PM$_{2.5}$ concentrations based on near-surface visibility ~~at 4011 sites~~ in the Northern Hemisphere from 1959 to 2022

Hongfei Hao[1], Kaicun Wang[2], Guocan Wu[1], Jianbao Liu[2], Jing Li[3]

[1]Global Change and Earth System Science, Faculty of Geographical Science, Beijing Normal University, Beijing 100875, China

[2]Institute of Carbon Neutrality, Sino French Institute of Earth System Science, College Urban and Environmental Sciences, Peking University, Beijing 100871, China

[3]Institute of Carbon Neutrality, Sino French Institute of Earth System Science, Department of Atmospheric and Oceanic Sciences, School of Physics, Peking University, Beijing 100871, China

Corresponding Author: *Kaicun Wang* Email: kcwang@pku.edu.cn

Abstract

Long-term PM$_{2.5}$ data are essential ~~needed to~~ for ~~study~~ the atmospheric environment, human health, and climate change. PM$_{2.5}$ measurements are sparsely distributed and of short duration. In this study, daily PM$_{2.5}$ concentrations are estimated ~~from 1959 to 2022~~ using a machine learning method from 1959 to 2022 ~~at 4011 terrestrial sites~~ in the Northern Hemisphere based on near-surface ~~hourly~~ atmospheric visibility ~~data~~, which are extracted from ~~the Me~~ the Integrated Surface Database (ISD)~~teorological Terminal Aviation Routine Weather Report (METAR)~~. Daily continuous monitored PM$_{2.5}$ concentration ~~monitoring~~ is set as the target ~~of machine learning~~, and near-surface atmospheric visibility and other related variables are used as the inputs. The 80% of the samples of each site are the training set, and the 20% are the testing set. The training result~~s~~ shows that the slope of linear regression with a 95% confidence interval (CI) between the estimated PM$_{2.5}$ concentration and the monitored PM$_{2.5}$ concentration is 0.955 ~~46~~[0.955, 0.955]~~±0.0002 within the 95% confidence interval (CI)~~, the coefficient of determination (R^2) is 0.95, the root mean square error (RMSE) is 7.2~~0~~ μg/m^3, and the mean absolute error (MAE) is 3.2~~1~~ μg/m^3. The test result~~s~~ shows that the slope within a 95% CI between the predicted PM$_{2.5}$ concentration and the monitored PM$_{2.5}$ concentration is 0.864~~2~~ [0.863, 0.865]~~± 0.0010 within a 95% CI~~, the R^2 is 0.79~~80~~, the RMSE is 1~~3.5~~4.8 μg/m^3, and the MAE is ~~–6.9~~7.6 μg/m^3. Compared with a global PM$_{2.5}$ concentration dataset derived from satellite aerosol optical depth product with 1 km resolution, the slopes of linear regression on the daily (monthly) scale are 0.817 (0.854) from 2000 to 2021, 0.758 (0.821) from 2000 to 2010, and 0.867 (0.879) from 2011 to 2022, indicating the accuracy of the model and the consistency of the estimated PM$_{2.5}$ concentration on the temporal scale. The interannual trends and spatial patterns of PM$_{2.5}$ concentration on the regional scale from 1959 to 2022 are analyzed by Generalized Additive Mixed Model (GAMM), suitable for the situation with an uneven spatial distribution of monitoring sites. The trend is the slope of the Sen-Theil estimator. In Canada, the trend is -0.10 μg/m^3/decade and the PM$_{2.5}$ concentration exhibits an east-high to west-low pattern. In the United States, the trend is -0.40 μg/m^3/decade, and PM$_{2.5}$ concentration decreases significantly after 1992, with a trend of -1.39 μg/m^3/decade. The high PM$_{2.5}$ concentration areas are in the east and west and the low are in the central and northern regions. In Europe, the trend is -1.55 μg/m^3/decade. High concentration areas are distributed in eastern Europe, and the low areas are in northern and western Europe. In China, the trend is 2.09 μg/m^3/decade. High concentration areas are distributed in northern China and the low areas are distributed in southern China. The trend is 2.65 μg/m^3/decade up to 2011 and -22.23 μg/m^3/decade since 2012. In India, the trend is 0.92 μg/m^3/decade. The concentration exhibits a north-high to south-low pattern, with high concentration areas distributed in northern India, such as Ganges Plain and Thar Desert and the low area is in Deccan Plateau. The trend is 1.41 μg/m^3/decade up to 2013 and -23.36 μg/m^3/decade since 2014. The variation in regional $PM_{2.5}$ concentrations is closely related to the implementation of air quality laws and regulations. The daily site-scale $PM_{2.5}$ concentration dataset from 1959 to 2022 in the Northern Hemisphere ~~The multiyear mean $PM_{2.5}$ concentrations from 1959 to 2022 in the United States, Canada, Europe, China, and India are 11.2 μg/m^3, 8.2 μg/m^3, 20.1 μg/m^3, 51.3 μg/m^3 and 88.6 μg/m^3, respectively. $PM_{2.5}$ is low and continues to decrease from 1959 to 2022. $PM_{2.5}$ in the United States increases slightly at a rate of 0.38 μg/m^3/decade from 1959 to 1990 and decreases at a rate of -1.32 μg/m^3/decade from 1991 to 2022. Trends in Europe are positive (5.69 μg/m^3/decade) from 1959 to 1972 and negative (-1.91 μg/m^3/decade) from 1973 to 2022. Trends in China and India are increasing (3.04 and 3.35 μg/m^3/decade, respectively) from 1959 to 2012 and decreasing (-38.82 and -42.84 μg/m^3/decade, respectively) from 2013 to 2022. The dataset~~ is available at National Tibetan Plateau / Third Pole Environment Data Center (https://doi.org/10.11888/Atmos.tpdc.301127) (Hao et al., 2024).

Keywords

Fine particulate matter; $PM_{2.5}$; Visibility; Machine learning; Dataset.

1 Introduction

Fine particulate matter ($PM_{2.5}$) refers to particulate matter suspended in air with an aerodynamic diameter of less than 2.5 micrometers. $PM_{2.5}$ has various shapes and is composed of complex components, such as inorganic salts (e.g., sulfate, nitrate, and ammonium), as well as organic carbon and elemental carbon, metallic elements, and organic compounds (Chen et al., 2020; Fan et al., 2021). $PM_{2.5}$ can be emitted directly into the atmosphere (Viana et al., 2008; Zhang et al., 2019) and generated through photochemical reactions and transformations (Guo et al., 2014). $PM_{2.5}$ exhibits high concentrations near emission sources, which gradually decreases with distance. Due to the smaller size and longer life span ~~of $PM_{2.5}$~~ compared with coarse particulate matter, $PM_{2.5}$ ~~it~~ can be transported over long distances by atmospheric movements, leading to wide-ranging impacts. Studies indicate that regional transport contributes significantly to local $PM_{2.5}$ concentration (Wang et al., 2014; Chen et al., 2020).

$PM_{2.5}$ reduces atmospheric visibility and facilitates the formation of fog and haze conditions (Fan et al., 2021). Direct and indirect effects of $PM_{2.5}$ on solar radiation in the atmosphere (Albrecht, 1989; Ramanathan et al., 2001; Bergstrom et al., 2007; Chen et al., 2022) alter the energy balance and the number of condensation nuclei, thereby influencing atmospheric circulation and the water cycle (Wang et al., 2012; Liao et al., 2015; Samset et al., 2019; Li et al., 2022).

$PM_{2.5}$ is also known as respirable particulate matter. Due to its complex composition, $PM_{2.5}$ may carry toxic substances that can significantly impair human health. The World Health Organization states explicitly that $PM_{2.5}$ is more harmful than coarse particles, and long-term exposure to high $PM_{2.5}$ concentrations increases the risk of respiratory diseases, cardiovascular diseases, and lung cancer (Lelieveld et al., 2015), regardless of a country's development status. A Global Burden of

Diseases study reveals~~ed~~ that exposure to environmental $PM_{2.5}$ causes thousands of deaths and millions of lung diseases annually (Chafe et al., 2014; Kim et al., 2015; Cohen et al., 2017).

$PM_{2.5}$ is an important parameter for assessing particulate matter pollution and air quality (Wang et al., 2012). $PM_{2.5}$ can lead to soil acidification, water pollution, disruption of plant respiration, and ecological degradation (Wu and Zhang, 2018; Liu et al., 2019). Due to globalization and economic integration, preventing and controlling particulate matter pollution is a challenge at city, country and global scales.

Therefore, long-term $PM_{2.5}$ concentration data are needed for studies on the environment, human health, and climate change. At present, ground-based measurements, chemical models, and estimations of alternatives are the primary sources of $PM_{2.5}$ concentration data.

Ground-based measurements are the most effective means to measure $PM_{2.5}$ concentration. $PM_{2.5}$ monitoring has been ongoing since the 1990s in North America and Europe (Van Donkelaar et al., 2010), and large-scale $PM_{2.5}$ monitoring has been implemented in other regions since 2000, including China in 2013 (Liu et al., 2017). As a result, the records for $PM_{2.5}$ concentration are short, with only a few years of data available in many countries. The scarcity of $PM_{2.5}$ measurements makes it challenging to provide long-term historical data for research.

Many studies have employed statistical methods, machine learning and deep learning methods to estimate $PM_{2.5}$ concentrations based on aerosol optical depth. Van Donkelaar et al. (2021) has utilized satellite aerosol optical depth data, aerosol vertical structure of chemical transport models, and ground-level measurements to estimate monthly $PM_{2.5}$ concentrations and their uncertainties over global land from 1998 to 2019, and there are several related studies (Van Donkelaar et al., 2010; Boys et al., 2014; Van Donkelaar et al., 2015; Van Donkelaar et al., 2016; Hammer et al., 2020). Many studies have been conducted at the regional scale, such as in the United States (Beckerman et al., 2013), China (Wei et al., 2019b; Xue et al., 2019; Wei et al., 2020a; He et al., 2021; Wei et al., 2021), and India (Mandal et al., 2020). Although the $PM_{2.5}$ concentrations derived from satellite retrievals have high spatial coverage, there are some limitations that need to be considered. Aerosol optical depth describes the column property of aerosol, while $PM_{2.5}$ concentration describes the near-surface properties of aerosol. Therefore, aerosol vertical structure is crucial in establishing the relationship between the two. The daily representativeness is also considerable, as $PM_{2.5}$ concentration is continuously monitored while the daily frequency of satellite observations is low (1-2 times). Surface types, cloud conditions (Wei et al., 2019a) and resolution (Nagaraja Rao et al., 1989; Hsu et al., 2017) affect the accuracy of satellite products, thereby increasing uncertainty of estimation of $PM_{2.5}$ concentration.

Reanalysis datasets provide estimates of long-term particulate matter concentrations. The Modern-Era Retrospective Analysis for Research and Applications version 2 (MERRA-2) is an excellent reanalysis dataset from NASA that uses the Goddard Earth Observing System version 5 (GEOS-5), which ~~has~~ provides~~d~~ global $PM_{2.5}$ data since 1980 (Buchard et al., 2015; Buchard et al., 2016; Buchard et al., 2017; Gelaro et al., 2017; Sun et al., 2019). There are some emission inventories in the aerosol model, including: volcanic material; monthly biomass burning from 1980 to 1996; monthly SO_2, SO_4, POM, and BC from 1997 to 2009; annual anthropogenic SO_2 between 100 and 500 m above the surface from 1980 to 2008; annual anthropogenic SO_4, BC, and POM concentrations from 1980 to 2006. In assimilation systems, satellite aerosol products from MISR and MODIS Aqua/Terra are assimilated after 2000. Another reanalysis dataset is the Copernicus Atmosphere Monitoring Service (CAMS) global reanalysis, which is a global reanalysis dataset of the atmospheric composition produced by the European Centre for Medium-Range Weather Forecasts (ECMWF) and has provided $PM_{2.5}$ data since 2003 (Che et al., 2014; Inness et al., 2019). Although reanalysis provides long-term $PM_{2.5}$ data, the uncertainty in emission inventories increases the uncertainty in $PM_{2.5}$ concentration (Granier et al., 2011). The validation of the reanalysis based on emission inventories shows that $PM_{2.5}$ concentration is still overestimated or underestimated in some regions~~The validation of $PM_{2.5}$ for CAMS shows severe overestimations in some areas~~ (Buchard et al., 2017; Ali et al., 2022; Jin et al., 2022). The assimilation of aerosol optical depth products improves the aerosol column properties (Buchard et al., 2017), thereby improving the estimation of surface $PM_{2.5}$ concentration, as it to some extent constrains the vertical structure of aerosols. However, the lack of high spatiotemporal resolution emission inventories and long-term assimilation data greatly limits the accuracy of surface $PM_{2.5}$ concentrations.

~~The MERRA-2 surface $PM_{2.5}$ assessment results are more consistent between observations located in rural areas, as cities and suburban areas are affected by high local emissions that do not represent the estimated grid average. Due to the lack of nitrate and low organic carbon emissions in GOCART, there is a difference in the total amount of $PM_{2.5}$ during winter in the western United States, and sea salt aerosols are overestimated (Buchard et al., 2017). Another reanalysis dataset is the Copernicus Atmosphere Monitoring Service (CAMS) global reanalysis, which is a global reanalysis dataset of the atmospheric composition produced by the European Centre for Medium-Range Weather Forecasts (ECMWF) and has provided $PM_{2.5}$ data since 2003 (Che et al., 2014; Inness et al., 2019). The validation of $PM_{2.5}$ for CAMS shows severe overestimations in some areas (Ali et al., 2022; Jin et al., 2022). Although reanalysis provides long-term $PM_{2.5}$ data, the uncertainty in emission inventories increases the uncertainty in $PM_{2.5}$, which remains challenging (Granier et al., 2011).~~

~~Many studies have employed statistical methods, machine learning, and deep learning methods to estimate $PM_{2.5}$ concentrations based on aerosol optical depth (AOD). Van Donkelaar et al. (2021) utilized satellite AOD, chemical transport models, and ground-level measurements of AOD to estimate monthly $PM_{2.5}$ concentrations and their uncertainties over global land from 1998 to 2019, and there are several related studies (Van Donkelaar et al., 2010; Boys et al., 2014; Van Donkelaar et al., 2015; Van Donkelaar et al., 2016; Hammer et al., 2020). Many studies have been conducted at the regional scale, such as in the United States (Beckerman et al., 2013), China~~ (Wei et al., 2019b; Xue et al., 2019; Wei et al., 2020a; He et al., 2021; Wei et al., 2021)~~, and India (Mandal et al., 2020). Although the $PM_{2.5}$ data derived from satellite retrievals have high spatial coverage, the temporal range depends entirely on the satellite retrievals. The estimation of $PM_{2.5}$ based on satellite products is also limited by bright surfaces, cloud conditions (Wei et al., 2019a) and resolution (Nagaraja Rao et al., 1989; Hsu et al., 2017).~~

Another alternative for estimating $PM_{2.5}$ concentrations is the near-surface atmospheric horizontal visibility, which is the maximum distance at which observers with normal visual acuity can discern target contours under current weather conditions. In addition to manual observations, automated visibility measurement~~s were~~ has been implemented early, typically relying on the aerosol scattering principle (Wang et al., 2009; Zhang et al., 2020). Both ~~V~~visibility and $PM_{2.5}$ concentration are measurements of near-surface aerosols. They describe atmospheric horizontal transparency and are used to describe atmospheric pollution. Long-term visibility records have been used to quantify long-term aerosol properties (Molnár et al., 2008; Wang et al., 2009; Zhang et al., 2017; Zhang et al., 2020). Visibility observation stations are densely distributed across the ~~country~~world. Compared to satellite~~-~~ retriev~~ed AOD data~~als, visibility observations have longer historical records dating back to the early 20th century ~~–~~(Noaa et al., 1998; Boers et al., 2015), are not affected by cloud interference and provide continuous measurements.

Visibility has been used as a proxy for $PM_{2.5}$ concentration (Huang et al., 2009) and to estimate $PM_{2.5}$ concentration (Liu et al., 2017; Li et al., 2020; Singh et al., 2020). Singh et al. (2020) has analyzed the air quality in East Africa from 1974 to 2018 using visibility data. Liu et al. (2017) has developed a statistical model and utilized ground-level visibility data to estimate long-term $PM_{2.5}$ concentrations in China from 1957 to 1964 and 1973 to 2014. Gui et al. (2020) has proposed a method to establish a virtual ground observation network for $PM_{2.5}$ concentration in China using extreme gradient boosting modeling in 2018. Zeng et al. (2021) has used LightGBM to establish a virtual network for hourly $PM_{2.5}$ concentrations in China in 2017. Zhong et al. (2021; 2022) has used LightGBM to predict 6-hour $PM_{2.5}$ concentrations based on visibility, temperature, and relative humidity in China from 1960 to 2020. Meng et al. (2018) has utilized a random forest model to estimate the daily $PM_{2.5}$ components in the United States from 2005 to 2015. These studies have provided various methods for estimating $PM_{2.5}$ using visibility data. However, some have focused on only methodological innovations without providing long-term trends in $PM_{2.5}$ concentration. Other studies offer long-term trends, but the primary focus ~~was~~ is at urban ~~and~~ ore national scale~~s~~. There are few studies on long-term and high-temporal-resolution $PM_{2.5}$ concentration at the global scale or across different countries.

This study uses a convenient, accurate, and easily understandable machine learning approach to estimate daily $PM_{2.5}$ concentrations based on visibility at ~~4,011~~5023 land-based sites from 1959 to 2022. ~~We also provide the long-term trends and characteristics of $PM_{2.5}$ in different regions. The $PM_{2.5}$ dataset provides support for climate change, human health, and pollution control research.~~ First, we build a machine learning model and then analyze the importance of the variables. Second, we evaluate the model's performance and predictive ability. Third, we discuss the errors and limitations of the dataset. Fourth, we compare the estimated $PM_{2.5}$ concentration with the other dataset~~s~~. Finally, we analyze ~~the spatial-temporal distributions of $PM_{2.5}$.~~the long-term trends and spatial patterns of $PM_{2.5}$ concentration in different regions. We hope ~~T~~the $PM_{2.5}$ dataset will provide~~s~~ support for the atmospheric environment, human health, and climate change studies~~climate change, human health, and pollution control research.~~

2 Data and methods

2.1 Study Area

The study area is the Northern Hemisphere. ~~includes Canada, the United States, Europe, China, and India in the Northern Hemisphere.~~ Figure 1 shows the ~~The~~ distributions of visibility stations (a) and the $PM_{2.5}$ monitoring sites (b) ~~(b) in each region are shown in Figure 1~~. Table 1 lists information of stations such as the number and time span in each region. The number of visibility stations ~~is~~ and $PM_{2.5}$ monitoring sites is 5023~~3177, and a total of 4011 $PM_{2.5}$ monitoring sites are selected for this study.~~, ~~with 1110 sites in the United States, 304 sites in Canada, 834 sites in Europe, 1557 sites in China, and 206 sites in India.~~ Due to its relevance to national or regional development, the record length and distribution of $PM_{2.5}$ observation are uneven. In this study, the site-scale $PM_{2.5}$

observations are met at least three years. These sites are densely populated in North America, East and South Asia, and Europe, and are very sparse in regions such as Africa and South America, and West Asia.

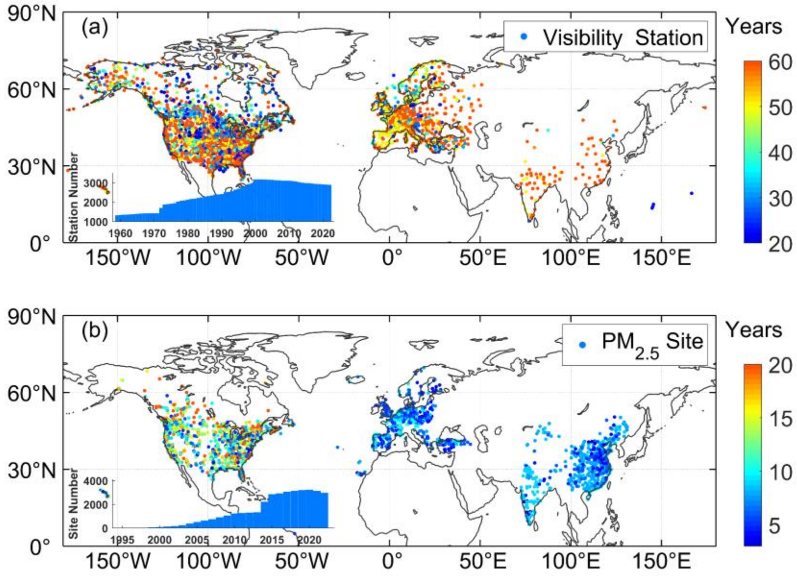

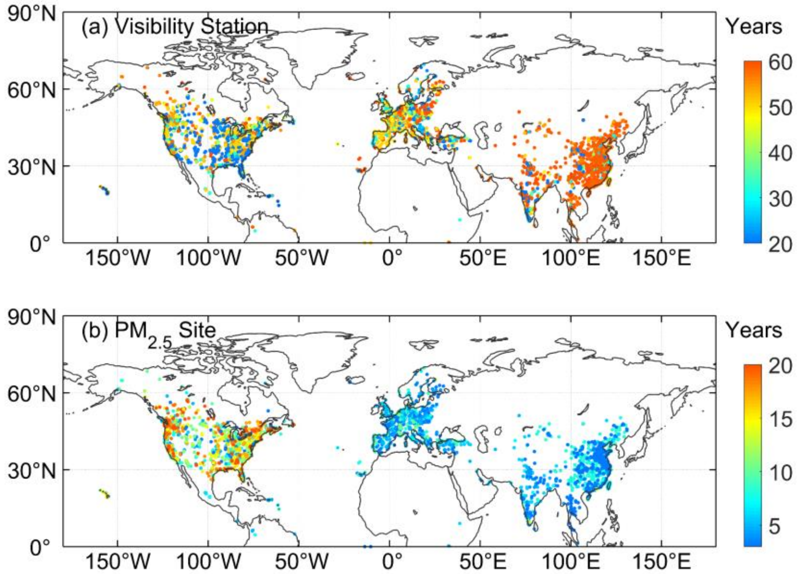

Figure 1. Study area and ~~the~~ distributions of visibility stations ~~from 1959 to 2022~~ (a) and $PM_{2.5}$ monitoring sites ~~from 1995 to 2022~~ (b). The color of marker (circle) represents ~~that~~ the ~~length~~ year number of ~~the observation record of~~ visibility observations and $PM_{2.5}$ concentration observations. ~~The bar chart shows the number of visibility stations and $PM_{2.5}$ monitoring sites per year. The number of visibility stations is 3177.The number of $PM_{2.5}$ sites is 4011 in this study (1110 in the United States, 304 in Canada, 834 in Europe, 1557 in China, and 206 in India).~~

Table 1. Data summary.

Region	Sites Number	Time Span	Temporal/Spatial Resolution	Data Source

Visibility	Global land	5023	1959-2022	Hourly/-	https://www.weather.gov/asos
	the United States	1111	1998-2022	Hourly/-	https://www.epa.gov/aqs
	Canada	311	1995-2022	Hourly/-	https://www.canada.ca
$PM_{2.5}$ observations	Europe	1073	1998-2022	Hourly/-	https://european-union.europa.eu;https://www.eea.europa.eu
	China	1887	2014-2022	Hourly/-	https://www.cnemc.cn
	India	270	2010-2022	Hourly/-	https://app.cpcbccr.com
	Other regions	371	2016-2022	Hourly/-	https://openaq.org
LGHAP	Land (-58~62°N)	--	2000-2021	Daily/1km	https://zenodo.org/communities/ecnu_lghap

2.2 $PM_{2.5}$ Data

2.2.1 $PM_{2.5}$ Data in the United States

The hourly $PM_{2.5}$ concentration data for the United States from 1998 to 2022 are sourced from the Air Data System (AQS), which are available at https://www.epa.gov/aqs. The AQS provides $PM_{2.5}$ mass monitoring and routine chemical speciation data and contains other ambient air pollution data collected by the Environmental Protection Agency (EPA), state, local, and tribal air pollution control agencies from thousands of monitors, comprising the Federal Reference Method (FRM) and Federal Equivalent Method (FEM). The primary purpose of both methods is to assess compliance with the $PM_{2.5}$ National Ambient Air Quality Standards (NAAQS). FRMs include in-stack particulate filtration, and FEMs include beta-attenuation monitoring, very sharp cut cyclones, and tapered element oscillating microbalances (TOEMs). The measurement precision is ± (1~2) $\mu g/m^3$ (hour) (Hall and Gilliam, 2016). The TEOM and beta-attenuation are automatic and near real-time monitoring methods. The TEOM, which is based on gravity, measures the mass of particles collected on filters by monitoring the frequency changes in tapered elements. The beta-attenuation method uses beta-ray attenuation and particle mass to measure the $PM_{2.5}$ concentration. In this study, we use two $PM_{2.5}$ measurement methods, FRM/FEM (88101) and non-FRM/FEM (88502). The 88502 monitors are "FRM-like" but are not used for regulatory purposes. Both the 88101 and 88502 monitors are used for reporting daily Air Quality Index values.

~~We set the conditions that each $PM_{2.5}$ monitoring event have a minimum of 3 years and more than 1000 days of overlapping records with nearby visibility stations. A total of 1110 sites in the United States are selected for this study.~~

2.2.2 $PM_{2.5}$ Data in Canada

The hourly $PM_{2.5}$ concentration data for Canada from 1995 to 2022 are sourced from the National Air Pollution Surveillance (NAPS) program, which are available at https://www.canada.ca. The NAPS program is a collaborative effort between the Environment and Climate Change Canada and provincial, territorial, and regional governments and is the primary source of environmental air quality data. Since 1984, $PM_{2.5}$ concentrations have been measured in Canada using a dichotomous sampler. Continuous or real-time particle monitoring began in the NAPS network in 1995 using TEOM and beta-attenuation monitoring (Demerjian, 2000). The samples are supplemented by EPA FRM samples obtained after 2009 (Dabek-Zlotorzynska et al., 2011). ~~The number of instruments is growing rapidly, with 410 sites in 2022. A total of 304 $PM_{2.5}$ monitoring sites in Canada are selected for this study.~~

2.2.3 $PM_{2.5}$ Data in Europe

The hourly $PM_{2.5}$ concentration data for Europe from 1998 to 2012 are obtained from the AirBase database, which is available at https://european-union.europa.eu. The hourly $PM_{2.5}$ concentration ~~verified~~ data (E1a) from 2013 to 2022 are obtained from the AirQuality database, which is available at https://www.eea.europa.eu. AirBase is maintained by the European Environment Agency (EEA) through its European Topic Center on Air Pollution and Climate Change Mitigation. Airbase contains air quality monitoring data and information submitted by participating countries throughout Europe. After the Air Quality Directive 2008/50/EC was enforced, the $PM_{2.5}$ concentration data began to be stored in AirQuality database. The main monitoring methods for $PM_{2.5}$ concentration include TEOM and beta attenuation (Green and Fuller, 2006; Chow et al., 2008). The sites are distributed across rural, rural-near city, rural-regional, rural-remote, suburban, and urban areas. ~~We merge the two datasets with the same site identifiers, and 834 sites in Europe are selected for this study.~~

2.2.4 $PM_{2.5}$ Data in China

The hourly $PM_{2.5}$ concentration data for China from 2014 to 2022 are obtained from the China National Environmental Monitoring Center, which are available at https://www.cnemc.cn. ~~China established air quality monitoring in 1980;~~ The continuous monitoring of $PM_{2.5}$ nationwide began in 2013 and $PM_{2.5}$ concentration data are available to the public. ~~74 cities were the first to publicly release real-time $PM_{2.5}$ in 2013~~(Su et al., 2022), and there ~~were~~ are ~~more than 18~~about 2000 air quality observation sites ~~as of 2000~~in 2022 ~~(Su et al., 2022)~~. $PM_{2.5}$ concentrations are measured using the TEOM and beta-attenuation method (Zhao et al., 2016b; Miao and Liu, 2019). According to the China Environmental Protection Standards, instrument maintenance, data transmission, data assurance and quality control ensure the reliability of $PM_{2.5}$ concentration measurements. The uncertainty in the $PM_{2.5}$ ~~mass~~ concentration is < 5 μg/m^{-3} (Pui et al., 2014). ~~In this study, a total of 1110 $PM_{2.5}$ monitoring sites are selected.~~

2.2.5 $PM_{2.5}$ Data in India

The hourly $PM_{2.5}$ concentration data for India from 2010 to 2022 are obtained from the Central Pollution Control Board (CPCB), which are available at https://app.cpcbccr.com. The Air (Prevention and Control of Pollution) Act of 1981 ~~was~~ is enacted by the Central Pollution Control Board (CPCB) of the Ministry of Environment, Forest and Climate Change (MoEFCC). ~~A standard of 60 μg/m^3 $PM_{2.5}$ concentration over 24 hours was added in 2009. The methods used by the Indian National Ambient Air Quality Standards (NAAQS) for $PM_{2.5}$ and related component measurements include the TEOM, FRM and FEM (Pant et al., 2019). The measurement precision is ± (1-2) μg/m^3 (hour).~~ The National Air Quality Monitoring Programme (NQAMP) is a key air quality monitoring programme employed by the Government of India, which is managed by the CPCB in coordination with the State Pollution Control Boards (SPCBs) and UT ~~(union territory)~~ Pollution Control Committees (PCCs). A standard of 60 μg/m^3 $PM_{2.5}$ concentration over 24 hours is added in 2009. The methods used by the Indian National Ambient Air Quality Standards (NAAQS) for $PM_{2.5}$ concentration and related component measurements include the FRM and FEM (Pant et al., 2019). The measurement precision is ± (1-2) μg/m^3 (hour).~~There were 703 $PM_{2.5}$ monitoring stations as of 2018. Most of these stations (residential and industrial) are located in urban areas, and others are located sparsely in rural areas. A total of 206 $PM_{2.5}$ monitoring sites are selected for this study.~~

2.2.6 $PM_{2.5}$ data in other regions

The hourly $PM_{2.5}$ concentration data of other regions from 2016 to 2022 are from openAQ (https://openaq.org), which is a nonprofit organization providing air quality data. These air quality data are collected from environmental protection departments and other departments over the world without any processing, therefore they have good accuracy. The $PM_{2.5}$ concentrations almost are measured by the TEOM and beta-attenuation method, and have been used for scientific research (Jin et al., 2022; Tan et al., 2022).

2.3 Visibility and Meteorological Data

~~The hourly meteorological data from 1959 to 2022 are collected from airport weather observations, which are available at . Automated observation minimizes the errors associated with human involvement in data collection, processing, and transmission. The data are extracted from the Meteorological Terminal Aviation Routine Weather Report (METAR). The World Meteorological Organization (WMO) sets guidelines for METAR reports, including report format, encoding, observation instruments and methods, data accuracy, and consistency. These requirements ensure the consistency and comparability of METAR reports globally. Visibility is a quantity that describes the atmospheric transparency, usually observed by automated sensors (scattering and transmission). More than 1000 stations are from the Automated Surface Observing System (ASOS) in the United States, and other data are sourced from airport reports worldwide. The forward-scatter visibility sensors at a wavelength of 550 nm for ASOS are consistent with the National Weather Service of the United States standard transmissometer, with more than 80% of the data within the limit of ±0.4 km when visibility is less than 2 km (Noaa et al., 1998).~~

The hourly visibility and meteorological data are from the Integrated Surface Database (ISD) (Smith et al., 2011), which is a global database consisted of hourly and synoptic surface observations and archived at the NOAA's National Centers for Environmental Information (NCEI), available at https://www.ncei.noaa.gov/products/land-based-station/integrated-surface-database. The ISD database integrates data from more than 100 original data sources and incorporates data from over 35000 stations around the world and includes observations data dating back to 1901. The strict quality control algorithms are used to ensure data quality by checking data format, extreme values and limits, consistency between parameters, and continuity between observations. Detailed information about the quality control are in http://www.ncei.noaa.gov/pub/data/inventories/ish-qc.pdf. The best spatial coverage of stations is evident in North America, Europe, Australia, and parts of Asia, and the coverage in the Northern Hemisphere is better than the Southern Hemisphere.

Visibility and meteorological records are filtered by the geophysical report type code. The codes of FM-12 and FM-15 are selected. FM-12 code represents the report is from Surface Synoptic Observations (SYNOP) report, which is a coding system developed by the World Meteorological Organization (WMO) for reporting observation data from ground meteorological stations. FM-15 code represents the report is from Meteorological Terminal Aviation Routine Weather Report (METAR), providing weather information at the airport and its surrounding areas. The format and content of the METAR report are consistent globally and comply with WMO's international meteorological observation and reporting standards. The frequency of SYNOP report is generally every three or six hours, and the frequency of METAR report is usually once per hour.

In this study, v~~V~~isibility is an essential variable for $PM_{2.5}$ concentration. ~~employed in this study, as research has shown that its~~ The reciprocal of visibility is directly proportional to the aerosol extinction coefficient ~~(Wang et al., 2009)~~, which is closely related to the $PM_{2.5}$ concentration (Wang et al., 2009; Wang et al., 2012). Considering that temperature, wind speed, ~~wind direction,~~ humidity, and precipitation are factors that impact particle dispersion, particle growth, and secondary generation ~~influenced by humidity, as well as the cleansing effect of precipitation~~ (Zhang et al., 2020), temperature, dew point temperature, ~~temperature-dew point difference, relative humidity, sea-level pressure,~~ wind speed ~~and direction~~, and precipitation are selected~~, and sky conditions are also employed in this study~~.

2.4 Data Preprocessing

When processing the visibility and meteorological variables, we use some screening conditions from previous studies (Husar et al., 2000; Wang et al., 2009; Li et al., 2016; Zhong et al., 2021). ~~The following data preprocessing steps are performed:~~ We remove the records with missing visibility, temperature, dew point temperature, ~~temperature-dew point difference, relative humidity, sea-level pressure,~~ wind speed~~, and wind direction data and remove records with~~ and hourly precipitation greater than 0.1 mm~~, sky conditions marked as 'VV', and~~ . ~~r~~Relative humidity is calculated using the Goff-Gratch formula (Goff, 1957). When relative humidity is greater than 90%, the record is removed to reduce the influence of fog, even precipitation. In high latitude regions, the low visibility records caused by ice fog and snow are removed, when the temperature is less than -29 °C and the wind speed is greater than 16 km/h. Since $PM_{2.5}$ exhibits hygroscopic growth, ~~we calculated the~~ dry visibility is calculated, ~~for~~ when relative humidity ~~values~~ is between 30% and 90% (Yang et al., 2021).

$$VISD = VIS/(0.26 + 0.4285 * log(100 - RH)) \qquad (1)$$

where VIS is the visibility, RH is the relative humidity, and VISD is the dry visibility.

For a single visibility site, there should be at least 5 non-repetitive visibility values and at least three valid records per day. The upper limit of visibility is set to the 99% percentile of visibility (Li et al., 2016). The harmonic mean is used to calculate the daily VIS and ~~daily~~ VISD because it can better capture rapid weather changes and enhance daily representativeness (Noaa et al., 1998). The arithmetic ~~average~~mean is used for other variables.

The maximum hourly $PM_{2.5}$ concentration is set to 1000 μg/m^3. The daily $PM_{2.5}$ concentration needs at least 3 hourly records. We select the $PM_{2.5}$ monitoring sites with a condition of at least 3-year continuous monitoring. The distribution of $PM_{2.5}$ sites is shown in Figure 1, and the details are shown in Table 1.

The spatial matching between $PM_{2.5}$ site and visibility station adopts the nearest principle, and the upper limit of distance is set to 100 km. Through experiments that the upper limit of distance has little effect on model training and prediction, but when the upper limit is small, the number of site pairs significantly decreases, especially in Asia. Matched visibility stations are not be used again. To match more $PM_{2.5}$ monitoring sites, we construct a 'virtual' visibility station, whose variables are established by the average of variables of the two nearest visibility stations.

We merge daily $PM_{2.5}$ concentration and visibility and other meteorological variables. We have adopted two matching methods: (1) merge at the hourly scale first and then calculate the daily mean (2) and calculate the daily mean first and then match. The results of two methods have no impact on the training of the model, but there are differences in the predicted results. Since SNOPY's visibility is not continuously observed hourly, we select the second method to merge $PM_{2.5}$ concentration and visibility data on the daily scale to improve the daily representativeness of estimated $PM_{2.5}$ concentration.

~~At least three hourly daily records are needed. The harmonic mean is used to calculate the daily VIS and daily VISD because it can better capture rapid weather changes and enhance daily representativeness (Noaa et al., 1998). The arithmetic average is used for other variables.~~

2.5 $PM_{2.5}$ Data for Comparison

~~In this study, our data are compared with other datasets, including two $PM_{2.5}$ datasets based on satellite AOD data and two reanalysis datasets.~~The long-term gap-free high-resolution air pollutants (LGHAP) dataset provides daily $PM_{2.5}$ concentrations from 2000 to 2021 over global land, with a 1 km grid resolution, which is available at https://zenodo.org/communities/ecnu_lghap. The $PM_{2.5}$ concentration is estimated using aerosol optical depth and other factors such as geographic location, land cover type, climate zone, and population density, based on a deep-learning approach, termed the scene-aware ensemble learning graph attention network. The correlation coefficient with ground-based measurements is 0.95 and the RMSE is 5.7 μg/m^3 (Bai et al., 2024). This dataset provides global $PM_{2.5}$ concentration with a high spatiotemporal resolution.

For most regions in the Northern Hemisphere, except for North America and Europe, the duration of continuous monitoring $PM_{2.5}$ concentration data is relatively short, making it difficult to evaluate historical $PM_{2.5}$ concentration. For example, $PM_{2.5}$ monitoring network in China was implemented from the end of 2012, resulting in the inability to verify the $PM_{2.5}$ concentrations before 2012. Therefore, we compare our data with the LGHAP $PM_{2.5}$ concentration to evaluate the predictive ability of the model and the consistency of our data on the temporal scale.

~~2.5.1 ACAG Dataset~~

~~The monthly global $PM_{2.5}$ dataset (version V5.GL.04) from 1980 to 2022, with a spatial resolution of 0.1°, is available from the Atmospheric Composition Analysis Group (ACAG) of Washington University in St. Louis (https://sites.wustl.edu/acag/datasets/surface-pm2-5/) (Van Donkelaar et al., 2021). The ACAG $PM_{2.5}$ concentrations are estimated based on satellite (MODIS, VIIRS, MISR and SeaWiFS) AOD and global vertical aerosol profiles from the Cloud-Aerosol Lidar and Infrared Pathfinder Satellite Observation (CALIPSO) satellites. The AOD of GEOS-Chem is used to simulate the spatiotemporally varying geophysical relationship with $PM_{2.5}$. Ground-based $PM_{2.5}$ values are incorporated at a monthly timescale using geographically weighted regression (Van Donkelaar et al., 2016; Hammer et al., 2020; Van Donkelaar et al., 2021). The coefficients of determination (R^2) for the monthly mean and monitor-based $PM_{2.5}$ concentrations are 0.86 (January), 0.81 (April), 0.72 (July), and 0.78 (October). The R^2 with WHO-collocated monitors is between 0.88 and 0.93. The EMSE is between 8 and 13.3 μg/m^3.~~

~~2.5.2 CHAP Dataset~~

~~The monthly $PM_{2.5}$ dataset of China High Air Pollutants (CHAP) from 2000 to 2021 is a product with coverage over China, with a spatial resolution of 1 km, which is available at https://zenodo.org/records/6398971. The CHAP $PM_{2.5}$ concentration is estimated based on the MODIS Collection 6 MAIAC AOD product and meteorological variables, surface conditions, pollutant emissions, and population distributions using a space-time extra-trees model. The R^2 and RMSE of the monthly $PM_{2.5}$ concentration are 0.92-0.94 and ~5.1-10.0 μg/m^3, respectively, from 2013 to 2018 (Wei et al., 2020b; Wei et al., 2021).~~

~~2.5.3 MERRA-2 Dataset~~

~~The monthly $PM_{2.5}$ dataset of Modern-Era Retrospective Analysis for Research and Applications version 2 (MERRA-2) from 1980 to 2022 is a NASA reanalysis dataset with a spatial resolution of 0.5×0.625° and uses the Goddard Earth Observing System version 5 (GEOS-5) coupled to the Goddard Chemistry Aerosol Radiation and Transport (GOCART) model, which is available at https://gmao.gsfc.nasa.gov. The aerosol data of GOCART include dust, sea salt, sulfate, black carbon, and organic carbon, and there are 72 vertical layers from the surface to more than 80 km altitude. MERRA-2 $PM_{2.5}$ is a dataset produced by the GEOS-5 atmospheric model and data assimilation system and the three-dimensional variational data analysis (3DVAR) Grid-point Statistical Interpolation (GSI) meteorological analysis scheme (Randles et al., 2017). In the aerosol model (GOCART), a SO_2 emission database of volcanic material for secondary sources is included. Aerosol hygroscopic growth depends on the simulated relative humidity. The monthly scale biomass burning inventory is from RETROv2 from 1980 to 1996; the monthly SO_2, SO_4, POM, and BC emissions are from GFEDv3.1 from 1997 to 2009; and the daily scale data are from QFED 2.4-r6 after 2010. The annual anthropogenic SO_2 is from EDGARv4.2 between 100 and 500 m above the surface from 1980 to 2008. The annual Anthropogenic SO_4, BC, and POM concentrations are obtained from AeroCom Phase II from 1980 to 2006. In assimilation systems, satellite AOD retrievals are used, including AVHRR (over the oceans) from 1998 to 2002, MISR from 2000 to 2014, MODIS Aqua since 2002, and MODIS Terra since 2000 (Buchard et al., 2017; Randles et al., 2017). The direct observations of the AOD AERONET station from 1999 to 2014 are also assimilated.~~

~~The surface $PM_{2.5}$ concentration in MERRA-2 can be computed using the concentrations of black carbon [BC], organic carbon [OC], dust [$DUST_{2.5}$], sea salt [$SS_{2.5}$], and sulfate [SO_4] (Provençal et al., 2017) and is expressed as follows (please refer to https://gmao.gsfc.nasa.gov/reanalysis/MERRA-2/FAQ/#Q4):~~

~~$[PM_{2.5}] = [DUST_{2.5}] + [SS_{2.5}] + [BC] + 1.6\times[OC] + 1.375\times[SO_4]$.~~

~~In this study, we conduct spatiotemporal matching between MERRA-2 $PM_{2.5}$ and the estimated $PM_{2.5}$.~~

~~2.5.4 CAMS Dataset~~

~~The Copernicus Atmosphere Monitoring Service (CAMS) reanalysis is the latest global reanalysis dataset of atmospheric composition produced by the European Centre for Medium-Range Weather Forecasts (ECMWF). We use the single-level monthly $PM_{2.5}$ product from the CAMS reanalysis~~

~~from 2003 to 2022, which is available at https://ads.atmosphere.copernicus.eu/cdsapp#!/dataset/cams-global-reanalysis-eac4. The resolution is 0.75°. The CAMS reanalysis builds on the experience gained during the earlier Monitoring Atmospheric Composition and Climate (MACC) reanalysis and CAMS interim reanalysis (Inness et al., 2019). The ECMWF's Integrated Forecast System (IFS) aerosol and chemistry modules are applied, and more details on the modules are provided in (2015). The data at 60 model levels are interpolated to 25 pressure levels. Anthropogenic emissions are from the MACCity inventory from 1960 to 2010 (Granier et al., 2011). The emissions of anthropogenic SOAs are estimated from MACCity CO emissions. The monthly biogenic emissions of the chemical species are from MEGAN2.1 (Guenther et al., 2006). The natural NO_2 emissions from soils and oceans are obtained from the Precursors of Ozone and Their Effects in the Troposphere (POET) database for 2000. Daily biomass burning emissions are from the Global Fire Assimilation System version 1.2 (GFASv1.2) (Kaiser et al., 2012). More details regarding emissions are provided in Granier (2011). The incremental 4D-Var data assimilation system is used for the CAMS reanalysis, and the total aerosol mixing ratio of the single species is derived from the assimilation of satellite retrievals (Benedetti et al., 2009). The AODs from satellite retrievals are assimilated, including those from AATSR Envisat from 2002 to 2012 and those from MODIS Terra and Aqua since 2002. For additional information, please refer to Inness et al. (2019).~~

~~The surface $PM_{2.5}$ concentration is estimated by the air density [ρ], sea salt [$SS_{1,2}$], dust [$DD_{1,2,3}$], nitrate [$NI_{1,2}$], organic matter [OM], black carbon [BC], ammonium [AM], and sulfate [SO_4] and is expressed as follows (Inness et al., 2019):~~

~~$[PM_{2.5}] = \rho \times([DD_1] + [DD_2] + [SS_1/4.3] + [0.5 \times SS_2/4.3] + [0.7 \times (AM + OM + 0.7NI_1 + SO_4)] + [BC] + 0.25 \times [NI_2])$.~~

2.6 Decision Tree Regression

We employ decision tree regression ~~using the CART algorithm~~ (Teixeira, 2004) to estimate daily $PM_{2.5}$ concentrations. The key to decision tree regression is to find the optimal split variable and optimal split point. The optimal split point of the predictor is determined by the minimum mean squared error, which determines the optimal tree structure. Decision tree regression is a commonly used nonlinear machine learning method that partitions the feature space based on the mapping between feature attributes and response values, with each leaf node representing a specific output for each feature space region. It'~~'~~s ability to handle complex relationships with relatively few model parameters is advantageous, minimizing the risk of overfitting and enabling the prediction of continuous and categorical predictive variables.

The sample data includes predictor and response. The predictor is composed of 9 variables~~includes 11 variables~~: the reciprocal of dry visibility (Vis_Dry_In), the reciprocal of visibility (Vis_In), temperature (Temp), dew point temperature (Td), temperature-dew point difference (Temp-Td), relative humidity (RH), ~~sea-level pressure (SLP),~~ wind speed (WS), wind ~~direction (WD),~~ numerical time (DateTime) and daily record number (DailyObsNum). Both visibility and meteorological variables are daily means. The response variable is the daily ~~observed~~ monitored $PM_{2.5}$ concentration.

For each site, we sort the sample data by time, with the first 80% being the training set and the last

20% being the test set. Due to the inconsistent sample length among different sites, this approach is friendly for sites with small sample sizes (such as only 3-year observations).We ~~randomly select 80% of the sample data to establish the decision tree regression model, and the remaining 20% of the sample data are used to test the model's predictive ability. To obtain a stable model, a~~ use10-fold cross-validation method (Browne, 2000) ~~is used~~ to train the model. The test set is used to evaluate the predictive ability of the model.

2.7 Evaluation Metrics

2.7.1 Statistical Metrics

We use the root mean squared error (RMSE), mean absolute error (MAE), and correlation coefficient (ρ) as evaluation metrics to evaluate the model's performance and predictive ability. The formulas are given as follows:

$$\boldsymbol{MSE} = \sqrt{\frac{1}{n}\sum_{i=1}^{n}(y_i - \hat{y}_i)^2} \qquad (2)$$

$$\boldsymbol{MAE} = \frac{1}{n}\sum_{i=1}^{n}|y_i - \hat{y}_i| \qquad (3)$$

$$\rho = \frac{\sum_{i=1}^{n}(y_i-\bar{y})(\hat{y}_i-\bar{\hat{y}})}{sqrt(\sum_{i=1}^{n}(y_i-\bar{y})^2\sum_{i=1}^{n}(\hat{y}_i-\bar{\hat{y}})^2)} \qquad (4)$$

where y_i and $\bar{y}$ are the predicted value and the average of the predicted values. $\hat{y}_i$ and $\bar{\hat{y}}$ are the target and the average of the target. $i = 1,2,\ldots,n$. n is the length of sample.

2.7.2 Partial Dependence

The importance of predictor variables is assessed via partial dependence. Partial dependence represents the relationship between the individual predictive variable and the predicted response (Friedman, 2001). By marginalizing the other variables, the expected response of the predicted variable is calculated. All the partial dependences of the predicted response on the subset of predicted variables are calculated. The calculation process of the partial dependency method is described as follows:

The dataset of the predictor is X, $X = [X^1, X^2, \ldots, X^n]$, and n represents the number of predictive factors. The complement of subset X^s is X^c, where X^s is a single variable in X and X^c is all other variables in X. The predicted response f(x) depends on all variables in X, and it is expressed as follows:

$$\boldsymbol{f(x) = f(X^s, X^c)} \qquad (5)$$

The partial dependence of the predicted response to X^s is expressed as follows:

$$\boldsymbol{f^s(X^s) = \int f(X^s, X^c)pC(X^c)dX^c} \qquad (6)$$

where $pC(X^c)$ is the marginal probability of X^c, that is, $pC(X^c) \approx \int f(X^s, X^c)dX^s$. Assuming that the likelihood for each observation is equal, the dependence between X^s and X^c and the interactions of X^s and X^c in response are not strong. The partial dependence is shown below:

$$f^s(X^s) \approx \frac{1}{N}\sum_{i=1}^{N} f(X^s, X_i^s) \qquad (7)$$

where N is the number of observations and i represents the ith observation.

2.7.3 ~~Mean Center~~ Generalized Additive Mixed Model

Generalized Additive Mixed Model (GAMM) originates from two independent yet complementary statistical methods: Generalized Additive Model (GAM) and Mixed Effects Models. GAM is introduced by Trevor Hastie and Robert Tibshirani in the 1980s (Hastie and Tibshirani, 1987). GAM employs smooth functions (such as splines) to replace linear terms in traditional regression, capturing nonlinear relationships between response and explanatory variables. The primary aim of GAM is to enhance model flexibility, allowing the data to determine the form of the nonlinear relationships rather than pre-specifying them. Mixed Effects Model includes both fixed and random effects, enabling the analysis of hierarchical and correlated data (Verbeke and Lesaffre, 1996). Fixed effects apply to the entire sample, whereas random effects account for variations within individuals or groups, explaining data correlation and variability. GAMM represents the evolution of statistical models from linear to nonlinear, from simple to complex, and from single effects to mixed effects. GAMM has been widely applied in various fields such as ecology and climate, air pollution becoming essential tools for studying complex nonlinear relationships and hierarchical data (Park et al., 2013; Polansky and Robbins, 2013; Chang et al., 2017; Ravindra et al., 2019).

The relationship between $PM_{2.5}$ concentrations and time (e.g., months, seasons) is typically nonlinear and exhibits seasonal variation. GAMM model uses smooth functions (such as splines) to capture the nonlinear variations and model the periodic features with cyclical smooth functions. Interannual variations in $PM_{2.5}$ concentrations can also be captured using smooth functions. Due to the inherent autocorrelation in time series, GAMM model effectively handles the autocorrelation by incorporating time-related smooth functions or random effects, thereby enhancing the model accuracy. $PM_{2.5}$ concentrations from neighboring locations often exhibit spatial correlation. GAMM model can address this spatial correlation by introducing spatially correlated smooth functions or random effects. Therefore, it is also suitable for spatial variations, especially when the spatial distribution of sites observations is uneven.

Based on the GAMM, the $PM_{2.5}$ concentration $y(i,t)$ at site i and time t can be expressed as:

$$y(i,t) = x\beta + f(\cdot) + b(i,t) + \varepsilon(i,t) \qquad (8)$$

The following is an explanation of the expression and parameter settings.

Linear terms $x\beta$: x is the vector of explanatory variables, including site elevation and the overall mean $PM_{2.5}$ concentration. β is a coefficient vector.

Smooth terms $f(\cdot)$ can be decomposed into three individual smooth terms: seasonal smooth term, interannual smooth term, and spatial smooth term, as shown in equation (9).

$$f(\cdot) = f(month) + f(year) + f(\mathrm{spatial}) \qquad (9)$$

They are composed of linear combinations using spline basis functions. For seasonal smooth term, it is a function of the month, smooth function is the penalized regression cyclic cubic splines (assumed with periodic nature) (Wood et al., 2016) and the knot number is 12. For interannual smooth term, it is a function of the year, smooth function is the penalized regression cubic splines (Wood et al., 2016) and the knot number is 64. For spatial smooth term, it is a function for longitude and latitude, smooth function is the gaussian process penalized regression splines (Kammann and Wand, 2003) and the knot number is 80. In this study, they are used to describe the regional long-term $PM_{2.5}$ concentration annual cycle, interannual trends and spatial distribution, respectively.

Station-specific effects term $b(i,t)$ is a random effect term to describe the differences between observation sites, based on the assumption that observations are independent.

The residual noise term $\varepsilon(i,t)$ 1-order autoregressive term.

More explanations about GAMM model are detailed in the package mgcv of R. Some studies also provide an introduction and selection of parameters (Polansky and Robbins, 2013; Chang et al., 2017; Ravindra et al., 2019). ~~(2017)~~

~~The mean center is a geostatistical method used to describe the average position of a set of geographical coordinates. It represents the central tendency of a set of geographical data and aids in understanding the overall distribution and trends in the dataset. The mean center of the $PM_{2.5}$ concentration shows the overall trend and variability in $PM_{2.5}$. If the mean center is located at the edge of the dataset, the data distribution is dispersed. Conversely, if the mean center is located at the center of the dataset, the data distribution is concentrated. This may be relevant for aspects, such as population distribution, urban development, and economic activities. It is particularly helpful in understanding the spatial patterns of $PM_{2.5}$. The expression is given as follows:~~

$$\cancel{x_{ct} = \sum_{i=1}^{N} c_i * x_i / \sum_{i=1}^{N} c_i}$$

$$\cancel{y_{ct} = \sum_{i=1}^{N} c_i * y_i / \sum_{i=1}^{N} c_i}$$

~~where x_{ct} and y_{ct} represent the longitude and latitude of the mean center, respectively, and c_i represents the $PM_{2.5}$ concentration at the i-th site (x_i, y_i).~~

~~2.7.4 Standard Deviation Ellipse~~

~~The standard deviation ellipse (SDE) is used in statistics and geography to describe the variability and correlation of multivariate data. The SDE is calculated based on the mean and covariance matrix of the data (Gong, 2002). This variable shows the dispersion and correlation of the data across different dimensions. The center of the ellipse corresponds to the mean of the data, while the shape and size of the ellipse reflect the variability in the data in different directions.~~

~~We calculate the SDE using the locations and concentration measurements associated with the $PM_{2.5}$ points. The major axis of the ellipse indicates the primary direction of data variation. The shape and size of the ellipse reflect the spatial dispersion of the $PM_{2.5}$ concentration. A larger ellipse indicates greater variability in the $PM_{2.5}$ concentration distribution, while a smaller ellipse denotes a more concentrated distribution. A circular ellipse indicates little or weak spatial correlation among $PM_{2.5}$ concentrations. A flattened ellipse indicates a spatial correlation between $PM_{2.5}$ concentrations.~~

3. Results and Discussion

3.1 Evaluation of Variable Importance

We ~~analyze~~ evaluate the contribution ~~influence~~ of ~~predictive~~ each variable~~s~~ ~~over~~ to the ~~predicted~~ response by partial dependence. The ~~predictive~~ variable with the highest partial dependence value is the most important ~~predictive~~ variable in the model. ~~The partial dependence of the predicted response on each predictive variable is calculated for every model.~~ Figure 2 (a) shows the proportion of the most important variables for all sites and Figure 2 (b) shows the ranking of the importance of all variables. Reciprocal of dry visibility is the most important variable at 65.8% of sites, and Reciprocal of visibility is the second most important variable at 14.9% of sites. The contribution of meteorological variables ranges from 2.1% to 6.6%. The time variable contributes 1.7%. The lowest contribution is daily number of visibility record at only 0.9%, because it is only a variable that describes the daily representativeness of visibility. It also indicates that daily visibility has high daily representativeness (under the conditions of at least three hourly records)

The $PM_{2.5}$ concentration level varies spatially, which are related to regional geographical environment, climate, and air quality laws and regulations. Therefore, we analyze the importance of variables in different regions, as shown in Figure 2 (c-h). The two most important variables are still reciprocal of dry visibility and reciprocal of visibility, with a proportion of 73.1% in the United States, 77.5% in Canada, 80.8% in Europe, 98.8% in China, and 60.2% in India. It indicates that $PM_{2.5}$ concentration is the most significantly correlated with visibility in China. The contribution of meteorological variables is significantly higher in the United States and India than in other regions. It indicates that meteorological conditions have a significant contribution to $PM_{2.5}$ concentration in these regions, which may be related to the formation mechanism and transport of particulate matter.

~~the ranking results of the importance of all the predictive variables. The variable with the highest dependence on the predicted response is Vis_Dry_In, and the second highest dependence is Vis_In. The dependence of the predicted response on Temp, Td, Temp-Td, RH, WS, and wind WD is moderate. The predictive variables with lower dependence include SLP, DateTime and DailyObsNum.~~

~~We count the frequency and proportion of the most important variables in all the models, as shown in Figure 2 (b). Vis_Dry_In is the most important variable at 2600 sites, contributing 64.8%. Vis_In was the second most important variable at 575 sites, accounting for 14.3%. This finding indicates that visibility is the most crucial variable, with a percentage of 79.1%. Temp and Td contribute 6.7% and 3.5%, respectively. The contribution of other variables combined is 10.7%. The percentages of the second most important predictive variable are 25.4% for Vis_In, 39.6% for Vis_Dry_In, 14.6% for Temp, 7.1% for Td and 3.4% for Temp-Td. Among the three most important variables, the proportions of Temp and Td are 15.7% and 14.3%, respectively.~~

The above results indicate a strong correlation between the $PM_{2.5}$ concentration and visibility, as visibility can be considered an indicator of air quality without fog or precipitation. Meteorological factors ~~Temperature and dew~~ play secondary roles~~, and other meteorological predictive variables play lesser roles in the model~~, ~~.Meteorological factors~~which influence the formation, dispersion and deposition of $PM_{2.5}$ (Gui et al., 2020; Zhong et al., 2022). ~~Temperature and dew play secondary roles, and other meteorological predictive variables play lesser roles in the model.~~ Although the number of daily records and time have the most negligible impacts on the $PM_{2.5}$ concentration in the model, they have significant impacts on the cyclical changes and daily representativeness of $PM_{2.5}$ concentration (Wang et al., 2012; Zhang et al., 2020).

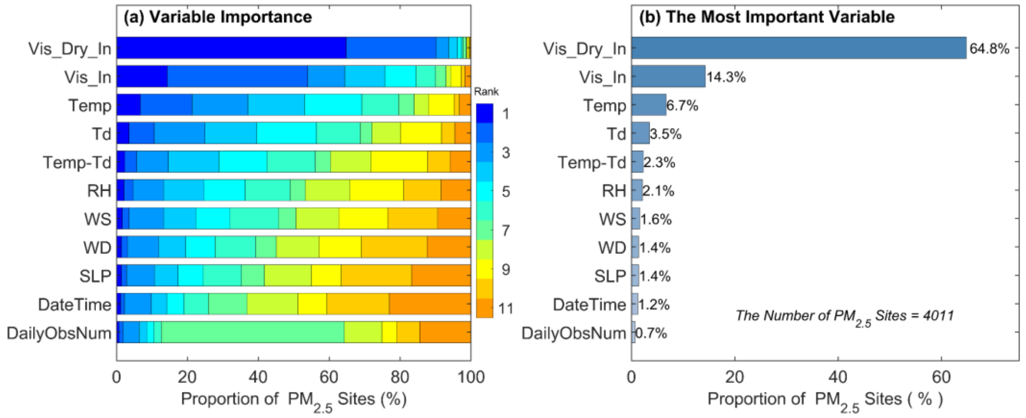

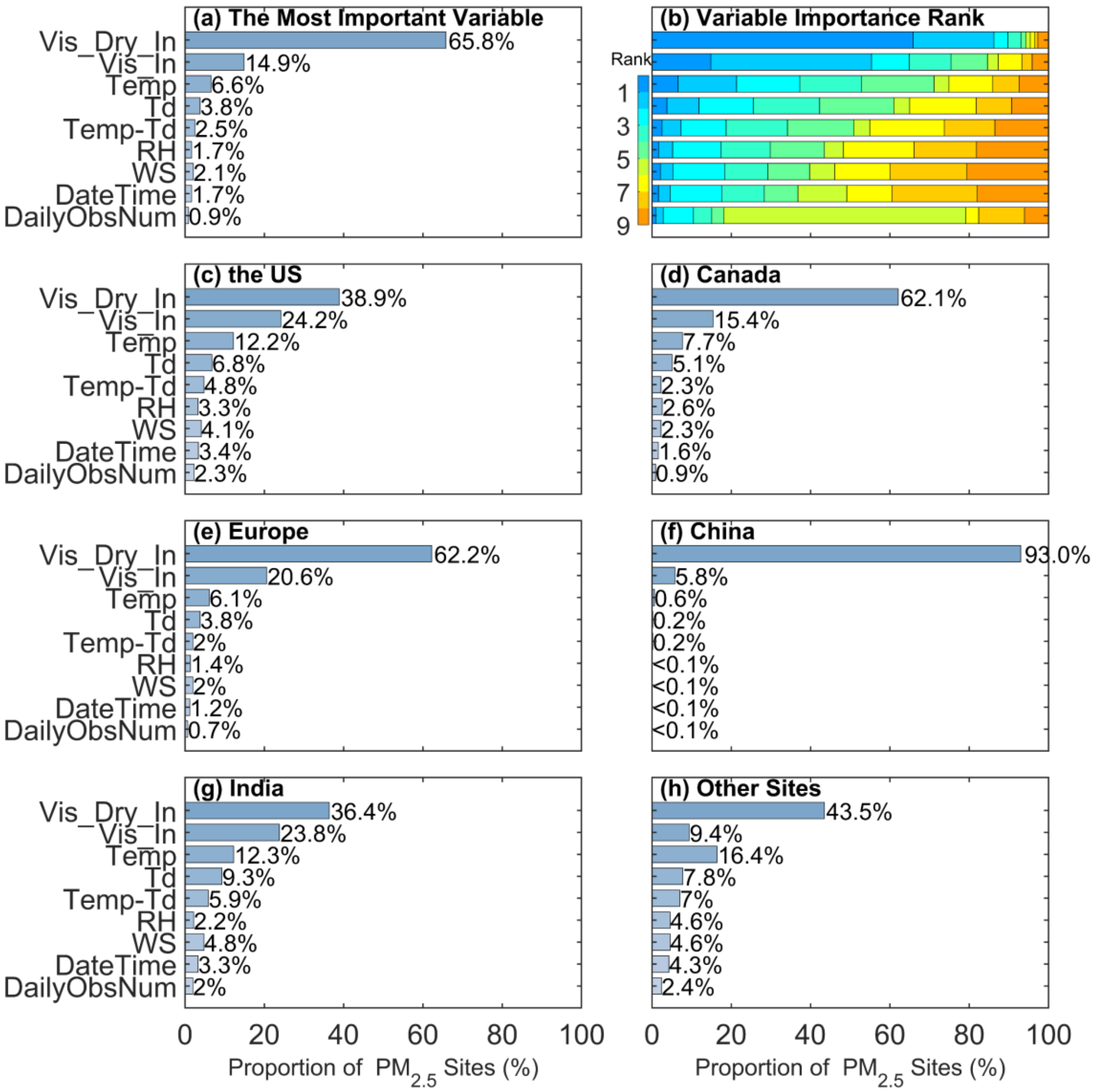

Figure 2. The most important~~ce of predictive~~ variables (a) and the ranking (b) at all sites. The most

important variable in each region (c-h).~~.~~ The stacked bar ~~(a)~~ shows the importance rankings of the ~~predictive~~ variables ("~~'~~rank=1"~~'~~ represents the most important variable). The bar ~~(b)~~ shows the ~~percentage~~ proportion of the most important ~~predictive~~ variable. The ~~predictive~~ variables are the reciprocal of dry visibility (Vis_Dry_In), reciprocal of visibility (Vis_In), temperature (Temp), dew point temperature (Td), temperature-dew point difference (Temp-Td), relative humidity (RH), ~~sea level pressure (SLP),~~ wind speed (WS), ~~wind direction (WD),~~ numerical time (DateTime) and daily ~~record~~ number of visibility record (DailyObsNum). ~~The total number of $PM_{2.5}$ sites is 4011.~~

3.2 Evaluation of Model Performance

~~3.2.1 For All Data~~

We analyze the linear regression ~~fitting~~ relationship between all estimated and corresponding response values to evaluate the model's performance. Figure 3 ~~shows~~ is the density scatter plot of the monitored $PM_{2.5}$ concentration (response values) and the estimated $PM_{2.5}$ concentration (estimated values). There is a total of ~~8,680,796~~8031473 data pairs for all the sites. The linear regression ~~coefficient~~ slope (95% confidence interval) is 0.9~~46 ±0.0002 within the 95% confidence interval~~55 [0.955, 0.955], the R^2 is 0.95, the RMSE is 7.2~~0~~ μg/m³, and the MAE is 3.2~~1~~ μg/m³.

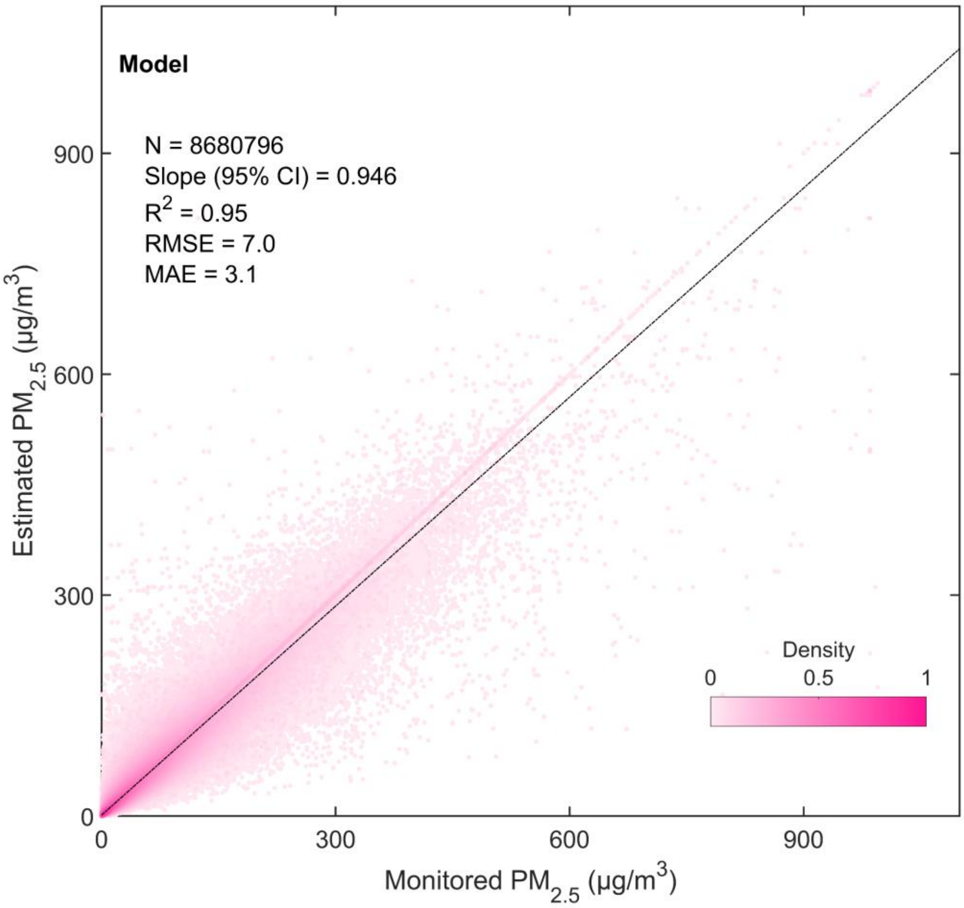

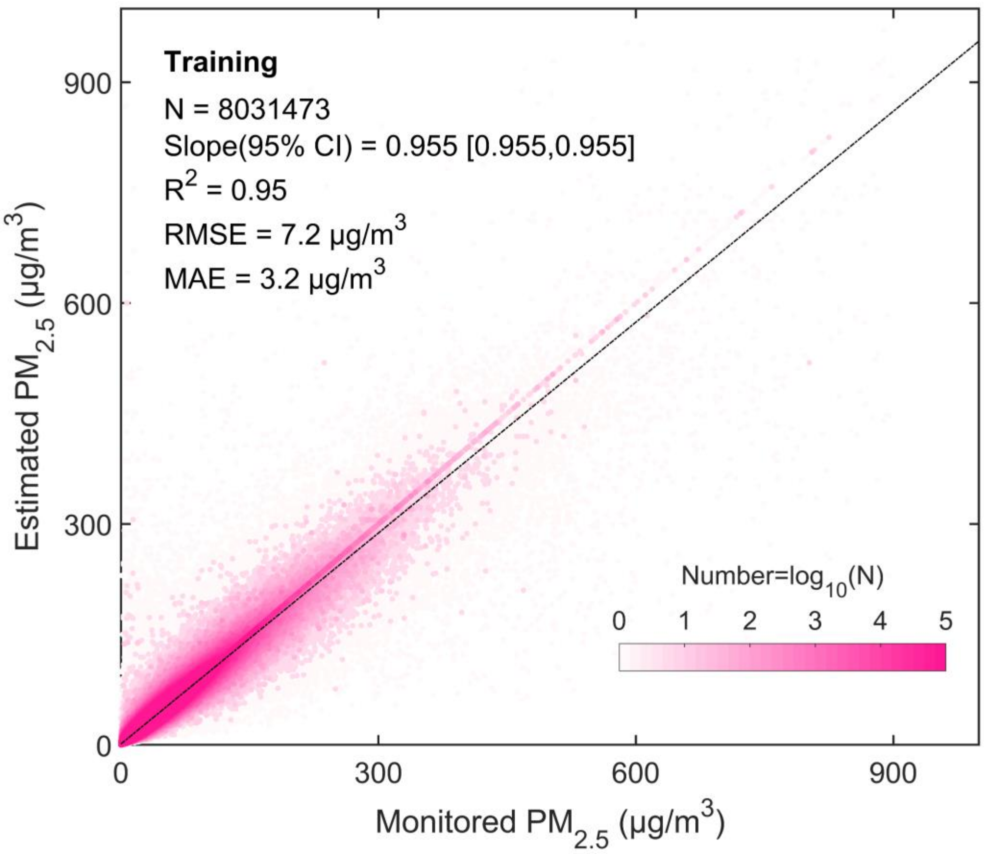

Figure 3. Density scatter plot (a) between ~~estimated values (~~estimated PM$_{2.5}$~~)~~ concentration and ~~the corresponding response values (~~monitored ~~Pd~~PM$_{2.5}$~~)~~ concentration~~at the daily scale~~. The dashed black line is the linear regression line. N is the length of the data pairs, and Slope is the linear regression coefficient within a 95% confidence interval (CI). R^2 is the coefficient of determination, RMSE is the root mean square error, and MAE is the mean absolute error.

~~3.2.2 For the Site and Region Scales~~

~~We evaluate the model's performance using the RMSE, MAE, and ρ of the estimated and response values at the site and region scales.~~ Figure 4 (a-c) shows the spatial distribution (a-c) and frequency ~~distribution (d-f) of the model's~~of training of ~~–~~RMSE, MAE, and ρ~~ at all sites~~. Table 2~~1~~ lists the model's performance metrics~~ for all sites and sites~~ in the United States, Canada, Europe, China, and India.

For all sites, the average RMSE is 6.9~~7.4~~2 μg/m^3, with a median of 4.76~~97~~ μg/m^3. The RMSE of 80% of the sites is less than 10~~1~~.01~~95~~ μg/m^3. The ~~ratio of the~~ RRMSE (the percentage of RMSE to mean of PM$_{2.5}$ concentration) ~~to the average PM$_{2.5}$ concentration~~ is ~~29.2~~28.7%. The ~~average~~ MAE is ~~4.01~~3.77 μg/m^3, with a median of 2.~~66~~72 μg/m^3. The MAE is less than ~~6.62~~5.66 μg/m^3 for 80% of the sites. The RMAE~~ to mean ratio~~ (the percentage of MAE to mean of PM$_{2.5}$ concentration) is 15.4~~8~~%. The average ρ is 0.91~~0~~, and the median is 0.92~~1~~. The ρ of 80% of the sites is greater than 0.87. Previous studies have shown that for PM$_{2.5}$ concentration retrieved from daily visibility or satellite ~~AOD~~ aerosol optical depth~~data~~, the R^2 range of the model is from 0.42 to 0.89, and the

RMSE range is from 9.59 μg/m^3 to 32.09 μg/m^3 (Shen et al., 2016; Liu et al., 2017; Wei et al., 2019b; Gui et al., 2020; Li et al., 2021; Zhong et al., 2021). This finding indicates that our model performs well at the daily scale.

~~At~~ On the regional scale, the ~~average~~ RMSE values for the United States, Canada, Europe, China, and India are ~~78, 2.86~~3.10 μg/m^3, ~~4.63~~2.78 μg/m^3, ~~11.62~~4.92 μg/m^3, 9.65 μg/m^3 and 1~~8.73~~7.46 μg/m^3, respectively.~~;~~ and the ~~mean~~ RRMSE values ~~$PM_{2.5}$ concentrations~~ are 3~~1.2~~4.9%, 40.~~9~~4%, ~~33.0~~29.8%, 2~~8.0~~3.1%, and 2~~7.9~~8.8%, respectively. The ~~average~~ MAEs for the United States, Canada, Europe, China, and India are 1.61~~42~~ μg/m^3, 1.3~~6~~5 μg/m^3, 2.54~~45~~ μg/m^3, ~~6.48~~5.47 μg/m^3, and 9.13~~56~~ μg/m^3, respectively.~~;~~ The RMAEs are ~~these values correspond to 15~~17.9%, 19.~~4~~5%, ~~17~~16.~~5~~3%, ~~15~~13.~~6~~1%, and 14.~~2~~4%, respectively.~~;~~ ~~of the mean $PM_{2.5}$ concentration.~~ The ρ values ~~average correlation coefficients~~ for the United States, Canada, Europe, China, and India are 0.87~~8~~, 0.88, 0.~~89~~91, 0.~~92~~94, and 0.92, respectively. The correlation coefficients are higher in China and India, low in the United States and Canada.

The largest~~values of~~ RMSE and MAE are ~~the largest~~ in India, ~~,~~and ~~–~~the smallest are in Canada. ~~The RMSE is the smallest in the United States, and the MAE is the smallest in Canada.~~ The ~~ratios of the~~ RRMSE and RMAE ~~to the mean~~ are larger in the United States, Canada and Europe than ~~in other regions and smaller~~ in China and India ~~than in~~and other regions. ~~Although the $PM_{2.5}$ concentration varies among regions, the MAE-to-mean concentration ratio remains at approximately 16%. This finding demonstrates the stability and reliability of the model.~~

Table 2.~~1~~ The ~~results of the model's performance~~ metrics for all sites and sites in the United States (the US), Canada, Europe, China and India. RRMSE is the percentage of RMSE to mean of $PM_{2.5}$ concentration. RMAE is the percentage of MAE to mean of $PM_{2.5}$ concentration.

Region	*RMSE (μg/m^3)*	*MAE (μg/m^3)*	*ρ*	*Mean (μg/m^3)*	*RRMSE (%)*	*RMAE (%)*
All	6.92	3.77	0.91	26.7	28.7	15.4
the US	3.10	1.61	0.87	9.1	34.9	17.9
Canada	2.78	1.35	0.88	6.9	40.4	19.5
Europe	4.92	2.54	0.91	15.7	29.8	16.3
China	9.65	5.47	0.94	42.1	23.1	13.1
India	17.46	9.13	0.92	63.1	28.8	14.4
Other	6.11	3.32	0.91	23.4	24.8	14.1

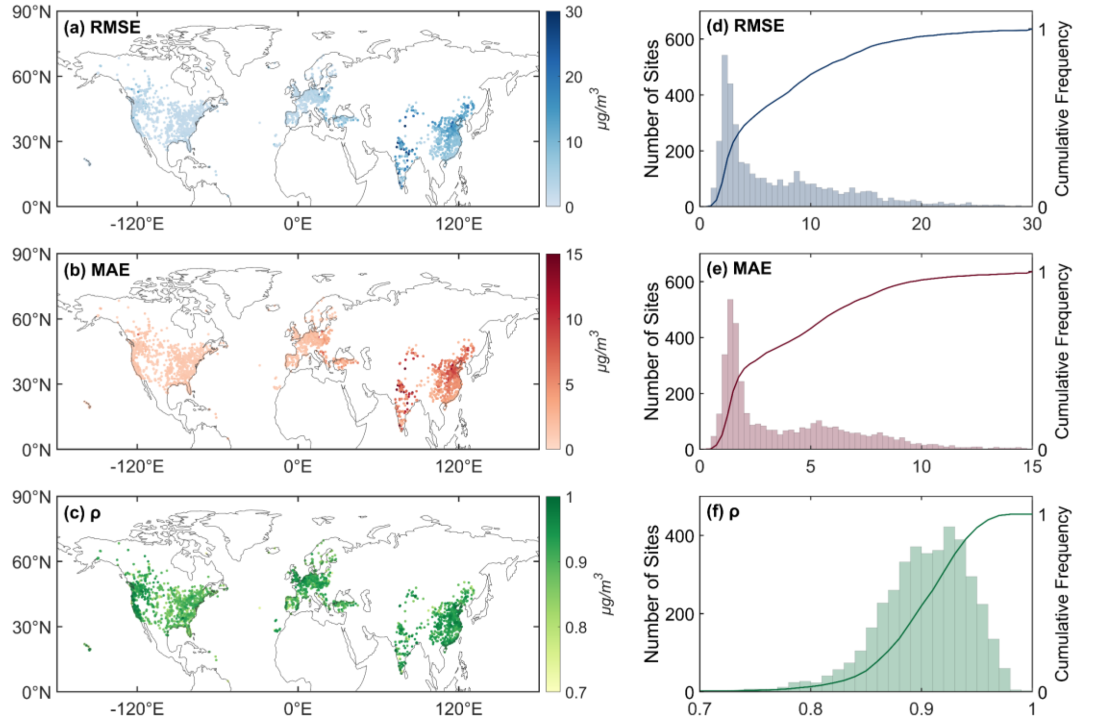

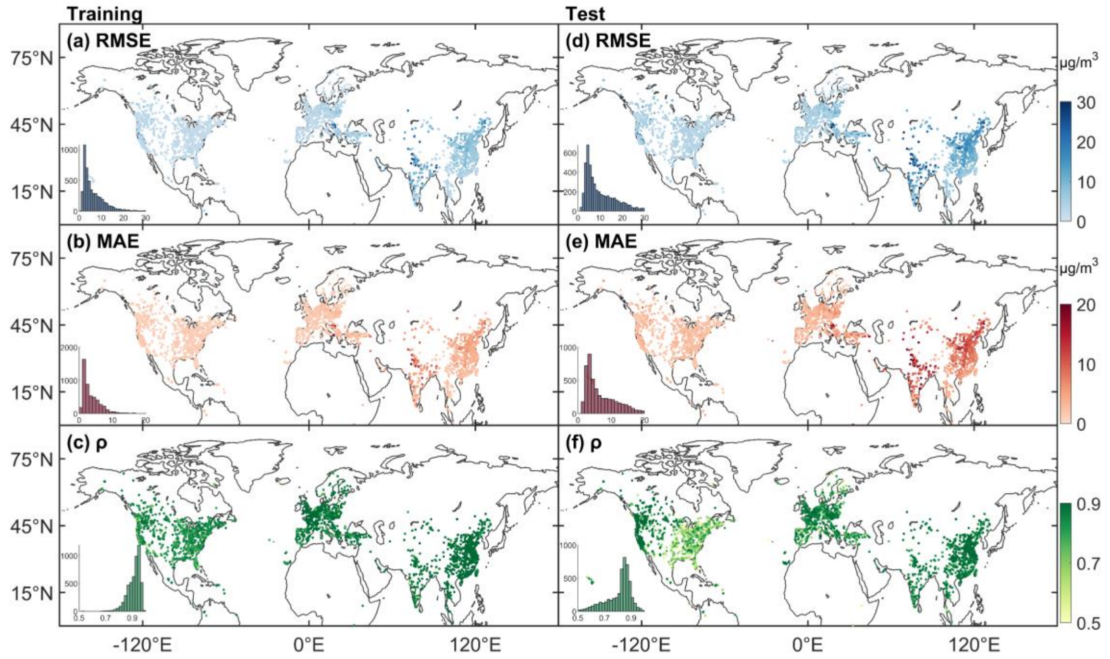

Figure 4. Statistical Metrics ~~Spatial~~ distribution of training (~~a-e~~left) and test (right). ~~of~~The bar is the frequency of sites. RMSE is the root mean square error, MAE is the mean absolute error, and ρ is the correlation coefficient. ~~the root mean squared error (RMSE), mean absolute error (MAE), and correlation coefficient (ρ) between the model's estimated values and response values. Number of sites (bar) and cumulative frequency (curve) (d-e) of the RMSE, MAE, and ρ.~~

~~3.2.3 Dependence on the Distance between the $PM_{2.5}$ Site and the Visibility Station~~

~~Although the previous analysis elucidates the stability and predictive capability of the model, it is necessary to understand the potential impact of the distance between $PM_{2.5}$ monitoring sites and visibility stations on the model. Most $PM_{2.5}$ monitoring sites are in urban areas, resulting in a relatively concentrated spatial distribution. Visibility stations are strategically placed to capture the characteristics of meteorological factors and have relatively uniform spatial distributions. Consequently, visibility stations and $PM_{2.5}$ monitoring sites are often not collocated, resulting in a certain spatial distance between them. Therefore, we consider the impact of the distance between sites on the model's performance.~~

~~Figure 5 shows the relationship between the model performance (ρ and RMSE) and the distance between the visibility stations and the $PM_{2.5}$ monitoring sites. The average distance between all sites is 0.964°, and the correlation coefficient between the model's RMSE and distance is 0.44, which is a moderate correlation. The average ρ of 3786 sites (within a distance of 3°) is 0.90, and the average RMSE is 7.13 μg/m^3. The RMSE values of 471 sites are greater than twice the average RMSE of all sites; however, their average ρ (0.91) is greater than the average of all sites. This finding indicates that the model's performance decreases as the distance increases.~~

~~For the United States, the average distance is 0.29°. The distance between the 919 (82.8%) sites was less than 0.5°, with ρ and RMSE values of 0.88 and 2.7 μg/m^3, respectively. The ρ and RMSE of the 191 sites (more than 0.5°) are 0.88 and 3.1 μg/m^3, respectively. The performance of the model is not significantly related to distance.~~

~~For Canada, 212 (69.7%) sites have distances of less than 0.5°, with ρ and RMSE values of 0.89 and 2.6 μg/m^3, respectively. The ρ and RMSE for 92 sites (more than 0.5°) are 0.87 and 3.3 μg/m^3, respectively. The correlation coefficient between the RMSE and the distance is 0.33, and the correlation coefficient between the ρ and the distance is -0.17. The performance of the model decreases as the distance increases.~~

~~For Europe, 541 (64.8%) sites have distances of less than 0.5°, with ρ and RMSE values of 0.90 and 4.0 μg/m^3, respectively. The ρ and RMSE of the 293 sites (more than 0.5°) are 0.88 and 5.7 μg/m^3, respectively. The correlation coefficient between the RMSE and the distance is 0.19.~~

~~For China, 303 (19.5%) sites have a distance of less than 0.5°, with ρ and RMSE values of 0.95 and 9.5 μg/m^3, respectively. The ρ and RMSE for 1254 sites (more than 0.5°) are 0.91 and 12.1 μg/m^3, respectively. The correlation coefficient between the RMSE and the distance is 0.23. The correlation coefficient between ρ and distance is -0.71. As the distance increases, the correlation coefficient significantly decreases.~~

~~For India, the ρ and RMSE of 117 (56.8%) sites with a distance of less than 0.5° are 0.94 and 18.7 μg/m^3, respectively. The ρ and RMSE of 89 sites (more than 0.5°) are 0.89 and 18.8 μg/m^3, respectively. The correlation coefficient between ρ and distance is -0.36.~~

~~The above results indicate no significant correlation between model performance and distance in the United States and Europe, as these regions have adequate visibility stations. However, in China, India, and Canada, the performance of models is influenced by distance. Particularly in China, due to the limited number of visibility stations, although the correlation coefficient decreases with distance, there is no significant change in the RMSE. The correlation coefficient for visibility remains near 0.4. Even when the distance between two visibility stations reaches 1000 km, the~~

~~maximum correlation coefficient for visibility remains near 0.4 (Fei et al., 2023). To acquire more $PM_{2.5}$ sample data, we do not disregard these distant sites since the models still shows a good performance for these sites. Nevertheless, more sufficient visibility stations in the same locations can enhance the model's performance.~~

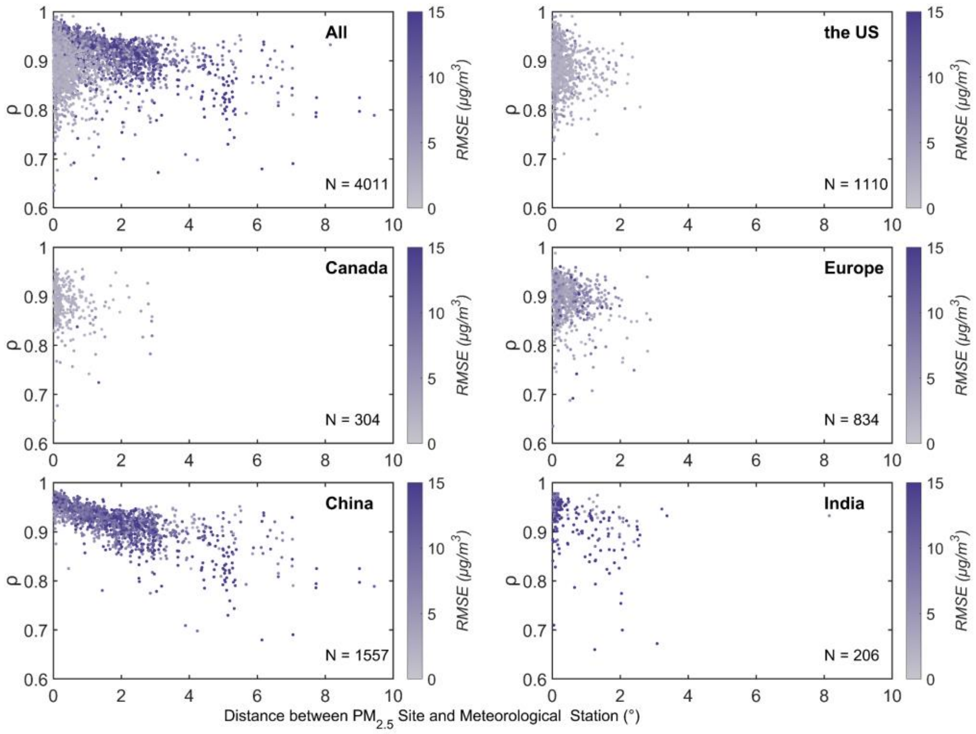

~~**Figure 5** Scatter plots of the distance between the $PM_{2.5}$ site and visibility station and the model's correlation coefficient (ρ) for all sites and sites in the United States, Canada, Europe, China, and India. The color bar represents the root mean square error (RMSE) of the model. N is the number of sites.~~

3.3 Evaluation of Model's Predictive Ability

~~3.3.1 For All Data~~

A total of ~~1,149,152~~1911183 pairs of test data is employed to evaluate the model's predictive ability. Figure 5~~6~~ ~~shows~~ is the density scatter plot between the predicted $PM_{2.5}$ concentration and the test $PM_{2.5}$ concentration. ~~The results indicate that t~~The linear regression ~~coefficient~~ slope (95% CI) is 0.864~~2~~ [0.863, 0.865], ~~± 0.001 within a 95% confidence interval,~~ R^2 is 0.79~~80~~, RMSE is 1~~3.5~~4.8 μg/m^3, and MAE is ~~6.9~~7.6 μg/m^3. Previous studies have shown that the R^2 range of the model's predictive results at the daily scale is 0.31~~42~~ - 0.84~~9~~, and the RMSE range is ~~9.59~~13.8-~~32.09~~29.0 μg/m^3 (Gui et al., 2020; Zhong et al., 2021). The test results exhibit excellent predictive capability.

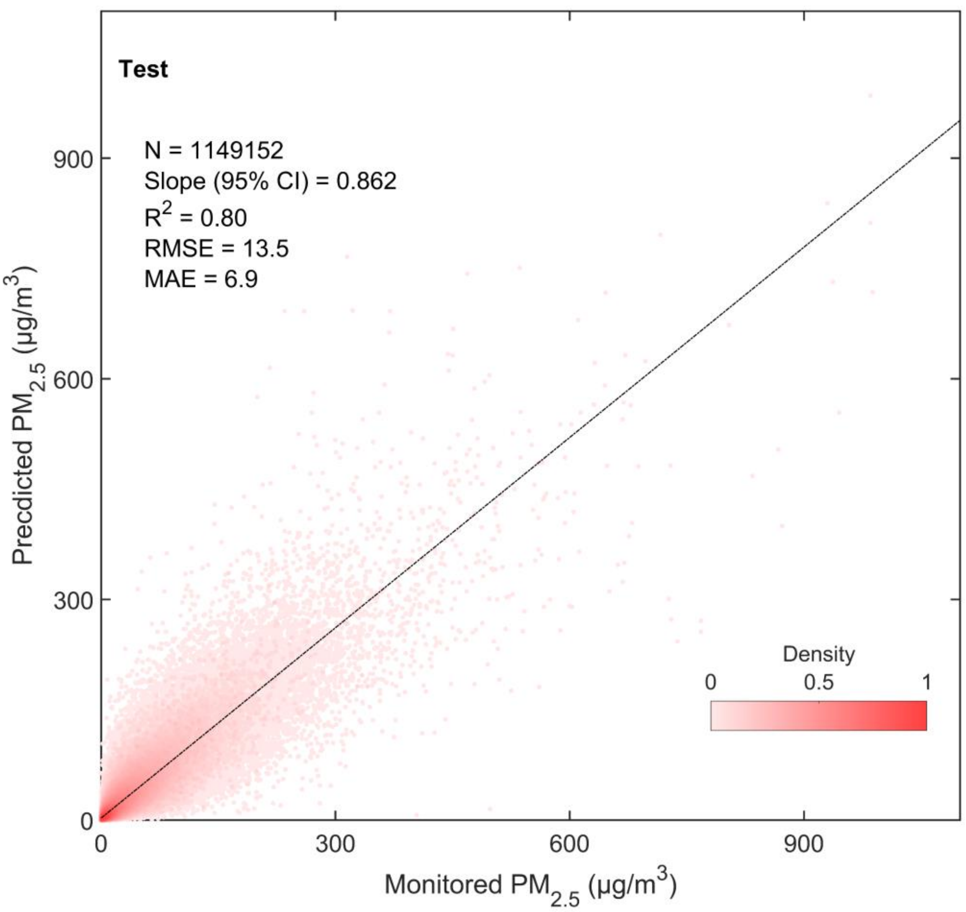
Test
N = 1149152
Slope (95% CI) = 0.862
R2 = 0.80
RMSE = 13.5
MAE = 6.9
Density
0
0.5
1
900
600
300
0
0
300
600
900
Predicted PM2.5 (μg/m3)
Monitored PM2.5 (μg/m3)

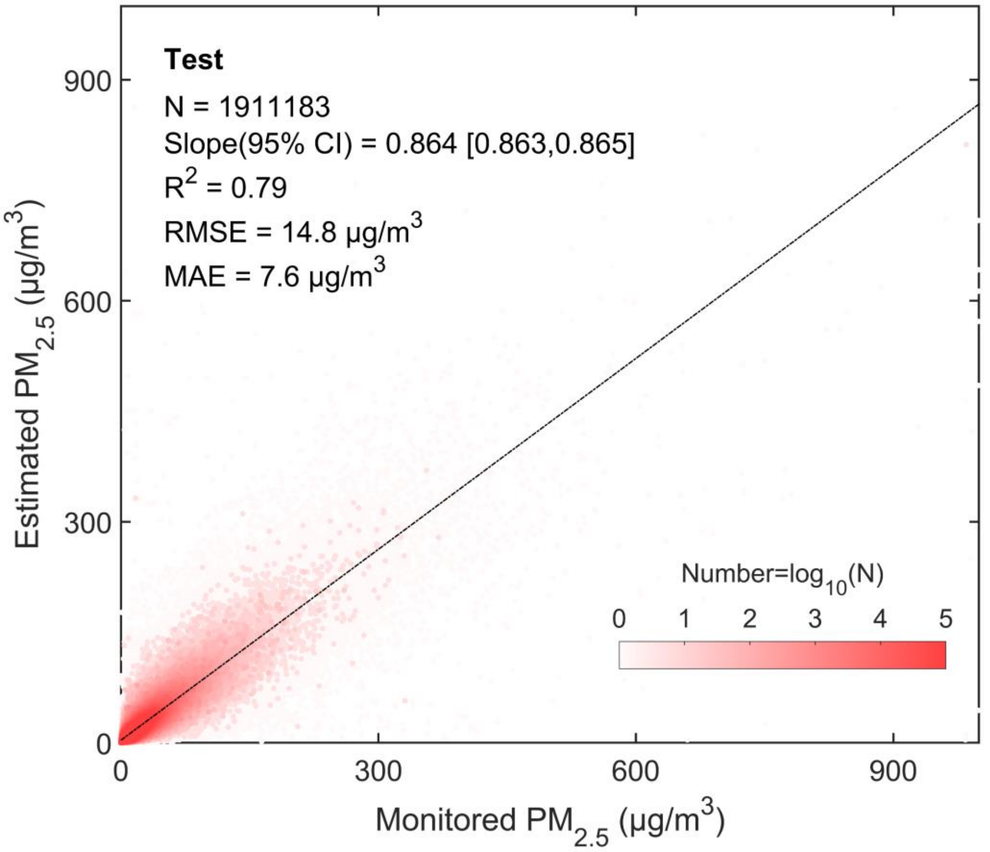

Figure 5.~~6~~ Density scatter plot (a) between the predicted $PM_{2.5}$ concentration and monitored $PM_{2.5}$ concentration of the test results~~ at the daily scale~~. The dashed black line is the linear regression line. N is the length of the data pairs, and Slope is the linear regression coefficient within a 95% confidence interval (CI). R^2 is the coefficient of determination, RMSE is the root mean square error, and MAE is the mean absolute error.

~~3.3.2 For the Site and Region Scales~~

We analyze the test results for Canada, the United States, Europe, China, and India to assess the predictive ability of the model in different regions. Figure ~~7~~ 4 (d - f) shows the spatial distributions of the test RMSE, MAE, and ρ and their frequency~~ and cumulative frequency distributions~~. Table 3~~2~~ lists the test results of the metrics.

For all sites, the average RMSE is ~~12.60~~11.50 µg/m^3. The RRMSE~~-to-mean ratio~~ is 4~~8.6~~6.0%. The average MAE is ~~8.52~~7.72 µg/m^3. The RMAE~~-to-mean ratio~~ is 30~~2~~.7~~9~~%. The ~~average~~ ρ is 0.81~~77~~.

For the United States, the RMSE, MAE, and ρ are ~~4.90~~5.06 µg/m^3, ~~3.15~~3.25 µg/m^3, and 0.72~~1~~, respectively. For Canada, the RMSE, MAE, and ρ are 4.73~~89~~ µg/m^3, ~~3.01~~2.88 µg/m^3, and 0.77~~4~~, respectively. The results in the United States and Canada are better in the west than in the east. The RMSE, MAE, and ρ for Europe are 7.~~54~~ 79 µg/m^3, ~~4.91~~5.10 µg/m^3, and 0.80~~77~~, respectively. For China, the RMSE, MAE, and ρ are ~~20.16~~16.83 µg/m^3, 1~~3.81~~1.50 µg/m^3, and 0.85~~1~~, respectively. For India, the RMSE, MAE, and ρ are 2~~8.84~~7.05 µg/m^3, 1~~9.57~~7.89 µg/m^3, and 0.85~~3~~, respectively. The results show that in developing regions (China and India), ρ is better than that in developed regions (the United States, Canada, and Europe), which means that the predictive ability of the model is better for severely polluted regions.

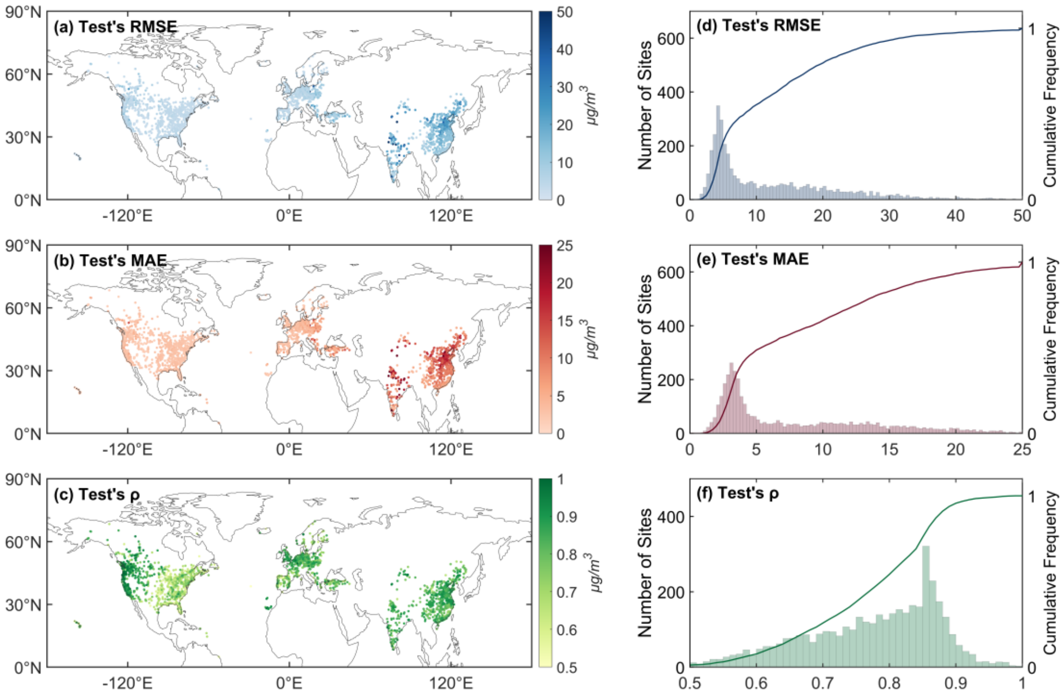

~~**Figure 7** Spatial distribution (a-c) of the root mean squared error (RMSE), mean absolute error (MAE), and correlation coefficient (ρ) between the model's predicted values and test values. Number of sites (bar) and cumulative frequency (curve) (d-e) of the RMSE, MAE, and ρ.~~

Table 3.~~2~~ The test results of the model's performance metrics for all sites and sites in the United States, Canada, Europe, China and India. RRMSE is the percentage of RMSE to mean of $PM_{2.5}$ concentration. RMAE is the percentage of MAE to mean of $PM_{2.5}$ concentration.

Region	*RMSE ($\mu g/m^3$)*	*MAE ($\mu g/m^3$)*	*ρ*	*Mean ($\mu g/m^3$)*	*RRMSE (%)*	*RMAE (%)*
All	11.50	7.72	0.81	27.1	46.0	30.7
the US	5.06	3.25	0.72	9.4	54.3	35.0
Canada	4.73	2.88	0.77	7.2	65.6	40.0
Europe	7.79	5.10	0.80	15.9	47.0	32.0
China	16.83	11.50	0.85	42.6	39.6	27.1
India	27.05	17.89	0.85	63.7	42.9	27.8
Other	8.86	6.16	0.81	23.4	36.7	26.1

~~*Test*~~	~~RMSE ($\mu g/m^3$)~~	~~MAE ($\mu g/m^3$)~~	~~ρ (Pearson's correlation)~~	~~Mean ($\mu g/m^3$)~~	~~RMSE/Mean (%)~~	~~MAE/Mean (%)~~
~~*All*~~	~~12.60~~	~~8.52~~	~~0.77~~	~~25.9~~	~~48.6~~	~~32.9~~
~~*America*~~	~~4.90~~	~~3.15~~	~~0.71~~	~~9.1~~	~~53.8~~	~~34.6~~
~~*Canada*~~	~~4.89~~	~~3.01~~	~~0.74~~	~~7.2~~	~~67.9~~	~~41.1~~
~~*Europe*~~	~~7.54~~	~~4.91~~	~~0.77~~	~~14.4~~	~~52.3~~	~~34.1~~

~~*China*~~	~~20.16~~	~~13.81~~	~~0.81~~	~~42.2~~	~~47.7~~	~~32.7~~
~~*India*~~	~~28.94~~	~~19.62~~	~~0.83~~	~~67.6~~	~~42.8~~	~~29.0~~

3.4 Uncertainties and Limitations

3.4.1 Uncertainty in the Pollution Level

Figure ~~8~~ 6 shows the uncertainty in the predicted $PM_{2.5}$ concentration with respect to the pollution level of the monitored $PM_{2.5}$ concentration. For all sites, the uncertainty in the bias increases as the pollution level increases. The mean ~~bias~~ and ~~the~~ median of the bias shift from positive to negative with increasing pollution levels. 83.6% of $PM_{2.5}$ concentration data is less than 45 μg/m^3, and ~~The~~ the mean bias (< 0.8 μg/m^3)~~–~~ is positive.~~of 88.4% of the data is less than 2 μg/m^3.~~ 36.8% is less than 10 μg/m^3, and the median (< 0.4 μg/m^3) of the bias is positive.~~A mean bias of 86.9% (<40 μg/m^3) is positive, and a median bias of 38.9% (<8 μg/m^3) is positive.~~ 16.4% of $PM_{2.5}$ concentration is great than 45 μg/m^3, and the mean bias is negative. 63.2% of $PM_{2.5}$ concentration is great than 10 μg/m^3, and the median is negative. ~~This result~~It indicates that the model overestimates at low pollution level ~~concentrations~~and underestimates at high pollution level.

The bias for each region also increases with pollution level. For ~~sites in~~ the United States, the mean bias of ~~92.1~~69.4% is positive and less than 0.8~~2~~ μg/m^3, and the $PM_{2.5}$ concentration is less than 10 μg/m^3. When the $PM_{2.5}$ concentration is greater than 10 μg/m^3, the mean bias is negative. ~~. A total of 69.1% (<10 μg/m^3) are positive.~~ For ~~sites in~~ Canada, the mean bias of ~~82.5~~74.1% is positive and less than ~~2~~ 0.7 μg/m^3. When the $PM_{2.5}$ concentration is greater than 8 μg/m^3, the mean bias is negative. ~~A total of 73.3% are positive (<8 μg/m^3). Among the data (<8 μg/m^3), 57.9% of the median is positive.~~ For ~~sites in~~ Europe, the mean bias of 6~~4.8~~7.1% is positive and ~~is~~ less than ~~2~~ 0.9 μg/m^3~~, and 69.8% is positive~~. When the $PM_{2.5}$ concentration is greater than 15 μg/m^3, the mean bias is negative.~~A total of 49.0% of the median is positive.~~ For ~~sites in~~ China, ~~81.8~~67.7% of the bias is positive and less than 2.7~~5~~ μg/m^3~~,~~.~~and 68.9% (<45 μg/m^3) is positive.~~ When the $PM_{2.5}$ concentration is greater than 45 μg/m^3, the mean bias is negative.~~A total of 48.0% (<30 μg/m^3) of the median is positive.~~ For ~~sites in~~ India, 80.~~5~~1% of the bias is positive and less than ~~8~~4.2 μg/m^3, and when the $PM_{2.5}$ concentration is greater than 100 μg/m^3, the mean bias is negative.~~73.5% (<80 μg/m^3) is positive.~~ When the $PM_{2.5}$ concentration is greater than 60 μg/m^3, the bias median is negative, with a percentage of 40.3%. ~~A total of 52.6% (<60 μg/m^3) of the median values are positive.~~The uncertainty in each region is similar, and the uncertainty increases as the pollution level increases.

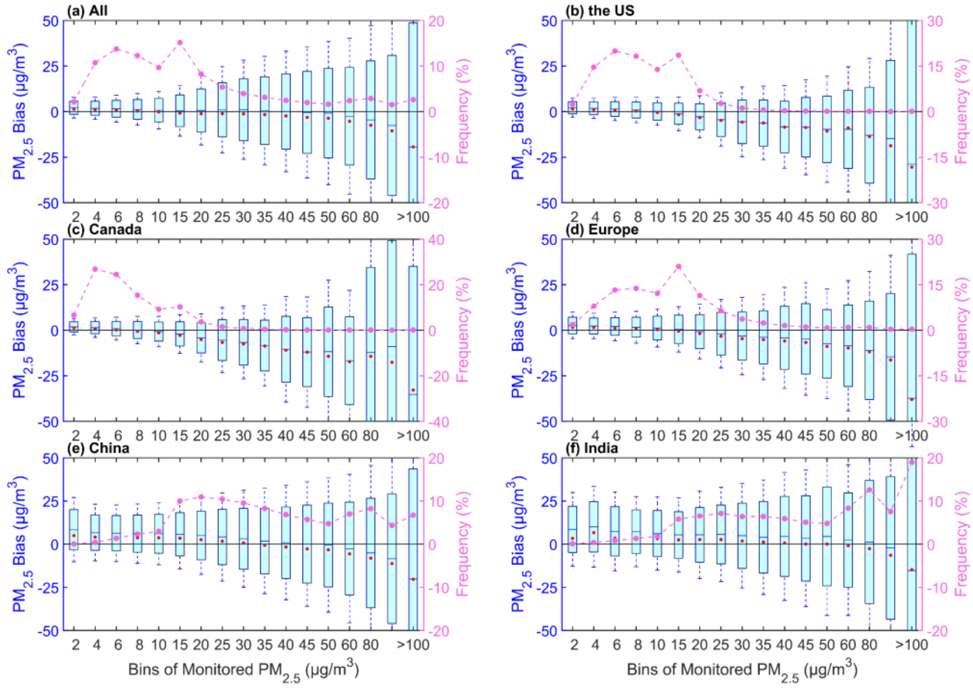

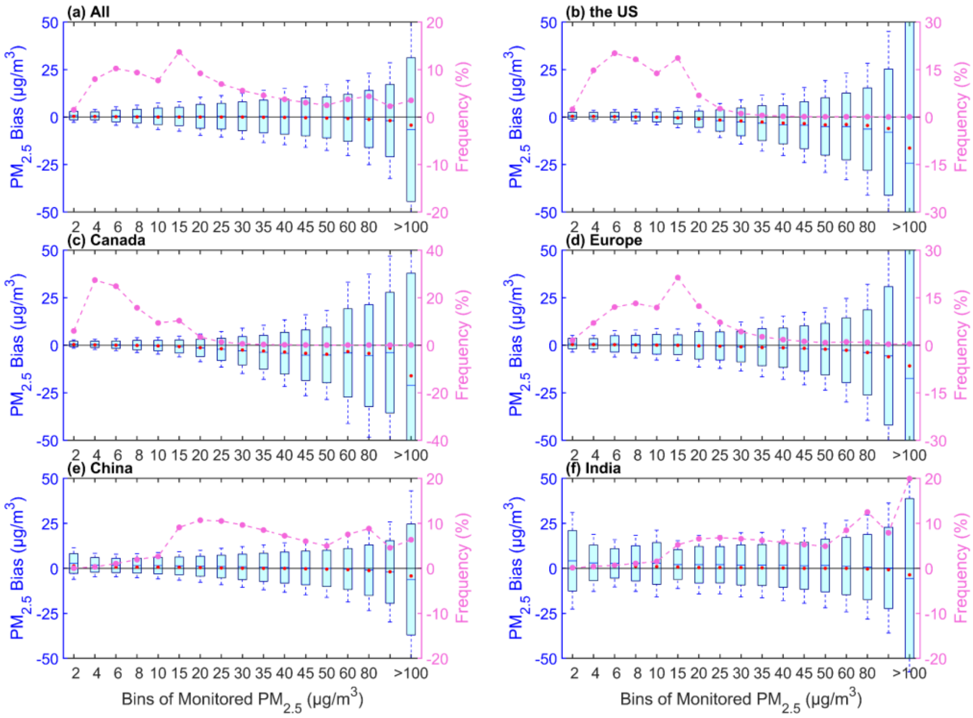

Figure 6.~~8~~ Boxplots of the pollution level and bias (predicted $PM_{2.5}$ concentration - monitored $PM_{2.5}$ concentration) for all sites (a), sites in the United States (b), Canada (c), Europe (d), China (e), and India (f). The box's upper and lower limits represent ± 1 standard deviation, the whiskers represent 2 times the standard deviation, the red circle represents the median, and the short line represents the mean bias. The frequency (%) on the right y-axis represents the percentage of data with different pollution levels (dashed line).

3.4.2 Uncertainty in the Station Elevation

With the spatial variability in $PM_{2.5}$ concentration, we analyze the mean bias at different visibility station elevations. Figure ~~9~~ 7 shows the relationships between the elevations of the visibility stations and the bias. The bias exhibits variations across different elevations for all ~~sites~~stations. The mean bias of all sites ranges from -0.04 to 0.02 μg/m^3. A total of ~~88.5~~90.1% of the ~~data~~stations ~~have~~ has positive ~~mean~~ biases. The median of the bias is almost positive, with a positive bias of 99.5% stations, except for the elevation at 4 km. The~~A~~ elevations ~~total~~ of ~~89~~86.5% of the ~~data~~ stations are ~~at an elevation of~~less than 1 km, with a positive median of the bias. ~~The mean bias ranges from -0.1 to 0.5 μg/m^3.~~ High uncertainties in bias occur at elevations ~~below~~ of 0.05~~2~~ km, 0.~~4-0.5~~2 km, and ~~1-3~~0.3 km. ~~A total of 88.5% of the data have positive mean biases.~~ Negative biases are observed at elevations of ~~0.6-0.8~~0.4 km, ~~3~~ 0.9-1 km, and ~~5~~4 km. ~~A total of 57.7% of the data have a positive median.~~ This finding indicates a nonsignificant overestimation of the predicted $PM_{2.5}$ concentration due to the various elevations.

The bias patterns vary across regions. For the United States, a total of 88.8% of the stations have negative biases. The median of the bias is negative with a percentage of 63.4%. High uncertainties in bias occur at elevations of 0.05 km, 2 km, and 0.3 km~~92.8% of the data correspond to elevations below 1 km. The mean bias ranges from -0.1 to 0.5 μg/m^3. A total of 88.8% of the mean biases are positive, and the median of 99% is positive~~. For Canada, 52.3% of the stations have positive biases. The median of the bias is negative with a percentage of 33.8%. High uncertainties in bias occur at elevations of 0.05 km and 1 km~~90.1% of the data correspond to elevations below 1 km. The mean bias ranges from -0.1 to 0.2. A total of 46.5% of the mean bias is positive, and the median is positive except at elevations of 0.7 km and 4 km. A higher uncertainty in the bias occurs at elevations ranging from 0.5-0.8 km~~. For Europe, 58.9% of the stations have positive biases. The median of the bias is negative with a percentage of 40.2%. High uncertainties in bias occur at elevations of 0.05 km and 0.9 km~~92.9% of the data correspond to elevations below 1 km. The bias ranges from -0.2 to 0.2 μg/m^3. A total of 62.7% of the mean bias is negative, and the median is positive. High standard deviations are observed at elevations of 0.2 km, 0.05 km, and 0.5-0.6 km. A significant bias occurs at 0.6 km~~. For China, 76.7% of the stations have negative biases. The median of the bias is negative with a percentage of 54.1%. High uncertainties in bias occur at elevations of 0.05 km, 0.5 km and 3 km.~~81.9% of the data correspond to elevations below 0.5 km. The median is positive, and the mean bias is positive except at 0.1 km. The lowest standard deviation occurs at an elevation of 0.3 km.~~ For India, 68.1% of the stations have positive biases. The median of the bias is negative with a percentage of 63.8%. The elevation of most stations with a high uncertainty is at 0.05 km. High uncertainties in bias occur at elevations of 0.1 km and 3 km.~~the mean bias ranges from -0.3 to 0.9 μg/m^3. The highest bias occurs at an elevation of 0.3 km. There is a negative mean bias in the range of 0.1-0.4 km. The medians are positive except at an elevation of 0.4 km.~~ More stations with negative bias are in the United States and China. More stations with positive bias are in Canada, Europe and India.

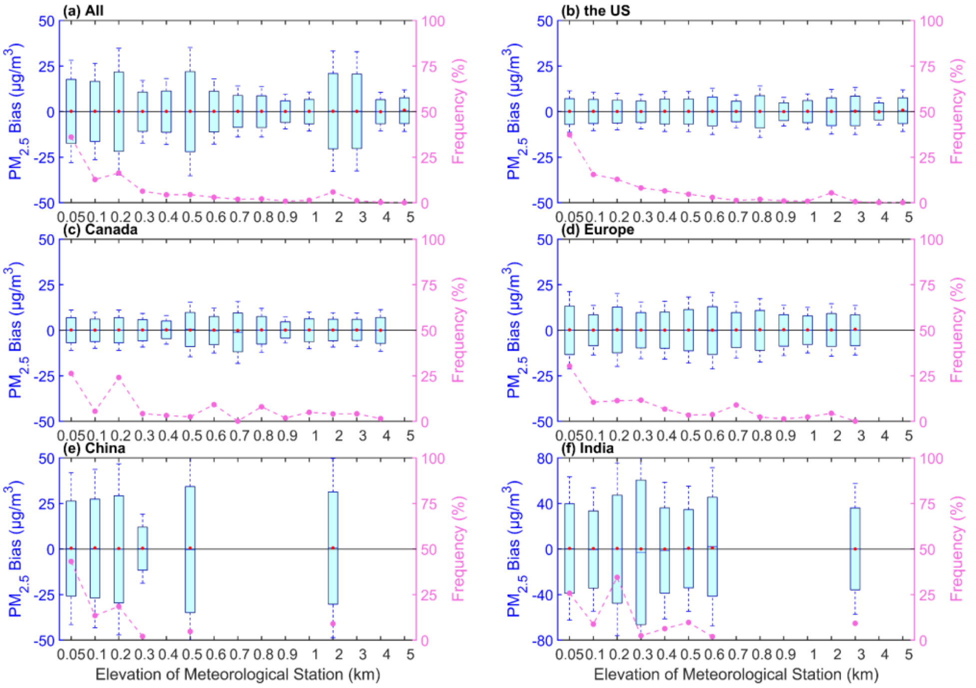

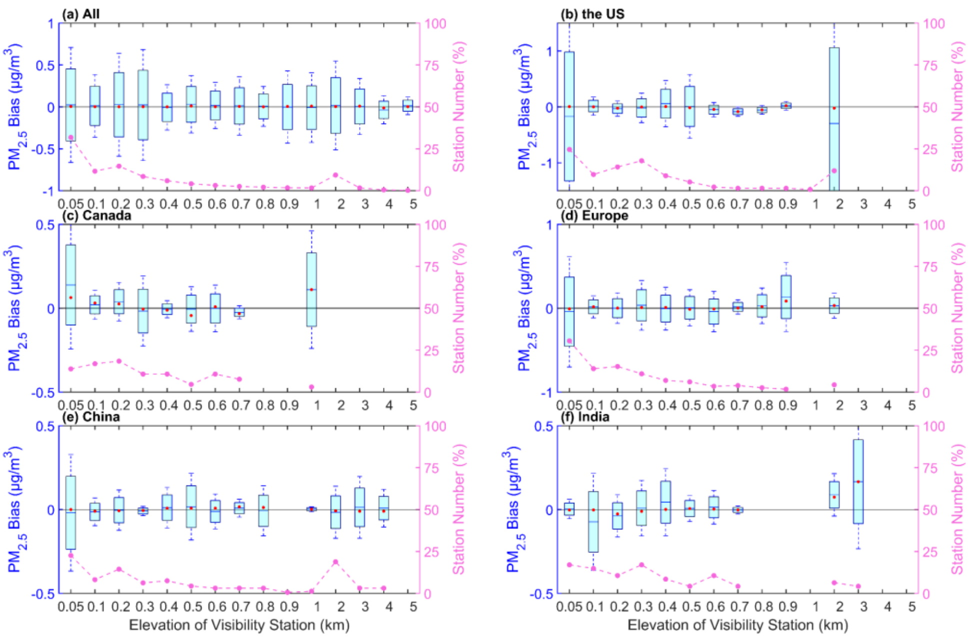

Figure 7~~.9~~ Boxplots of the bias (predicted $PM_{2.5}$ concentration - monitored $PM_{2.5}$ concentration) and the elevation of the visibility station ~~and bias (predicted $PM_{2.5}$ – monitored $PM_{2.5}$)~~ for all sites (a), sites in the United States (b), Canada (c), Europe (d), China (e), and India (f). The box's upper and lower limits represent ± 1 standard deviation, the whiskers represent 2 times the standard deviation, the red circle represents the median, and the short line represents the mean bias. The station number ~~frequency~~ (%) on the right y-axis represents the percentage of ~~data~~ station number at different elevations ~~pollution levels~~ (dashed line).

3.4.3 Uncertainty in the Station Distance

As the visibility stations and $PM_{2.5}$ sites are not collocated, we analyze the ~~$PM_{2.5}$~~ mean bias of $PM_{2.5}$ concentration at different distances, as shown in~~.~~ Figure ~~10~~8. ~~shows the distance between the visibility of the station and the $PM_{2.5}$ site and bias.~~ For all sites, 86.1% of the stations have negative biases. The median of the bias is negative with a percentage of 70.8%. More stations have a negative bias caused by the distance. T~~t~~he uncertainty has no signification with the distance. The distances with low uncertainties are at 1 km and 20-40 km. The distances with high uncertainties are at 5 km and 60 km.~~standard deviation gradually increases with distance, indicating an increase in uncertainty with increasing distance. Except at distances of 0.05° and 1°, the mean bias is positive. The median is positive.~~

For the United States, 63.1% of the stations have negative biases. The median of the bias is negative with a percentage of 69.2%. The distance with the lowest uncertainty is at 1 km. The distances with high uncertainties are at 5 km and 60 km. For Canada, 60.0% of the stations have positive biases. The median of the bias is positive with a percentage of 80.0%. The uncertainty shows an increase with the distance increasing. For Europe,72.7% of the stations have negative biases. The median of the bias is positive with a percentage of 67.1%. When the distance is less than 10 km, the uncertainty increases with the distance. The distances with low uncertainties are at 1 km and 30-40 km. The distances with high uncertainties are at 10 km and 75 km. For China, 64.3% of the stations have negative biases. The median of the bias is negative with a percentage of 72.7%. The distance with a low uncertainty is at 30 km. The distance with a high uncertainty is at 60 km. For India, 62.3% of the stations have negative biases. The median of the bias is positive with a percentage of 59.1%. The distance with the lowest uncertainty is at 30 km. The distance with the highest uncertainty is at 20 km.

More visibility stations have negative biases, except for the stations in Canada. For the stations in the United States, Canada and Europe, the lowest uncertainty is at 1 km. For the stations in China and India, the uncertainty has no significant relationship with distance, though the distance has caused a negative bias.~~For each region, the distance of the largest average bias is 3° in the United States, 3° in Canada, 0.8° in Europe, 10° in China, and 0.4° in India. The distances are below 1° in the United States, Canada, Europe, and India, while they are 1-3° in China. This finding is due to the limited number of visibility sites in China. The mean bias exhibits greater uncertainties in China and India.~~

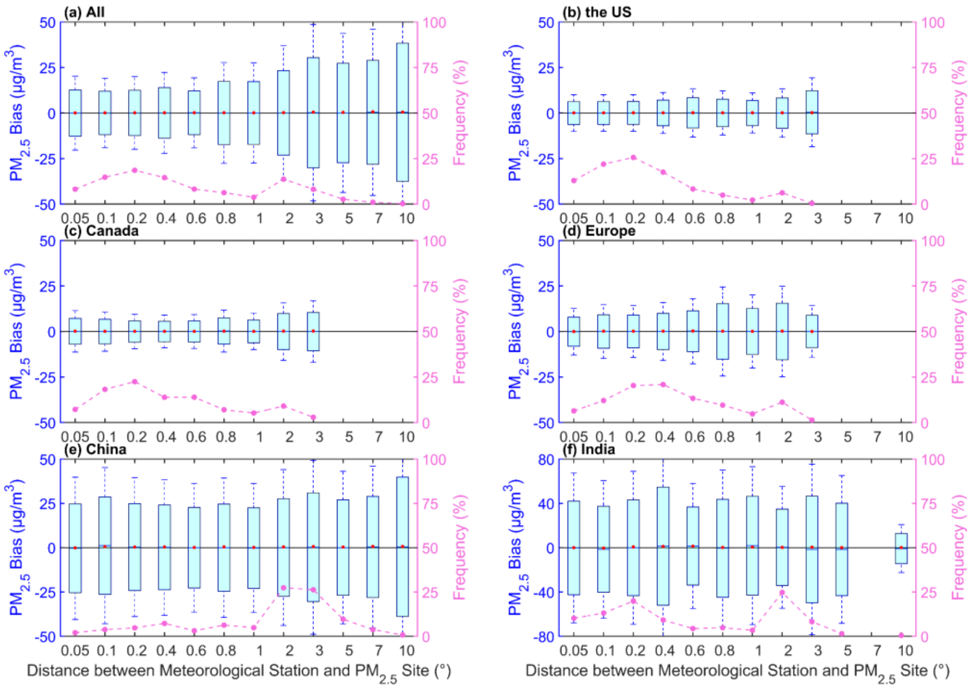

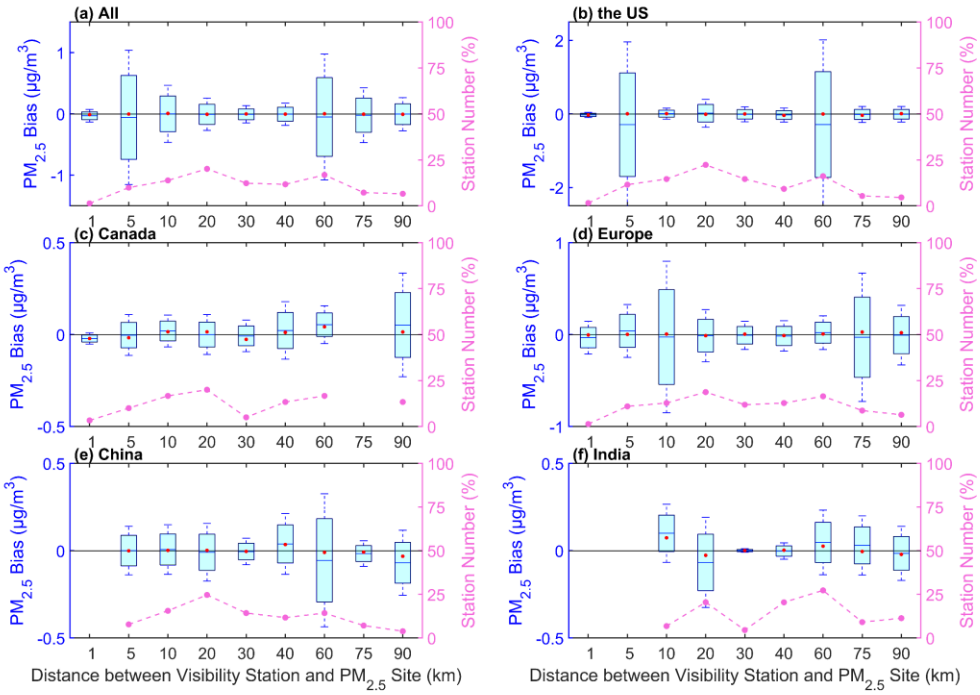

Figure ~~10~~ 8. Boxplots of the mean bias (predicted $PM_{2.5}$ concentration - monitored $PM_{2.5}$ concentration) and the distance between the visibility station and the $PM_{2.5}$ site and ~~bias (predicted $PM_{2.5}$ - monitored $PM_{2.5}$)~~ for all sites (a), sites in the United States (b), Canada (c), Europe (d), China (e), and India (f). The box's upper and lower limits represent ±1 standard deviation, the whiskers represent 2 times the standard deviation, the red circle represents the median, and the short line represents the mean bias. The ~~frequency~~ station number (%) on the right y-axis represents the percentage of ~~data~~ station number under different distances~~pollution levels~~ (dashed line).

3.4.4 Discussion on the Uncertainties and Limitations

There are some uncertainties and limitations in this study. The upper limit of visibility and ~~(~~$PM_{2.5}$ concentration~~) is 10 km (1000 μg/m^3), which~~ can cause some uncertainties in model training~~ing~~. The maximum distance ~~for spatial matching~~ between the visibility stations and $PM_{2.5}$ monitoring sites is 100 km~~0°~~ due to the spatial variability in aerosols, which may increase the uncertainty in the estimated $PM_{2.5}$ concentration. ~~The boundary layer height is closely related to the vertical structure of $PM_{2.5}$, and reanalysis data may introduce uncertainty to the model.~~ Because of the nonuniform vertical distribution of aerosols, the different elevations of the visibility stations and the $PM_{2.5}$ monitoring sites further increase the uncertainty in estimating $PM_{2.5}$ concentration. In addition, the spatial coverage of visibility stations, especially in China and India, is still limited, which may increase the uncertainty in the representativeness of regional $PM_{2.5}$ concentration ~~trends~~ and pollution levels. With the increasing human concern ~~about~~ of air pollution and the implementation of air pollution control measures, the types of major atmospheric pollutants may have changed at regional scale, the composition of particulate matter has also evolved, the scattering and absorption characteristics may have changed, and the relationship between visibility and $PM_{2.5}$ concentration may change. These changes may lead to uncertainties~~y~~ in estimating historical $PM_{2.5}$ concentration~~,~~. It is challenging to validate by ~~especially before 2000 (~~ground observations and satellite-based ~~observations~~ estimation prior to 2000~~are limited)~~. Despite these limitations and challenges, we establish a long-term $PM_{2.5}$ concentration dataset based on visibility from 1959 to 2022, which has been carefully validated and evaluated, providing insights into the long-term spatiotemporal characteristics of concentration $PM_{2.5}$ in the Northern Hemisphere.

4 Comparisons with Other $PM_{2.5}$ Concentration Dataset~~s~~

We compare the daily and monthly estimated $PM_{2.5}$ concentration with the LGHAP $PM_{2.5}$ concentration from 2000 to 2021 to further demonstrate the reliability the estimated $PM_{2.5}$ concentration. When comparing on the regional scale, we split the time range into 2000-2010 and 2011-2021, to further validate the accuracy and consistency of estimated $PM_{2.5}$ concentrations, as in some regions such as India and China, there are almost no continuous $PM_{2.5}$ monitoring data before 2010.

~~of those derived from a satellite AOD and two reanalysis datasets, including (1) ACAG, the monthly satellite-derived $PM_{2.5}$ from 1998 to 2022 (Van Donkelaar et al., 2019; Hammer et al., 2020); (2) MERRA-2, the monthly $PM_{2.5}$ from 1980 to 2022 (Buchard et al., 2016; Buchard et al., 2017; Gelaro et al., 2017); and (3) CAMS, the monthly $PM_{2.5}$ from 2003 to 2022 (Inness et al., 2019). The time ranges for comparing the estimated $PM_{2.5}$ with the ACAG, MERRA-2, and CAMS data are 1998-2022, 1980-2022, and 2003-2022, respectively. The monthly average should meet a minimum requirement of at least ten days per month.~~

4.1 Comparisons on the Daily Scale~~Monthly Frequency and Annual Cycle of $PM_{2.5}$~~

We spatiotemporally match the LGHAP $PM_{2.5}$ concentration with the estimated $PM_{2.5}$ concentration. Figure 9 shows the density scatter plot between the estimated $PM_{2.5}$ concentration and LGHAP $PM_{2.5}$ concentration. There is a total of 96188682 pairs during the period of 2000 and 2021, 46846389 pairs during the period from 2000 to 2010, and 49342302 during the period of 2011 and 2021, with slopes of 0.817, 0.758 and 0.867. The intercepts are 6.928 μg/m^3, 8.933 μg/m^3, and 5.377

μg/m³, respectively. The slope decreases before 2010, which may be related to the upper limit of LGHAP $PM_{2.5}$ concentration with a significantly decreasing quantity of the concentration (> 300 μg/m³).

We further compare the $PM_{2.5}$ concentrations of the annual calendar cycles on the regional scale in Figure 10. The $PM_{2.5}$ concentration of each day is the mean of the $PM_{2.5}$ concentrations at all sites in the region. The correlation coefficients of the $PM_{2.5}$ concentrations are greater than 0.89 from 2011 to 2021 and greater than 0.92 from 2000 to 2010. The correlation is greater in Europe, China, and India than in the United States and Canada. There is no significant difference in the variation of annual calendar cycles between two periods on the regional scale. In the United States, $PM_{2.5}$ concentration between 2000 and 2010 is more similar than the concentration between 2011 and 2021, and the bias decreases. In Canada, the correlation coefficient increases, although the bias increases. In Europe, the correlation coefficient and bias increase. There are similar changes in China and India. The bias increases on days 1 to 60 and 300 to 366, but the correlation remains significant. The difference of $PM_{2.5}$ concentration during the two periods is mainly reflected in the increasing bias in Canada and Europe, which is a non-seasonal bias and the increasing bias in winter in China and India, which is a seasonal bias. Overall, $PM_{2.5}$ concentrations show a good consistency before and after 2010 on the daily scale.

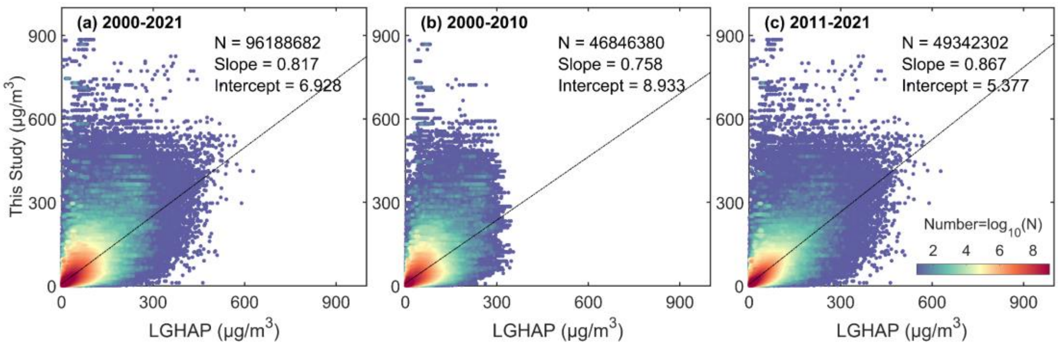

Figure 9. Density scatter plot between the estimated $PM_{2.5}$ concentration (this study) and LGHAP $PM_{2.5}$ concentration on the daily scale from 2000 to 2021 (a), from 2000 to 2010 (b) from 2011 to 2021. The dashed black line is the linear regression line. N is the length of the data pairs, and Slope is the linear regression coefficient. Intercept represents the y-intercept.

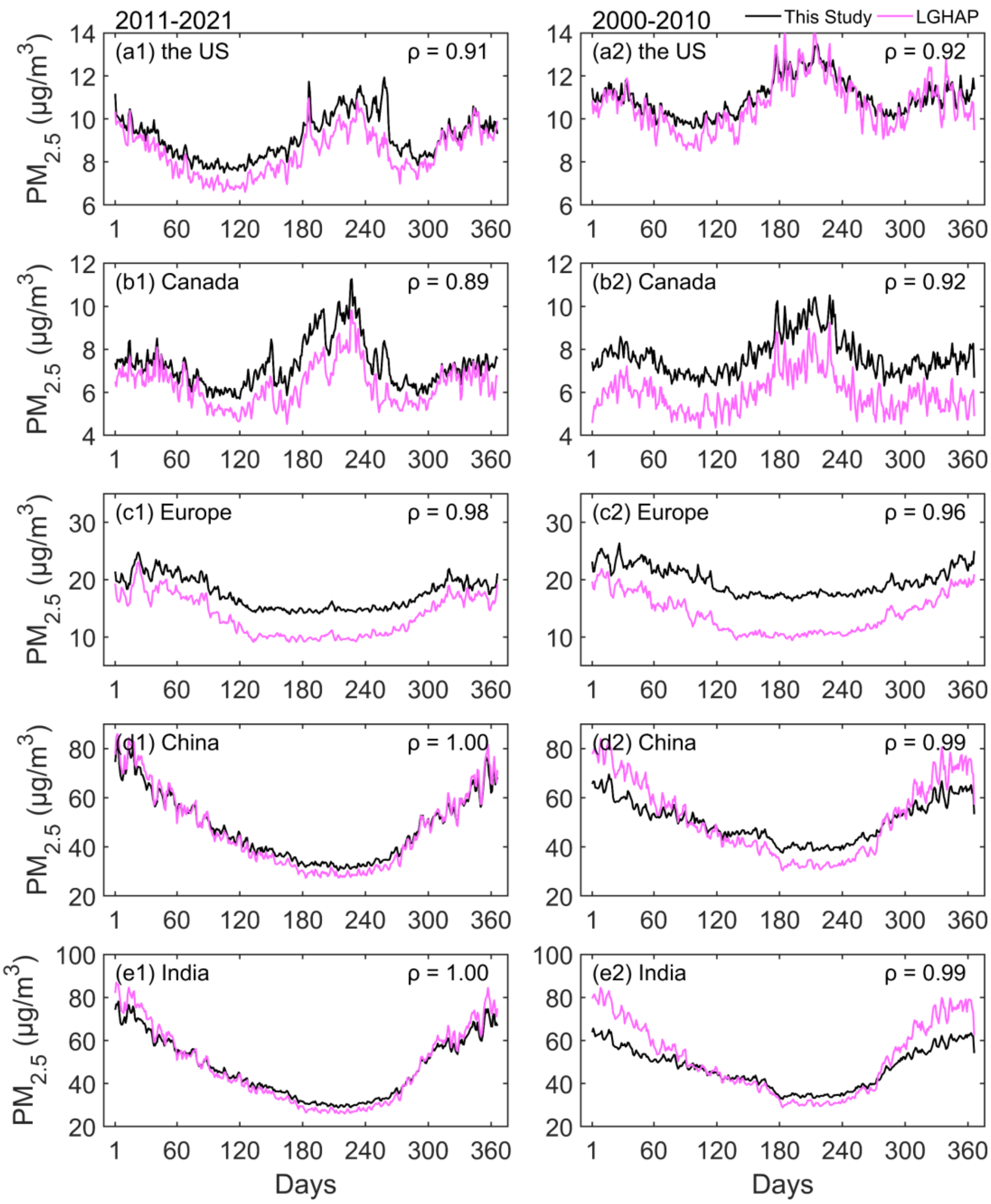

Figure 10. Comparison of annual calendar cycle of $PM_{2.5}$ concentration on the regional scale from 2011 to 2021 (left) and from 2000 to 2010 (right) between the estimated $PM_{2.5}$ concentration (this study) and LGHAP $PM_{2.5}$ concentration on the daily scale. ρ is the correlation coefficient.

~~We compare the frequency of the estimated PM2.5 concentration at different pollution levels, with an interval of 1 μg/m3, with three other datasets. Figure 11 shows the monthly PM2.5 frequencies of the estimated, ACAG, MERRA-2, and CAMS datasets for all sites and regional sites.~~

~~Compared with the ACAG data, they exhibit similar frequency distributions. However, the frequency of estimated PM2.5 concentrations is greater at high pollution levels at all sites. Regionally, the frequency distributions are similar at different pollution levels in the United States and Canada. In Europe, China, and India, the frequency of high concentrations is greater than that of the ACAG.~~

~~Compared with the MERRA-2 data, the frequency distribution of the estimated data is similar to that of the ACAG for all the sites. Regionally, the frequency distributions of the estimates are comparable in the United States and Canada. However, in Europe, China, and India, the differences in the frequency of high pollution levels are greater than those in the ACAG.~~

~~Compared with the CAMS data, the frequency distributions at high pollution levels are similar, but the frequency at high pollution levels is lower. Regionally, Europe differs from other regions, as the frequency of high pollution levels is higher.~~

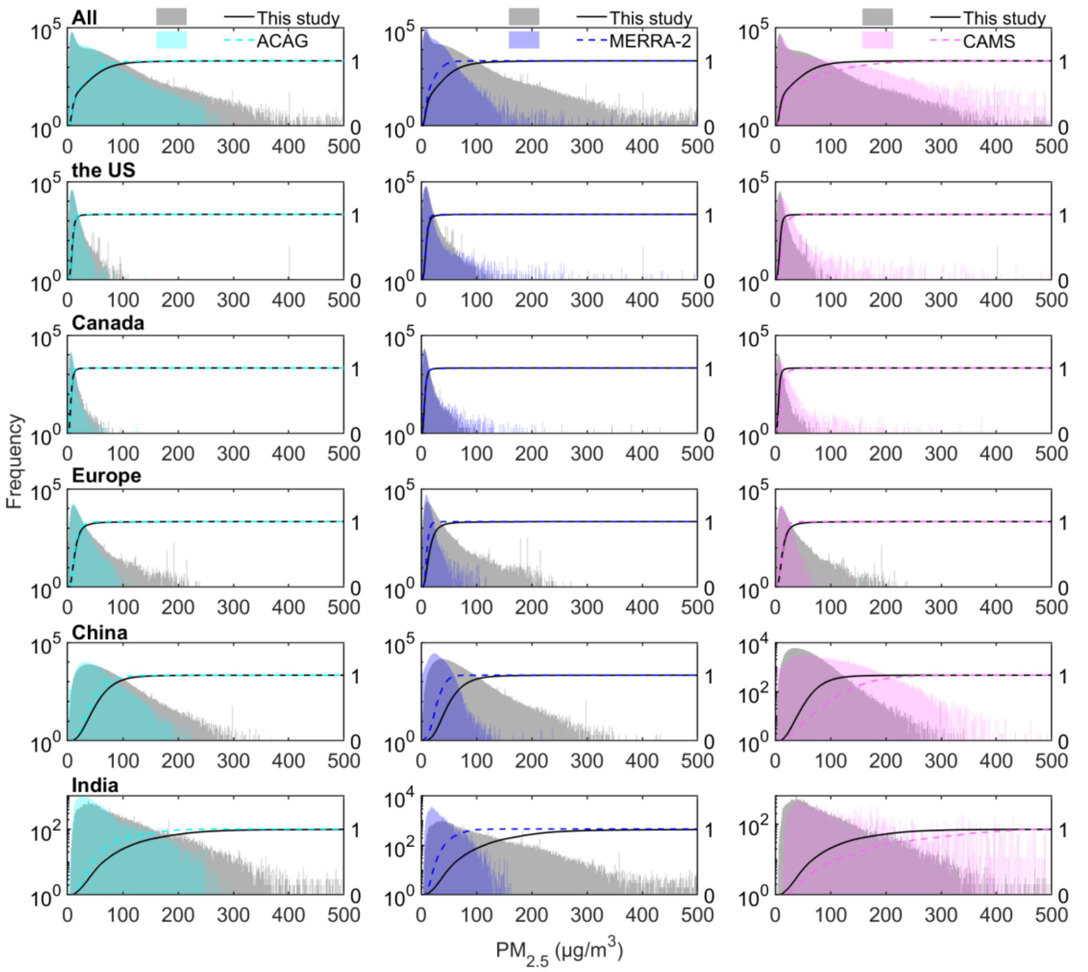

~~**Figure 11** Frequency (left axis) and cumulative frequency (right axis) of monthly $PM_{2.5}$. The time range of the estimated $PM_{2.5}$ corresponds to the time range of the three datasets (ACAG from 1998 to 2022, MERRA-2 from 1980 to 2022, and CAMS from 2003 to 2022). The bins range from 0 to 500 μg/m^3 with an interval of 1 μg/m^3.~~

~~In Figure 12, we compare the multiyear monthly average $PM_{2.5}$ concentration with that of the three datasets. For all sites, the correlation coefficients between the estimated and ACAG, MERRA-2, and CAMS data are 0.99, 0.42, and 0.93, respectively, and the average biases (average relative biases) are 6.6 μg/m^3 (26%), 14.1 μg/m^3 (76%), and -19.1 μg/m^3 (-37%), respectively. The estimated multiyear average monthly $PM_{2.5}$ concentrations are higher for ACAG and MERRA-2 and lower for CAMS. The correlation coefficient is highest for ACAG and lowest for MERRA-2.~~

~~Compared with the ACAG data, the correlation coefficients are 0.97, 0.96, 0.98, 0.99, and 0.99, with~~

~~average biases (average relative biases) of 0.8 μg/m^3 (9%), 0.5 μg/m^3 (7%), 2.2 μg/m^3 (16%), 10.8 μg/m^3 (26%), and 31.4 μg/m^3 (62%) in the United States, Canada, Europe, China, and India, respectively. The annual variations in the two datasets are nearly consistent across all regions. The bias is less than 10% for the United States and Canada, while India exhibits the largest bias.~~

~~Compared with the MERRA-2 data, the correlation coefficients are 0.30, 0.61, -0.25, 0.80, and 0.45, with average biases (average relative biases) of 1.1 μg/m^3 (16%), 0.2 μg/m^3 (5%), 7.5 μg/m^3 (67%), 24.1 μg/m^3 (83%), and 56.1 μg/m^3 (169%) in the United States, Canada, Europe, China, and India, respectively. There are differences in the annual variations between the two datasets, particularly during winter (November to January) and spring (February to March), in all regions. The largest difference occurs in March and September to December in Europe, showing the opposite trend. The highest correlation coefficient is observed in China, which has the second largest bias. The largest bias is in India.~~

~~Compared with the CAMS data, the correlation coefficients are 0.29, 0.22, 0.02, 0.91, and 0.98, with average biases (average relative biases) of -5.4 μg/m^3 (-34%), -5.0 μg/m^3 (-38%), 2.7 μg/m^3 (21%), -38.7 μg/m^3 (-42%), and -52.7 μg/m^3 (-36%) in the United States, Canada, Europe, China, and India, respectively. The annual variations between the CAMS and ACAG data are similar in China and India but have more significant biases. The smallest differences in the United States and Canada occur in January and December. In Europe, the months with more significant biases are January to March and September to December, while biases are smaller in other months.~~

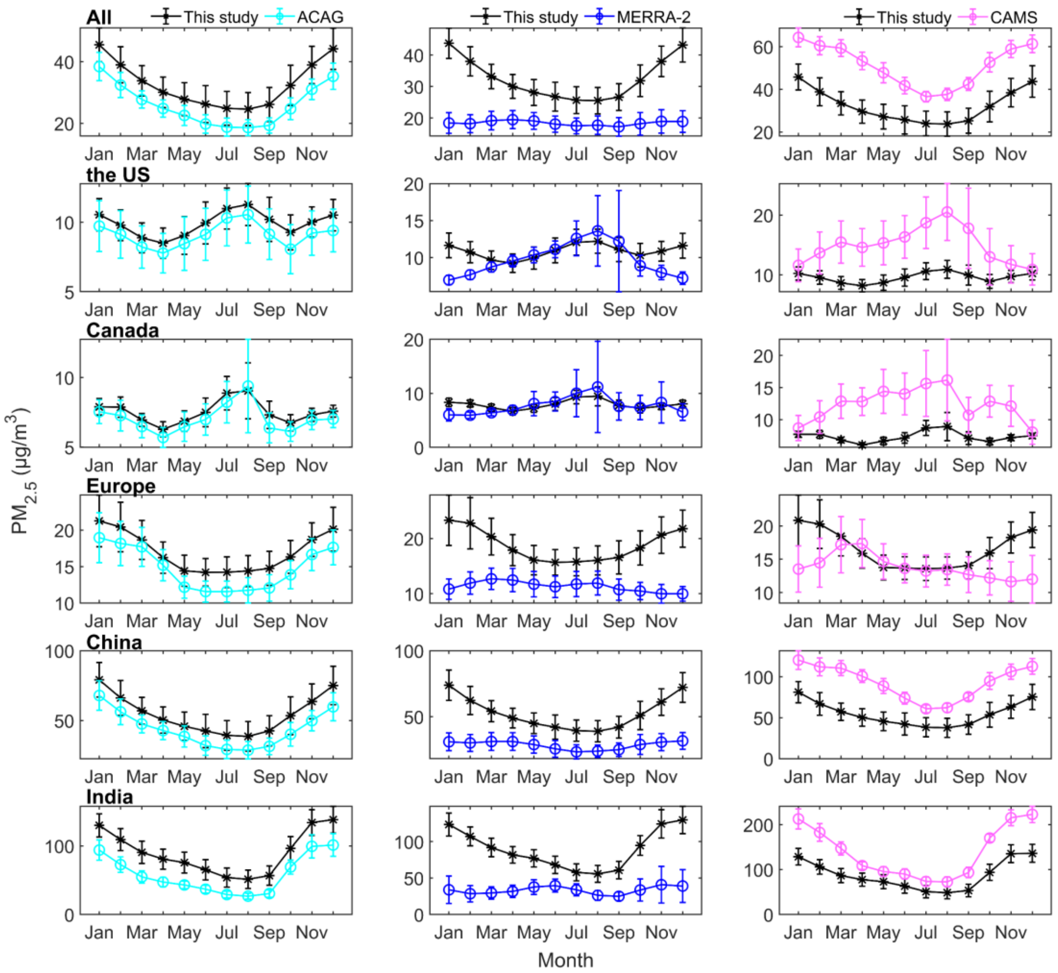

~~**Figure 12** Multiyear monthly average $PM_{2.5}$ of our data and the three datasets. The time range of the estimated $PM_{2.5}$ corresponds to the time range of the three datasets (ACAG data from 1998 to 2022, MERRA-2 data from 1980 to 2022, and CAMS data from 2003 to 2022).~~

4.2 Comparisons on the Monthly Scale~~Time Series at the Annual Scale~~

Figure 11 shows the density scatter plot between the estimated $PM_{2.5}$ concentration and LGHAP $PM_{2.5}$ concentration on the monthly scale. The monthly $PM_{2.5}$ concentration is calculated by the matched daily concentrations. There is a total of 3296739 pairs during the period from 2000 to 2021, 1582161 pairs during the period from 2000 to 2010, and 1714578 during the period from 2011 to 2021, with slopes of 0.857, 0.821 and 0.879. The intercepts are 6.774 μg/m^3, 8.716 μg/m^3, and 5.272 μg/m^3, respectively. The slope of monthly concentration significantly improves before 2010, and slightly increases after 2010 compared to the daily scale.

We also compare the $PM_{2.5}$ concentrations of the annual cycles on the regional scale in Figure 12. The $PM_{2.5}$ concentration of each month is the mean of the $PM_{2.5}$ concentrations at all sites in the region. The correlation coefficients of the $PM_{2.5}$ concentrations are greater than 0.92 from 2011 to 2021 and greater than 0.87 from 2000 to 2010. In the United States, the $PM_{2.5}$ concentrations before 2010 are closer compared to those after 2010, except in April and August, and the biases in other months has significantly decreased. In Europe and Canada, the biases have increased. In China, the result is similar with the result on the daily scale. In India, the performance of the two is almost consistent, with a correlation coefficient of 0.99 and 0.96. The two datasets have a very high similarity in annual cycles, indicating that the estimated $PM_{2.5}$ concentration in this study is accurate and consistent before and after 2010.

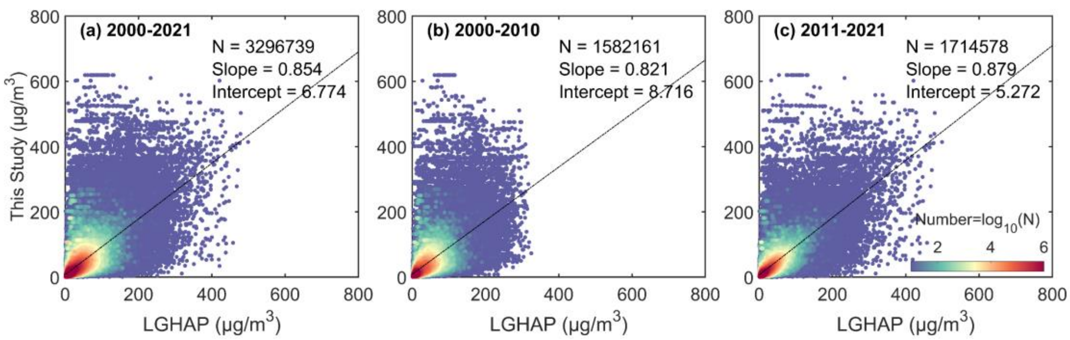

Figure 11. Density scatter plot between the estimated $PM_{2.5}$ concentration (this study) and LGHAP $PM_{2.5}$ concentration on the monthly scale from 2000 to 2021 (a), from 2000 to 2010 (b) from 2011 to 2021. The dashed black line is the linear regression line. N is the length of the data pairs, and Slope is the linear regression coefficient. Intercept represents the y-intercept.

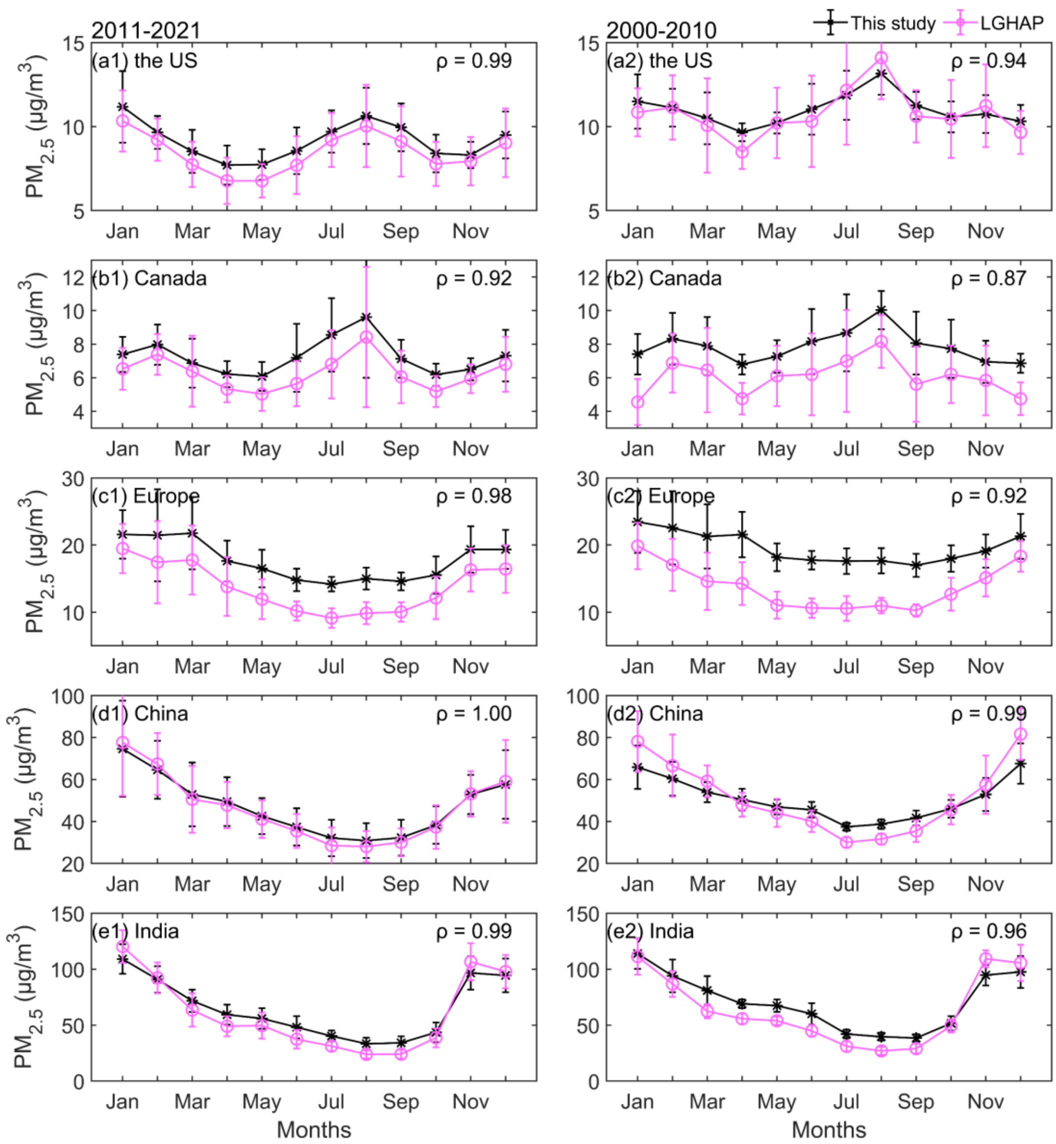

Figure 12. Comparison of annual cycle of monthly $PM_{2.5}$ concentration on the regional scale from 2011 to 2021 (left) and from 2000 to 2010 (right) between the estimated $PM_{2.5}$ concentration (this study) and LGHAP $PM_{2.5}$ concentration on the daily scale. ρ is the correlation coefficient.

~~Figure 13 shows the annual average $PM_{2.5}$ concentration from 1959 to 2022 in different regions, along with a comparison to the $PM_{2.5}$ concentrations derived from other datasets. Another dataset is used for comparison in China: the monthly $PM_{2.5}$ of the CHAP from 2000 to 2021 (Wei et al., 2020b; Wei et al., 2021). We use correlation coefficients, mean bias and mean relative bias to compare the relationships and differences among the $PM_{2.5}$ datasets.~~

~~In the United States, the estimated $PM_{2.5}$ concentrations exhibit correlation coefficients of 0.96, 0.88, and -0.38 with the ACAG, CAMS, and MERRA-2 data, respectively; the mean bias (mean relative bias) is 0.8 (10%), -5.4 (-35%), and 1.1 (13%) for each dataset, respectively.~~

~~In Canada, the estimated $PM_{2.5}$ concentrations exhibit correlation coefficients of 0.84, 0.62, and -0.46 with the ACAG, CAMS, and MERRA-2 data, respectively; the mean bias (mean relative bias) is 0.5 μg/m^3 (7%), -5.1 μg/m^3 (-40%), and 0.2 μg/m^3 (6%) for each dataset, respectively.~~

~~In Europe, the estimated $PM_{2.5}$ concentrations exhibit correlation coefficients of 0.96, 0.96, and 0.76 with the ACAG, CAMS, and MERRA-2 data, respectively; the mean bias (mean relative bias) is 2.3 $\mu g/m^3$ (15%), 2.6 $\mu g/m^3$ (20%), and 7.5 $\mu g/m^3$ (66%) for each dataset, respectively.~~

~~In China, the estimated $PM_{2.5}$ concentrations exhibit correlation coefficients of 0.78, 0.98, 0.81, and 0.51 with the ACAG, CHAP, CAMS, and MERRA-2 data, respectively; the mean bias (mean relative bias) is 10.7 $\mu g/m^3$ (24%), 2.5 $\mu g/m^3$ (4%), -39.1 $\mu g/m^3$ (-42%), and 24 $\mu g/m^3$ (90%) for each dataset, respectively.~~

~~In India, the estimated $PM_{2.5}$ concentrations exhibit correlation coefficients of -0.3, -0.02, and -0.09 with the ACAG, CAMS, and MERRA-2 data, respectively; the mean bias (mean relative bias) is 29.9 $\mu g/m^3$ (53%), -58.9 $\mu g/m^3$ (-40%), and 56.1 $\mu g/m^3$ (203%) for each dataset, respectively. From 2013 to 2022, the correlation coefficients with the ACAG and CAMS data are 0.71 and 0.70, respectively. The trend of visibility declines from 1961 to 2008. The frequency of visibility (exceeding 10 km) in the afternoon decreases by 46%, and the frequency of visibility (below 4 km) in the morning increases by 21% (Jaswal et al., 2013), particularly in the central and northern regions. The low cloud cover significantly increases from 1960 to 2010 in the Indo-Gangetic Plain and the northwestern and eastern coasts of India (Jaswal et al., 2017). The average total cloud cover is 3.4 okta from 1960 to 2007, with a decrease of 0.07 okta/decade (Jaswal, 2010). However, the indirect impact of aerosols on cloud formation do not influence cloud cover (Ramanathan et al., 2005). The prevalence of clouds poses challenges for satellite retrievals in these areas, potentially contributing to substantial disparities between $PM_{2.5}$ concentrations estimated based on visibility and satellite retrievals. The CAMS reanalysis data are calibrated using satellite data and thus show consistency with the trend in AOD retrievals from satellites; the anthropogenic emission data are from the MACCity inventory (Inness et al., 2019), and there are significant variations among different anthropogenic emission inventories, particularly before 2010, which leads to substantial uncertainties in India (Granier et al., 2011; Liu et al., 2022). These issues exist to a greater or lesser extent in other regions, which may contribute to the increased disparities between estimated $PM_{2.5}$ and reanalysis data before 2012.~~

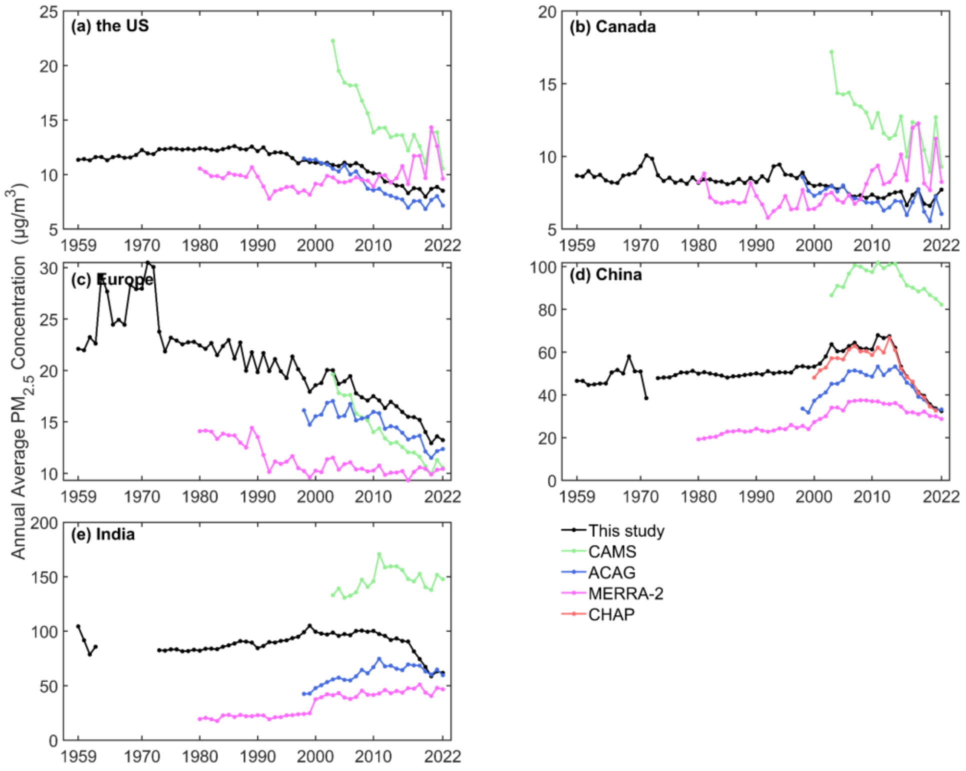

~~**Figure 13** Annual mean $PM_{2.5}$ concentration from 1959 to 2022 in the United States (US) (a), Canada (b), Europe (c), China (d), and India (e). The other four datasets are ACAG from 1998 to 2022, CHAP from 2000 to 2021, MERRA-2 from 1980 to 2022, and CAMS from 2003 to 2022.~~

4.3 Discussion on the Differences ~~among the~~ of $PM_{2.5}$ Concentration~~Datasets~~ from Visibility and Aerosol Optical Depth

Both visibility and aerosol optical depth are excellent alternatives for estimating $PM_{2.5}$ concentration, with its own advantages. However, they have differences in principle, which may be the reason for the difference between the two datasets in comparison.

Fine particulate matter near the ground surface affects atmospheric visibility through scattering. Studies have shown ~~$PM_{2.5}$ is considered a pollutant that decreases visibility. There is~~ visibility has a negative correlation ~~between visibility and~~with $PM_{2.5}$ concentration, and the reciprocal of visibility has a positive correlation with~~is proportional to~~ the extinction coefficient and has a negative correlation~~, which is closely related to~~ with the ~~concentration of~~ particulate matter concentration (Wang et al., 2012; Zhang et al., 2017; Zhang et al., 2020). Therefore, ~~Prior to the widespread implementation of $PM_{2.5}$ measurements or lack of measurement of particulate matter,~~ visibility is often used as a proxy for particulate matter pollution (Huang et al., 2009; Singh et al., 2020) and i~~.~~ ~~I~~t is the basis ~~for using visibility~~ to estimate $PM_{2.5}$ concentration. In addition, s~~S~~tudies have shown that meteorological observations such as temperature and humidity also play an important role in estimating $PM_{2.5}$ concentration using visibility (Shen et al., 2016; Xue et al., 2019; Zhong et al., 2021). Therefore, when estimating $PM_{2.5}$ concentration based on visibility data, only conventional meteorological variables need to be added, which is convenient and accurate observational data.

Besides, the ~~The~~ long-term, complete and high-temporal ~~advantages of~~ ground-based ~~visibility and other meteorological variables~~ observations are the advantage of historical estimation of $PM_{2.5}$ concentration. ~~include long-term records, high temporal resolution, and good data completeness, and the visibility observations from airports can be traced back to 1959 in this study.~~ The daily mean from continuous or equidistant hourly observations greatly increases the daily representativeness.~~Therefore, we employ a machine learning approach to establish the relationship between $PM_{2.5}$ and visibility and other meteorological variables, and estimate the long-term historical $PM_{2.5}$ concentration from 1959 to 2022, and discuss the limitations and uncertainties. It should be noted that not all sites of $PM_{2.5}$ have the time range from 1959 to 2022, which depends on the record length of matched visibility station.~~

~~There are differences between $PM_{2.5}$ based on visibility, $PM_{2.5}$ based on satellite retrievals, and $PM_{2.5}$ of reanalysis.~~ The aerosol optical depth is a physical quantity that describes aerosol column properties, which is the integration of the extinction coefficient in the vertical direction. When establishing a connection between aerosol optical depth and near-ground $PM_{2.5}$ concentration, it is essential to consider the vertical structure of aerosols. Studies have shown that ~~$PM_{2.5}$ based on satellite retrievals typically requires consideration of~~the aerosol vertical profiles usually are provided by observations, assumptions, or chemical transport models to obtain the aerosol properties near the surface (Van Donkelaar et al., 2010; Wei et al., 2019b; Van Donkelaar et al., 2021). Van Donkelaar et al. (2006; 2010) ~~(!!! INVALID CITATION !!! (2006; 2010))~~ have demonstrated that aerosol vertical profile errors in chemical transport models and aerosol optical depth ~~AOD~~ retrieval and sampling result in an approximately 25% uncertainty of one standard deviation. Sensitivity testing shows that a 1% estimation error in the aerosol optical depth ~~AOD~~ can lead to a 0.27% estimation error in the $PM_{2.5}$ concentration (Wei et al., 2021). Besides, the retrieval of aerosol optical depth ~~Visibility is a near-surface observation that~~ is ~~not~~ affected by clouds or surface types and a finite number of daily observations (usually 1-2 times), though it has the advantage of high spatial coverage ~~has high temporal resolution~~ (Liu et al., 2017; Singh et al., 2020; Zhong et al., 2021). ~~$PM_{2.5}$ from reanalysis usually requires accurate meteorological fields and emission inventories. Although ERA5 has provided meteorological reanalysis since 1940, the historical emission inventories and physical-chemical mechanisms in the chemical transport model still have significant uncertainties, which increase the uncertainty in particulate matter concentration. Additionally, the assimilated data in reanalysis mainly consist of satellite AOD and ground-based AOD, aiming to improve column aerosol properties, without considering near-surface $PM_{2.5}$ (Buchard et al., 2017; Gelaro et al., 2017; Provençal et al., 2017; Huijnen et al., 2019; Inness et al., 2019; Ali et al., 2022). These factors contribute to the differences in estimating $PM_{2.5}$ concentration among the three methods.~~

Another difference is the upper limit of $PM_{2.5}$ concentration. In this study, the upper limit of the estimated daily $PM_{2.5}$ concentration is set to 1000 $\mu g/m^3$ (the same for input data). ~~because~~ When the $PM_{2.5}$ concentration is greater than 500 $\mu g/m^3$ during heavy pollution ~~weather~~, which may contribute to the higher frequency at high pollution levels than in the ~~other~~ LGHAP dataset, ~~s.~~ especially before 2010. ~~Visibility is a near-surface observation that is not affected by clouds or surface types and has high temporal resolution (Liu et al., 2017; Singh et al., 2020; Zhong et al., 2021). In section 3.4, the uncertainty analysis provides an explanation for the overestimation.~~ We do not ~~delete~~ remove visibility records during ~~sand and~~ dust weather when preprocessing the data, which may lead to an overestimation of $PM_{2.5}$ concentration in dusty areas, such as northern China and northwestern India. ~~Visibility is a near-surface observation that is not affected by clouds or surface types and has high temporal resolution (Liu et al., 2017; Singh et al., 2020; Zhong et al., 2021).~~ In section 3.4, the uncertainty analysis has provided an explanation for the overestimation.

~~The frequency and monthly/annual variations in our data are consistent with those of $PM_{2.5}$ based on satellite retrievals (ACAG and CHAP). The concentration level is higher than in those datasets because their upper limits are lower. The AOD is a physical quantity that describes the properties of aerosol columns. It is important to consider the vertical structure of aerosols when establishing a connection between AOD and near-ground $PM_{2.5}$. Van Donkelaar et al. (2006; 2010) demonstrated that aerosol vertical profile errors in chemical transport models and AOD retrieval and sampling result in an approximately 25% uncertainty of one standard deviation. Sensitivity testing shows that a 1% estimation error in the AOD can lead to a 0.27% estimation error in the $PM_{2.5}$ concentration (Wei et al., 2021). Visibility is a near-surface observation that is not affected by clouds or surface types and has high temporal resolution (Liu et al., 2017; Singh et al., 2020; Zhong et al., 2021). In section 3.4, the uncertainty analysis provides an explanation for the overestimation.~~

~~In section 2.6.3, we introduce the chemical model, emission, and assimilation of MERRA-2. The $PM_{2.5}$ concentration from MERRA-2 does not include nitrates, and the assimilation of AOD mainly provides constraints on aerosols after 2000 (Buchard et al., 2016; Randles et al., 2017; Ali et al., 2022). The lack of nitrate is a limitation in areas with high nitrate concentrations. For example, an extreme pollution event over China in January 2013 is not captured well (Buchard et al., 2017). Ali et al. (2022) used 1.4 × [SO_4^{2-}] to represent nitrate concentration, and the results showed a correlation coefficient of 0.55 with the observed $PM_{2.5}$. Compared to the ACAG over the United States, which has a low nitrate concentration, the MERRA-2 surface $PM_{2.5}$ concentration is greater in rural areas than in urban and suburban areas, with high and localized emissions reducing the representation of the grid mean $PM_{2.5}$ (Buchard et al., 2017). Therefore, the lack of nitrate and insufficient assimilation data are the key factors leading to the significant differences between the two datasets.~~

~~In section 2.6.4, we introduce the CAMS $PM_{2.5}$. The $PM_{2.5}$ concentration from CAMS is significantly greater than the estimated $PM_{2.5}$ concentration and follows a similar annual cycle, except in Europe. In Europe, the CO and NO_2 concentrations in CAMS are lower than those in winter (Flemming et al., 2015), which may lead to the underestimation of nitrate emissions and its precursors, resulting in the underestimation of $PM_{2.5}$ concentrations. Some studies have reported similar results (Kong et al., 2021; Ryu and Min, 2021; Ali et al., 2022; Jin et al., 2022). This finding may be related to the vertical section structure, composition, and microphysical properties of aerosols (Ali et al., 2022). Because NO_2 emissions are obtained by multiplying CO emissions by a factor of 0.2, the uncertainty in nitrate increases. Studies have shown that the uncertainties in MACCity (Huijnen et al., 2019) and dust (Ukhov et al., 2020) also cause overestimation in CAMS $PM_{2.5}$.~~

Overall, our $PM_{2.5}$ concentration dataset has a good consistency with $PM_{2.5}$ concentration based on aerosol optical depth~~satellite AOD data~~. ~~There are some differences in the reanalysis $PM_{2.5}$ concentrations. We also hope that our dataset can provide auxiliary support for reanalysis datasets.~~

5 ~~$PM_{2.5}$ Variability from 1959 to 2022~~Regional Trends and Spatial Patterns

We use the estimated $PM_{2.5}$ concentrations (at least 10-day records in a site) to calculate monthly $PM_{2.5}$ concentrations, and analyze the annual cycles, interannual trends, and spatial patterns of $PM_{2.5}$ concentrations in different regions based on the GAMM model. The annual variation comes from the monthly smooth term of GAMM, the interannual variation comes from the annual smooth term, and the spatial pattern comes from the spatial smooth term. The regions include Canada, the United States, Europe, China, and India. The results are shown in Figure 13. The trend from 1959 to 2022 in each region is the slope of the Sen-Theil (ST Slope) estimators (Sen, 1968; Theil, 1992), and Mann-Kendall test (Mann, 1945; Kendall, 1948) is used to calculate the significance of the trend. The test results show the p-values are all less than 0.01 in all regions.

~~5.1 Monthly $PM_{2.5}$ and Trend~~

In the United States, the annual cycle curve shows that the $PM_{2.5}$ concentration is a 'double peaks and double valleys' shape. The peaks occur in July and December, respectively, with the highest $PM_{2.5}$ concentration in July throughout the year. The valley values are in April and October, and the $PM_{2.5}$ concentration levels are equivalent. The trend is -0.40 μg/m^3/decade, and $PM_{2.5}$ concentration decreases significantly after 1992, with a trend of -1.39 μg/m^3/decade. The high $PM_{2.5}$ concentration areas are in the east and west. The areas with low $PM_{2.5}$ concentrations are mainly located in the central and northern regions. The high concentration in the eastern and western regions is related to extensive industrial activities and densely populated cities. The low concentration in the central and northern regions is relatively to high vegetation coverage, low industrial activity and low population density.

In Canada, the annual cycle curve also shows that the $PM_{2.5}$ concentration is a 'double peaks and double valleys' shape. The peak values occur in August and February, with the highest $PM_{2.5}$ concentration in August. The valley values are in April and October. The trend is -0.10 μg/m^3/decade, and $PM_{2.5}$ concentration increases after 2010. The $PM_{2.5}$ concentration exhibits an east-high to west-low pattern. The eastern regions, such as Ontario and Quebec, are characterized by high population density and significant industrial and transportation activities.

In Europe, the annual cycle of $PM_{2.5}$ concentration shows that the $PM_{2.5}$ concentration is the highest in February, and is low from May to September. The valley values are in April and October. The trend is -1.55 μg/m^3/decade. High concentration areas are distributed in eastern Europe, while low concentration areas are in northern and western Europe. Eastern Europe exhibits more industrialization, particularly with a prevalence of traditional heavy industries and the use of coal and other high-pollution energy sources. In contrast, the energy structure in western Europe tends to favor cleaner energy sources.

In China, the annual cycle curve of $PM_{2.5}$ concentration presents a V-liked shape. It indicates that high concentrations are in winter, while low concentrations are in summer. The trend is 2.09 μg/m^3/decade. The trend is 2.65 μg/m^3/decade from 1959 to 2011 and -22.23 μg/m^3/decade from 2012 to 2022. High concentration areas are distributed in northern China, such as North China Plain, Northeast China, Sichuan Basin, Taklimakan Desert, and Badain Jaran Desert. Low concentration areas are in southern China and Northern Tianshan Mountains. Besides dust, industrial activities and coal combustion for heating during winter are significant contributors to the $PM_{2.5}$ concentration in northern regions.

In India, the annual cycle curve of $PM_{2.5}$ concentration also presents a V-liked shape. High concentrations are in winter, and low concentrations are in summer. The trend is 0.92 μg/m^3/decade. The trend is 1.41 μg/m^3/decade from 1959 to 2013 and -23.36 μg/m^3/decade from 2014 to 2022. Some studies have shown that the $PM_{2.5}$ concentration in India has decreased since 2014, especially in northern cities. Singh et al. (2021) have found that five major cities in India show a downward trend from 2014 to 2019, with the largest decline of approximately -4.2 μg/m^3 per year in New Delhi. Ravindra et al. (2024) also finds that the trend in New Delhi is about -5 μg/m^3 per year from 2014 to 2020. These studies have shown a faster downward trend than our study, as these $PM_{2.5}$ monitoring sites are mainly concentrated in urban areas. The $PM_{2.5}$ concentration exhibits a north-high to south-low pattern. High concentration areas are distributed in northern India, such as Ganges Plain and Thar Desert, because there are more industrial and densely populated areas and the terrain leads to the retention of air pollutants. Low concentration areas are in Deccan Plateau.

~~Figure 14 (a) shows the frequency of the estimated monthly $PM_{2.5}$ from 1959 to 2022, and Table 3 lists the maximum frequency for each region. The order of the concentrations with the greatest frequency was Canada (8 μg/m^3), the United States (12 μg/m^3), Europe (18 μg/m^3), China (42 μg/m^3) and India (64 μg/m^3). Canada and the United States are areas with less frequent $PM_{2.5}$ pollution. $PM_{2.5}$ pollution occurs frequently in China and India.~~ Above all, ~~The results indicate that~~ the $PM_{2.5}$ concentrations in developed countries and regions are significantly lower than those in developing countries in the Northern Hemisphere.

~~Figure 14 (b-f) shows the anomalies of the estimated monthly $PM_{2.5}$ concentration from 1959 to 2022, and Table 3 lists the trends for each region. The trends in each region from 1959 to 2022 are all negative; however, the trend in India does not pass the significance test ($p>0.05$). The fastest downward trend is in Europe, at -1.93 μg/m^3/decade. The trends in different regions vary at different times. Positive trends are detected in the United States from 1959 to 1990, in Canada from 1959 to 1993, and in China and India from 1959 to 2012. The most rapid upward trend is observed in India, at 3.35 μg/m^3/decade from 1959 to 2012. Negative trends are detected in the United States from 1991 to 2022, in Europe from 1959 to 1972 and from 1973 to 2022, and in China and India from 2013 to 2022. The most significant downward trend is observed in India, at -42.84 μg/m^3/decade. These~~ R~~r~~egional trends are similar ~~to~~ with those of previous studies in different periods (Van Donkelaar et al., 2010; Wang et al., 2012; Boys et al., 2014; Ma et al., 2016; Li et al., 2017; Hammer et al., 2020).

The trends in $PM_{2.5}$ concentration changes in different regions are closely associated with the implementation of relevant policies. The earlier pollution control measures are taken, the earlier the decreasing trend in the $PM_{2.5}$ concentration occurs, and the lower the threat of particulate matter pollution is to humans. In 1997, the United States ~~–~~EPA classified $PM_{2.5}$ as a hazardous substance in the National Ambient Air Quality Standard, and subsequent regulations in 2006 further strengthened the source control and management of fine particulate matter (Hall and Gilliam, 2016). In 1988, the Canadian federal government enacted the Canadian Environmental Protection Act, which enhanced the regulation of $PM_{2.5}$ (Davies, 1988). The European Union introduced the Air Quality Directive in 1996, followed by multiple revisions and updated~~s~~ to regulate and restrict air pollutants, including $PM_{2.5}$ (Kuklinska et al., 2015). However, Europe stands out due to its early adoption of clean production practices in heavy industries since the 1970s. Since 2012, China has implemented numerous regulations and standards for $PM_{2.5}$. For instance, the Monitoring Method for Atmospheric Particulate Matter ($PM_{2.5}$) was issued in 2012, and the Chinese Ministry of Environmental Protection released the Ambient Air Quality Standards in 2013, ~~which~~ includinge emission standards for $PM_{2.5}$ (Zhao et al., 2016a). In 2009, the Indian Ministry of Environment and Forests issued the National Ambient Air Quality Standards, which include control standards for ~~air pollutants, including~~ $PM_{2.5}$. Since 2015, the Indian government has launched the National Clean Air Programme (NCAP) to improve air quality ~~in India~~ by implementing a series of measures to reduce the emissions of $PM_{2.5}$ and other pollutants (Ganguly et al., 2020). These environmental regulations have contributed significantly to the decline ~~in~~ of $PM_{2.5}$ concentrations. Some studies have shown that the variation of $PM_{2.5}$ concentrations is also related to several factors, such as the energy structure, urbanization process, population distribution and vegetation coverage (Shi et al., 2018; Wu et al., 2018; Li et al., 2019; Wang et al., 2019; Lim et al., 2020; Qi et al., 2023).(2021; 2024)

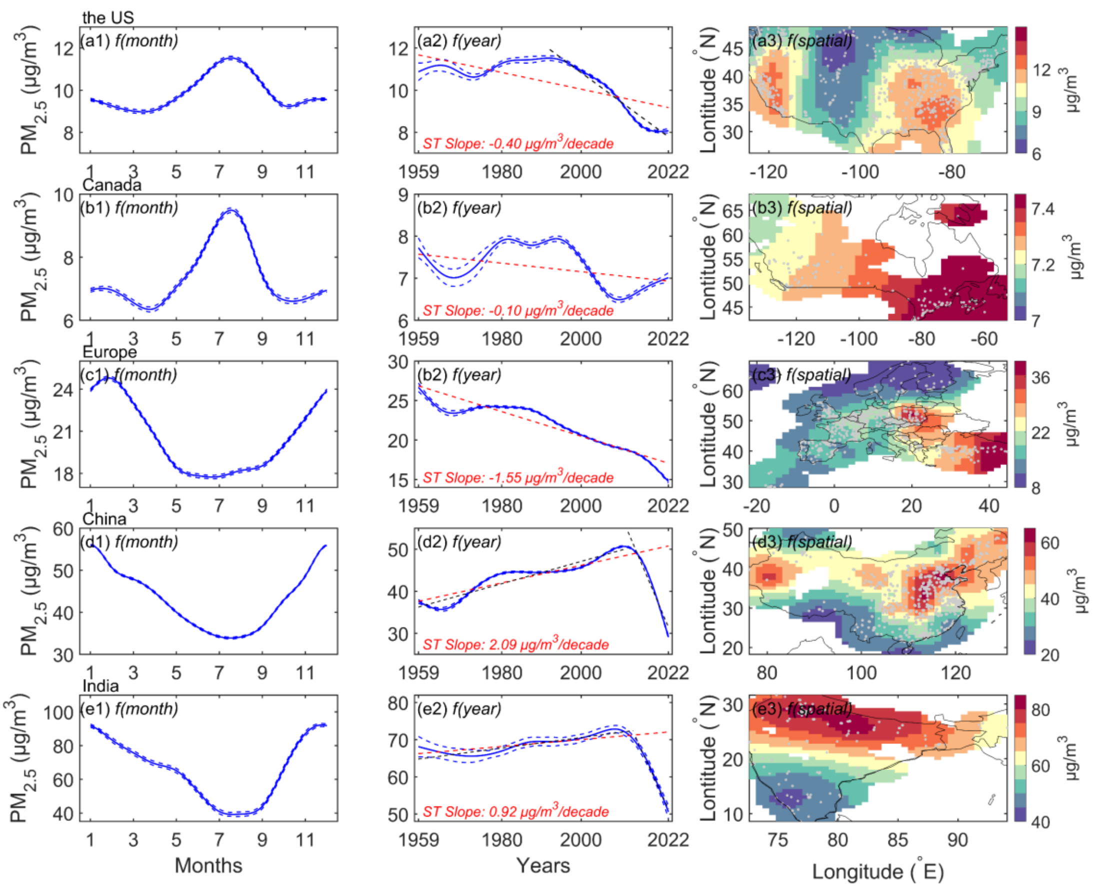

Figure 13. Annual cycles, interannual trends and spatial patterns of $PM_{2.5}$ concentrations in the United States (a1-a3), Canada (b1-b3), Europe (c1-c3), China (d1-d3), and India (e1-e3). The left column 'f(month)' is the annual cycle, the middle column 'f(year)' is the interannual trend, and the right column 'f(spatial)' is the spatial distribution from Generalized Additive Mixed Model (GAMM). The blue dashed lines represent ± 1 standard error of the month and annual mean of $PM_{2.5}$ concentrations. The red or black dashed lines represent the trends of the Sen-Theil estimators (ST Slope). Mann-Kendall test of trends shows that the p-values are less than 0.01 in all regions. The scatter points in right column are the locations of $PM_{2.5}$ monitoring sites.

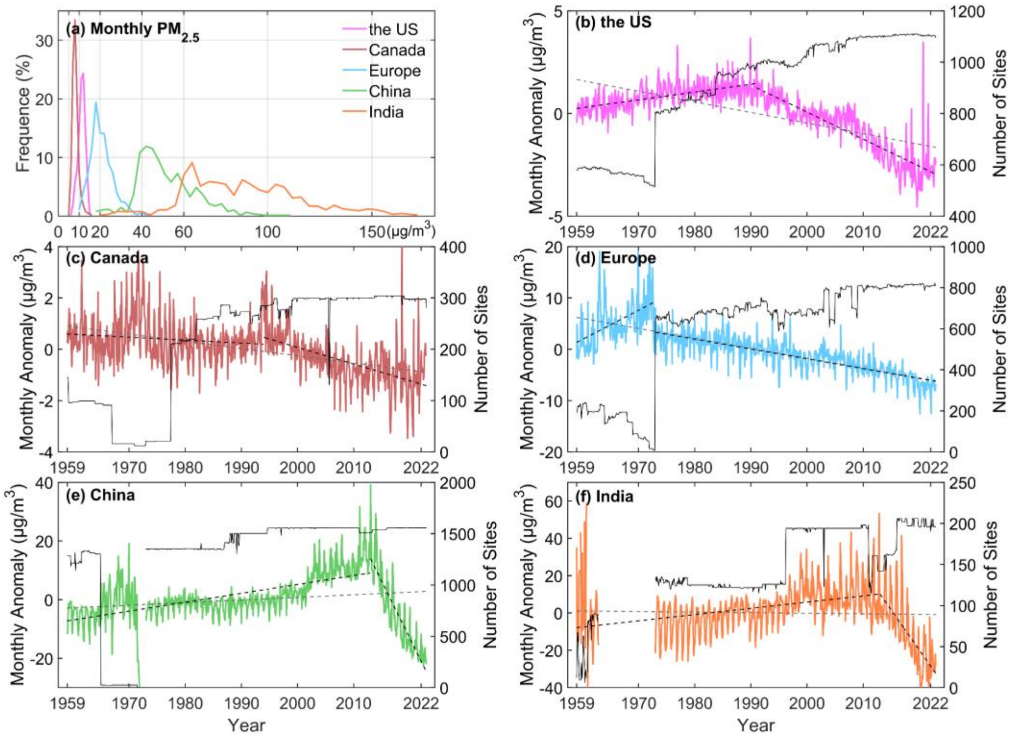

~~**Figure 14** Frequency (a) and anomalies (b-f) of monthly $PM_{2.5}$ from 1959 to 2022 in the United States (the US), Canada, Europe, China, and India. The right Y-axis (b-f) is the monthly number of sites.~~

~~**Table 3** The frequency and trend of the monthly $PM_{2.5}$ concentration from 1959 to 2022 in the United States (the US), Canada, Europe, China and India.~~

	~~*Concentration Mode (μg/m^3) and maximum frequency (%)*~~	~~*Trend (μg/m^3/decade)*~~		
~~*the US*~~	~~12 (24.3%)~~	~~-0.52* (1959-2022)~~	~~0.38* (1959-1990)~~	~~-1.32* (1991-2022)~~
~~*Canada*~~	~~8 (33.5%)~~	~~-0.28* (1959-2022)~~	~~-0.11* (1959-1993)~~	~~-6.48* (1994-2022)~~
~~*Europe*~~	~~18 (19.4%)~~	~~-1.93* (1959-2022)~~	~~5.69* (1959-1972)~~	~~-1.91* (1973-2022)~~
~~*China*~~	~~42 (11.9%)~~	~~-0.89* (1959-2022)~~	~~3.04* (1959-2012)~~	~~-38.82* (2013-2022)~~
~~*India*~~	~~64 (9.1%)~~	~~-0.31 (1959-2022)~~	~~3.35* (1959-2012)~~	~~-42.84* (2013-2022)~~

~~The symbol * indicates passing the significance test, $p<0.01$; otherwise, not passing the significance test, $p>0.05$.~~

~~5.2 Annual $PM_{2.5}$ and Distribution~~

~~We analyze the spatial distribution of the multiyear average $PM_{2.5}$ concentration in each region, and we investigate the yearly variations in the spatial distribution based on the SDE and the average center, as shown in Figure 15. The mean center and SDE describe the periodic changes in the spatial distribution and dispersion of the $PM_{2.5}$ concentration in each region. The larger the ellipse area is, the more dispersed the spatial distribution of $PM_{2.5}$ is. The flatter the ellipse is, the stronger the~~

~~spatial correlation of $PM_{2.5}$, and the direction of the major axis indicates the direction of the concentration.~~

~~The multiyear average $PM_{2.5}$ concentrations from 1959 to 2022 are 11.2 μg/m^3 in the United States, 8.2 μg/m^3 in Canada, 20.1 μg/m^3 in Europe, 51.3 μg/m in China, and 88.6 μg/m^3 in India. $PM_{2.5}$ concentrations in developed regions (North America and Europe) are significantly lower than those in developing regions (China and India).~~

~~For the United States, the concentration in the eastern region is greater than that in the western region. The $PM_{2.5}$ concentration at most sites in the eastern region is greater than 10 μg/m^3. Based on the area of the SDE, the spatial distribution is divided into three stages: 1959-1972, 1973-1976, and 1977-2022. The area decreases and then increases, indicating a changing trend in the spatial extent of the $PM_{2.5}$ concentration. The concentration distribution direction is east–west and rotates northward, and the mean center gradually moves northwest after 1977, indicating an increase in the $PM_{2.5}$ contribution in the western region.~~

~~For Canada, the concentrations in the eastern and western regions are greater than those in the central region. The area of the ellipse increases and then decreases. The concentration distribution direction is northwest-to-southeast, and the concentration rotates southward after 1977, indicating an increase in weight in the western region. The mean center gradually moves northwestward and then southeastward.~~

~~For Europe, high-concentration areas are mainly located in the central and eastern regions. The ellipse's area can be divided into three stages: 1959-1967, 1968-1972, and 1973-2022. The spatial variability decreases and then increases, corresponding to the mean centers moving north, south, and north. The concentration direction is northwest–southeast, and the major axis shortens after 1993, indicating that the directionality of the concentration weakens.~~

~~For China, high-concentration areas are in the central and eastern regions. The center of the SDE is located in the northeast region from 1965 to 1971, which may be related to Northeast China being the center of heavy industry during that period. After 1988, the area of the SDE increases significantly, and the center moves significantly southwestward and gradually northward after 2008. This finding indicates that the spatial distribution of $PM_{2.5}$ increases in a discrete pattern after 1988, and the concentration weight in the eastern region gradually increases. After 2008, the weight in the western region decreases again.~~

~~For India, the highest concentration is in the northern region, and the lowest concentration is in the southern region. The area, shape, and mean center of the SDE show significant changes and can be divided into three stages. The SDE flattens between 1959 and 1962. The flattening weakens, and the area increases from 1963 to 1995. The spatial variability in $PM_{2.5}$ increases, and the mean center moves southward. From 1996 to 2022, the flattening further weakens, the area decreases, the spatial variability in $PM_{2.5}$ decreases, and the mean center shifts northward.~~

~~Above all, the concentration distributions in the United States and India exhibit an east–west pattern. The concentration distribution in Canada and Europe shows a northwest-to-southeast concentration gradient. In China, the $PM_{2.5}$ concentration distribution ranges from northeast to southwest. There are strong correlations between the $PM_{2.5}$ concentration and the location of the sites in Europe and Canada. However, the spatial correlation in India is gradually weakening, and the spatial dispersion~~

~~of $PM_{2.5}$ in China is increasing. Studies have shown that the variation in $PM_{2.5}$ based on the mean center and the SDE is related to several factors, such as the energy structure, urbanization process, population distribution and vegetation coverage (Shi et al., 2018; Wu et al., 2018; Li et al., 2019; Wang et al., 2019; Lim et al., 2020; Qi et al., 2023).~~

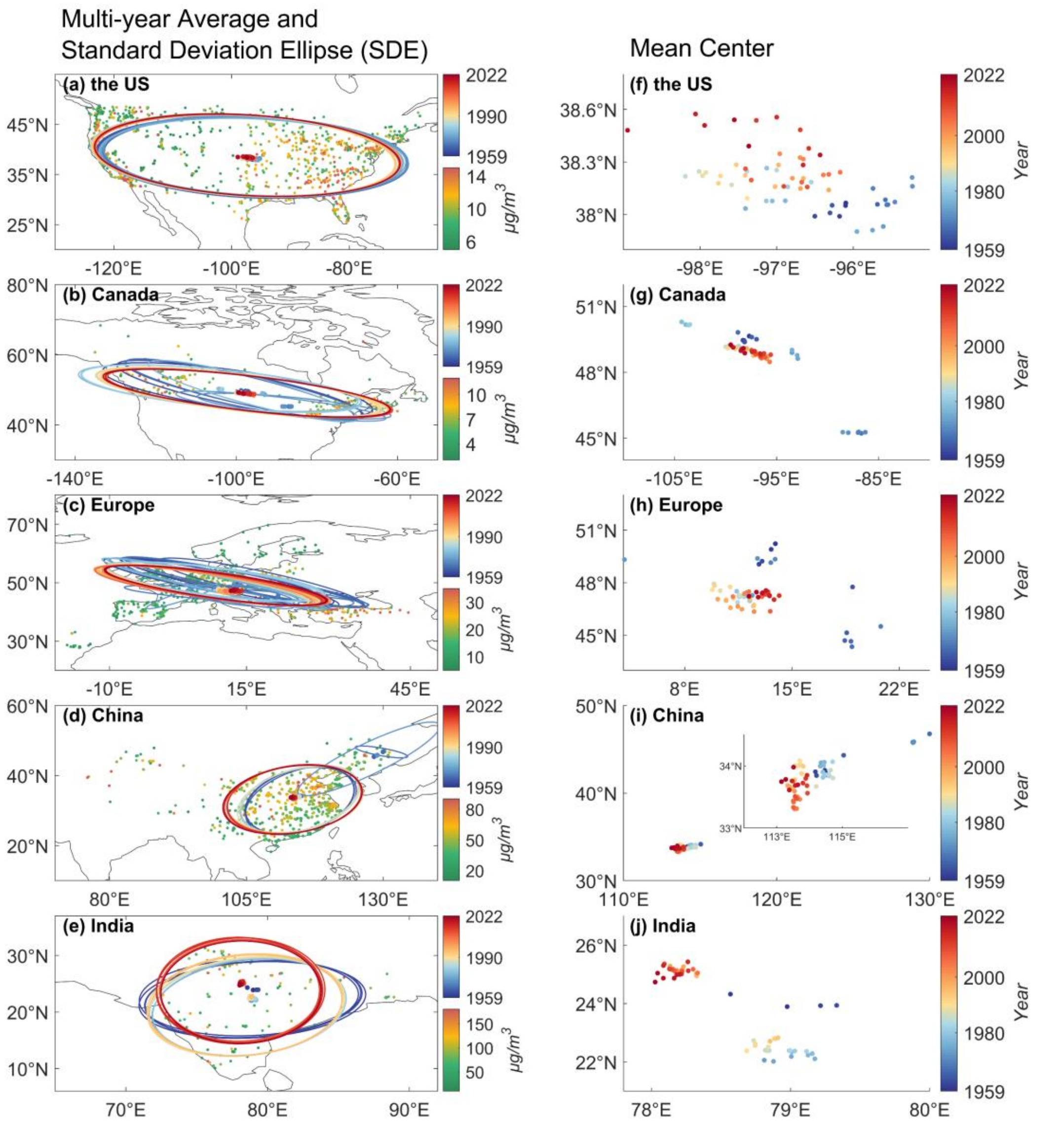

~~**Figure 15** The spatial distribution of the multiyear average and standard deviation ellipse (SDE) (a-e) and the mean center (f-j) of the $PM_{2.5}$ concentration from 1959 to 2022 in the United States (the US), Canada, Europe, China, and India. The mean center and SDE describe the changes in the spatial distribution. The larger the ellipse area is, the more dispersed the spatial distribution of $PM_{2.5}$ is. The flatter the ellipse is, the stronger the spatial correlation of $PM_{2.5}$ is. The direction of the major axis indicates the direction of the concentration.~~

6 Conclusions

In t~~T~~his study, we use~~s~~ a machine learning method to estimate daily $PM_{2.5}$ concentration for ~~4011~~ 5023 terrestrial sites in the Northern Hemisphere from 1959 to 2022 based on ~~hourly~~ daily visibility and related meteorological variables. The first 80% of $PM_{2.5}$ concentration data in each site ~~Eighty percent of the sample data~~ are used to train the model, and the last 20% are used ~~for~~ to test~~ing~~. The model's performance and predictive ability are evaluated and a dataset of daily $PM_{2.5}$ concentration based on aerosol optical depth is used to compare and evaluate the estimated $PM_{2.5}$ concentration. We analyze the uncertainty and discuss the limitations of ~~the~~ our dataset~~. We compare the estimated $PM_{2.5}$ with the $PM_{2.5}$ based on the satellite AOD and $PM_{2.5}$ of the reanalysis datasets~~. Finally, the $PM_{2.5}$ concentration ~~variability~~ variation (annual calendar cycle, interannual cycle and spatial distribution) in ~~each~~ 5 regions over the past 64 years is analyzed based on GAMM. We hope our dataset will be useful for studying the atmospheric environment, human health, and climate change and provide auxiliary support for assimilation. Several key results of this study are described as follows:

The most important variable. Visibility is the most important variable at ~~79.1~~80.7% of the $PM_{2.5}$ sites, as visibility can ~~also~~ be considered an indicator of $PM_{2.5}$ concentration without fog or precipitation. Other meteorological variables play a secondary role in the model, especially temperature and dew point temperature. ~~Visibility can serve as a good indicator of $PM_{2.5}$.~~

Model performance and predictive ability. The training results show that the slope between the estimated $PM_{2.5}$ concentration and the monitored $PM_{2.5}$ concentration within the 95% confidence interval is 0.~~946~~955, the R^2 is 0.95, the RMSE is 7.~~0~~2 μg/m^3, and the MAE is 3.2~~1~~ μg/m^3. The test results show that the slope between the predicted $PM_{2.5}$ concentration and the monitored $PM_{2.5}$ concentration is 0.~~862~~864 ± 0.0010 within a 95% confidence interval, R^2 is 0.~~80~~79, RMSE is 1~~3.5~~4.8 μg/m^3, and MAE is ~~6.9~~7.6 μg/m^3. The model shows good stability and predictive ability. Compared with a global $PM_{2.5}$ concentration dataset based on satellite retrieval, the slopes of linear regression on the daily (monthly) scale are 0.817 (0.854) from 2000 to 2021, 0.758 (0.821) from 2000 to 2010, and 0.867 (0.879) from 2011 to 2022. The result indicates the accuracy of the model and the consistency of the estimated $PM_{2.5}$ concentration on the temporal scale.

Regional trends and spatial patterns~~**Comparison with other datasets.** The estimated $PM_{2.5}$ concentration is consistent with the $PM_{2.5}$ concentration based on satellite AOD data at the monthly scale. The correlation coefficient of the annual cycles in each region is greater than 0.96. Compared with the reanalysis data, there are some differences among regions, which are closely related to the accuracy of emission inventories and the vertical structures of aerosols.~~

~~**Monthly $PM_{2.5}$**~~. The interannual trends and spatial patterns of $PM_{2.5}$ concentration on the regional scale from 1959 to 2022 are analyzed based on GAMM. In Canada, the trend is -0.10 μg/m^3/decade in Canada and the $PM_{2.5}$ concentration exhibits an east-high to west-low pattern. In the United States, the trend is -0.40 μg/m^3/decade, and $PM_{2.5}$ concentration decreases significantly after 1992, with a trend of -1.39 μg/m^3/decade. The high $PM_{2.5}$ concentration areas are in the east and west and the low are in the central and northern regions. In Europe, the trend is -1.55 μg/m^3/decade. High concentration areas are distributed in eastern Europe, while the low is in northern and western Europe. In China, the trend is 2.09 μg/m^3/decade. High concentration areas are distributed in northern China and the low are distributed in southern China and Northern Tianshan Mountains. The trend is 2.65μg/m^3/decade from 1959 to 2011 and -22.23 μg/m^3/decade from 2012 to 2022. In India, the trend is 0.92 μg/m^3/decade. The concentration exhibits a north-high to south-low pattern, with high concentration areas distributed in northern India, such as Ganges Plain and Thar Desert and the low in Deccan Plateau. The trend is 1.41 μg/m^3/decade from 1959 to 2013 and -23.36 μg/m^3/decade from 2014 to 2012. The variation of $PM_{2.5}$ concentration is inseparable with the implementation of pollution control laws and regulations, the energy structure, industrialization, population and vegetation coverage.~~From 1959 to 2022, the $PM_{2.5}$ concentration at the highest frequency is 12 μg/m^3, 8 μg/m^3, 17 μg/m^3, 40 μg/m^3 and 63 μg/m^3, and the trends are -0.52 μg/m^3/decade, -0.28 μg/m^3/decade, -1.93 μg/m^3/decade, -0.89 μg/m^3/decade, and -0.31 μg/m^3/decade, respectively, for the United States, Canada, Europe, China, and India. $PM_{2.5}$ concentrations in all regions show a periodic increase and decrease from 1959 to 2022. The decreasing trends are -1.32 μg/m^3/decade from 1991 to 2022 in the United States, -6.48 μg/m^3/decade from 1994 to 2022 in Canada, -1.91 μg/m^3/decade from 1973 to 2022 in Europe, and -38.82 μg/m^3/decade and -42.84 μg/m^3/decade from 2013 to 2022 in China and India, respectively. Although the $PM_{2.5}$ concentrations in developing countries are significantly greater than those in developed countries, they have declined more quickly in recent years.~~

~~**Annual $PM_{2.5}$.** The multiyear average $PM_{2.5}$ concentrations from 1959 to 2022 in the United States, Canada, Europe, China, and India are 11.2 μg/m^3, 8.2 μg/m^3, 20.1 μg/m^3, 51.3 μg/m^3 and 88.6 μg/m^3, respectively. Based on the features of the SDE and mean center, the spatial distribution of $PM_{2.5}$ has more spatial variability in the United States, Canada, and Europe and less variability in China and India. The changes in the mean center of the $PM_{2.5}$ concentration exhibit various patterns in each region.~~

7 Data Availability

Daily $PM_{2.5}$ concentration data ~~at 4011 sites~~ in the Northern Hemisphere from 1959 to 2022 are available at https://cstr.cn/18406.11.Atmos.tpdc.301127 (Hao et al., 2024).

All site-scale $PM_{2.5}$ data files are in "PM25-Daily_1959_2022. zip". The file name includes a region name and a site number. For example, the file name, 'China_1001. txt', means that the site is in China, and the site number is 1001, which describes the daily $PM_{2.5}$ concentration at a single site and can be directly opened using a text program (such as Notepad), separated by commas. The data includes four variables: Date, PM25(μg/m3), Longitude(degree_east), and Latitude(degree_north). Date is UTC time, PM25(μg/m3) is the daily $PM_{2.5}$ concentration (unit: μg/m^3), Longitude range is [-180 °E, 180 °E] and Latitude range is [0 °N, 90 °N].

Competing Interests

The contact author has declared that none of the authors has any competing interests.

Acknowledgments

This work was supported by the National Key Research & Development Program of China (2022YFF0801302) and the National Natural Science Foundation of China (41930970). The hourly visibility data are available at from https://www.ncei.noaa.gov/products/land-based-station/integrated-surface-database~~https://mesonet.agron.iastate.edu/ASOS/~~. The hourly $PM_{2.5}$ data for the United States are available at https://www.epa.gov/aqs. The hourly $PM_{2.5}$ data for Canada are available at https://www.canada.ca. The hourly $PM_{2.5}$ data for Europe available at

https://european-union.europa.eu. The hourly $PM_{2.5}$ data for China are available at https://www.cnemc.cn. The hourly $PM_{2.5}$ data for India are available at https://app.cpcbccr.com. The hourly $PM_{2.5}$ concentration data of other regions are from openAQ, available at https://openaq.org. The daily $PM_{2.5}$ concentration of long-term gap-free high-resolution air pollutants (LGHAP) concentration dataset over global land, with a 1 km grid resolution, is available at https://zenodo.org/communities/ecnu_lghap.~~The hourly visibility and meteorological data are available at https://www.weather.gov/asos. The monthly global PM2.5 dataset for the Atmospheric Composition Analysis Group version V5.GL.04 (ACAG) are available at https://sites.wustl.edu/acag/datasets/surface-pm2-5/). The monthly PM2.5 dataset of China High Air Pollutants (CHAP) are available at https://zenodo.org/records/6398971. The monthly PM2.5 dataset of Modern-Era Retrospective Analysis for Research and Applications, version 2 (MERRA-2) are available at https://gmao.gsfc.nasa.gov. The monthly PM2.5 of the Copernicus Atmosphere Monitoring Service (CAMS) reanalysis are available at https://ads.atmosphere.copernicus.eu/cdsapp#!/dataset/cams-global-reanalysis-eac4.~~

References

, !!! INVALID CITATION !!! (2006; 2010).

Albrecht, B. A.: Aerosols, cloud microphysics, and fractional cloudiness, Science, 245, 1227-1230, https://doi.org/10.1126/science.245.4923.1227, 1989.

Ali, M. A., Bilal, M., Wang, Y., Nichol, J. E., Mhawish, A., Qiu, Z., de Leeuw, G., Zhang, Y., Zhan, Y., Liao, K., Almazroui, M., Dambul, R., Shahid, S., and Islam, M. N.: Accuracy assessment of CAMS and MERRA-2 reanalysis PM2.5 and PM10 concentrations over China, Atmos. Environ., 288, 119297, https://doi.org/10.1016/j.atmosenv.2022.119297, 2022.

Bai, K., Li, K., Shao, L., Li, X., Liu, C., Li, Z., Ma, M., Han, D., Sun, Y., Zheng, Z., Li, R., Chang, N. B., and Guo, J.: LGHAP v2: a global gap-free aerosol optical depth and PM2.5 concentration dataset since 2000 derived via big Earth data analytics, Earth Syst. Sci. Data, 16, 2425-2448, https://doi.org/10.5194/essd-16-2425-2024, 2024.

Beckerman, B. S., Jerrett, M., Serre, M., Martin, R. V., Lee, S.-J., Van Donkelaar, A., Ross, Z., Su, J., and Burnett, R. T.: A hybrid approach to estimating national scale spatiotemporal variability of PM2. 5 in the contiguous United States, Environ. Sci. Technol., 47, 7233-7241, https://doi.org/10.1021/es400039u, 2013.

Benedetti, A., Morcrette, J.-J., Boucher, O., Dethof, A., Engelen, R. J., Fisher, M., Flentje, H., Huneeus, N., Jones, L., Kaiser, J. W., Kinne, S., Mangold, A., Razinger, M., Simmons, A. J., and Suttie, M.: Aerosol analysis and forecast in the European Centre for Medium-Range Weather Forecasts Integrated Forecast System: 2. Data assimilation, J. Geophys. Res-Atmos., 114, https://doi.org/10.1029/2008JD011115, 2009.

Bergstrom, R. W., Pilewskie, P., Russell, P. B., Redemann, J., Bond, T. C., Quinn, P. K., and Sierau, B.: Spectral absorption properties of atmospheric aerosols, Atmos. Chem. Phys., 7, 5937-5943, https://doi.org/10.5194/acp-7-5937-2007, 2007.

Boers, R., van Weele, M., van Meijgaard, E., Savenije, M., Siebesma, A. P., Bosveld, F., and Stammes, P.: Observations and projections of visibility and aerosol optical thickness (1956-2100) in the Netherlands: impacts of time-varying aerosol composition and hygroscopicity, Environ. Res. Lett., 10, https://doi.org/10.1088/1748-9326/10/1/015003, 2015.

Boys, B., Martin, R., Van Donkelaar, A., MacDonell, R., Hsu, N., Cooper, M., Yantosca, R., Lu, Z., Streets, D., and Zhang, Q.: Fifteen-year global time series of satellite-derived fine particulate matter, Environ. Sci. Technol., 48, 11109-11118, https://doi.org/10.1021/es502113p, 2014.

Browne, M. W.: Cross-validation methods, J. Math. Psychol., 44, 108-132, https://doi.org/10.1006/jmps.1999.1279, 2000.

Buchard, V., da Silva, A. M., Colarco, P. R., Darmenov, A., Randles, C. A., Govindaraju, R., Torres, O., Campbell, J., and Spurr, R.: Using the OMI aerosol index and absorption aerosol optical depth to evaluate the NASA MERRA Aerosol Reanalysis, Atmos. Chem. Phys., 15, 5743-5760, https://doi.org/10.5194/acp-15-5743-2015, 2015.

Buchard, V., da Silva, A. M., Randles, C. A., Colarco, P., Ferrare, R., Hair, J., Hostetler, C., Tackett, J., and Winker, D.: Evaluation of the surface PM2.5 in Version 1 of the NASA MERRA Aerosol Reanalysis over the United States, Atmos. Environ., 125, 100-111, https://doi.org/10.1016/j.atmosenv.2015.11.004, 2016.

Buchard, V., Randles, C. A., da Silva, A. M., Darmenov, A., Colarco, P. R., Govindaraju, R., Ferrare, R., Hair, J., Beyersdorf, A. J., Ziemba, L. D., and Yu, H.: The MERRA-2 Aerosol Reanalysis, 1980 Onward. Part II: Evaluation and Case Studies, J. Climate, 30, 6851-6872, https://doi.org/10.1175/JCLI-D-16-0613.1, 2017.

Chafe, Z. A., Brauer, M., Klimont, Z., Van Dingenen, R., Mehta, S., Rao, S., Riahi, K., Dentener, F., and Smith, K. R.: Household Cooking with Solid Fuels Contributes to Ambient PM2.5 Air Pollution and the Burden of Disease, Environ. Health Persp., 122, 1314-1320, https://doi.org/10.1289/ehp.1206340, 2014.

Chang, K.-L., Petropavlovskikh, I., Cooper, O. R., Schultz, M. G., and Wang, T.: Regional trend analysis of surface ozone observations from monitoring networks in eastern North America, Europe and East Asia, Elementa: Science of the Anthropocene, 5, https://doi.org/10.1525/elementa.243, 2017.

Che, H., Xia, X., Zhu, J., Hong, W., and Shi, G.: Aerosol optical properties under the condition of heavy haze over an urban site of Beijing, China, Environ. Sci. Pollut. R., 22, 1043-1053, https://doi.org/10.1007/s11356-014-3415-5, 2014.

Chen, A., Zhao, C., and Fan, T.: Spatio-temporal distribution of aerosol direct radiative forcing over mid-latitude regions in north hemisphere estimated from satellite observations, Atmos. Res., 266, 105938, https://doi.org/10.1016/j.atmosres.2021.105938, 2022.

Chen, Z., Chen, D., Zhao, C., Kwan, M.-p., Cai, J., Zhuang, Y., Zhao, B., Wang, X., Chen, B., Yang, J., Li, R., He, B., Gao, B., Wang, K., and Xu, B.: Influence of meteorological conditions on PM_{2.5} concentrations across China: A review of methodology and mechanism, Environ. Int., 139, https://doi.org/10.1016/j.envint.2020.105558, 2020.

Chow, J. C., Doraiswamy, P., Watson, J. G., Chen, L. W. A., Ho, S. S. H., and Sodeman, D. A.: Advances in Integrated and Continuous Measurements for Particle Mass and Chemical Composition, Japca J. Air Waste Ma., 58, 141-163, https://doi.org/10.3155/1047-3289.58.2.141, 2008.

Cohen, A. J., Brauer, M., Burnett, R., Anderson, H. R., Frostad, J., Estep, K., Balakrishnan, K., Brunekreef, B., Dandona, L., Dandona, R., Feigin, V., Freedman, G., Hubbell, B., Jobling, A., Kan, H., Knibbs, L., Liu, Y., Martin, R., Morawska, L., Pope, C. A., III, Shin, H., Straif, K., Shaddick, G., Thomas, M., van Dingenen, R., van Donkelaar, A., Vos, T., Murray, C. J. L., and Forouzanfar, M. H.: Estimates and 25-year trends of the global burden of disease attributable to ambient air pollution: an analysis of data from the Global Burden of Diseases Study 2015, Lancet, 389, 1907-1918, https://doi.org/10.1016/s0140-6736(17)30505-6, 2017.

Dabek-Zlotorzynska, E., Dann, T. F., Martinelango, P. K., Celo, V., Brook, J. R., Mathieu, D., Ding, L., and Austin, C. C.: Canadian National Air Pollution Surveillance (NAPS) PM_{2.5} speciation program: Methodology and PM_{2.5} chemical composition for the years 2003-2008, Atmos. Environ., 45, 673-686, https://doi.org/10.1016/j.atmosenv.2010.10.024, 2011.

Davies, J.: CEPA—The Canadian. Environmental Protection Act, JAPCA, 38, 1111-1113, https://doi.org/10.1080/08940630.1988.10466452, 1988.

Demerjian, K. L.: A review of national monitoring networks in North America, Atmos. Environ., 34, 1861-1884, https://doi.org/10.1016/S1352-2310(99)00452-5, 2000.

Fan, H., Zhao, C., Yang, Y., and Yang, X.: Spatio-Temporal Variations of the PM_{2.5}/PM₁₀ Ratios and Its Application to Air Pollution Type Classification in China, Front. Environ. Sci., 9, https://doi.org/10.3389/fenvs.2021.692440, 2021.

Fei, Y., Liao, J., and Zhang, Z.: Consistency and Discrepancy between Visibility and PM2. 5 Measurements: Potential Application of Visibility Observation to Air Quality Study, Sensors, 23, 898, https://doi.org/10.3390/s23020898, 2023.

Flemming, J., Huijnen, V., Arteta, J., Bechtold, P., Beljaars, A., Blechschmidt, A. M., Diamantakis, M., Engelen, R. J., Gaudel, A., Inness, A., Jones, L., Josse, B., Katragkou, E., Marecal, V., Peuch, V. H., Richter, A., Schultz, M. G., Stein, O., and Tsikerdekis, A.: Tropospheric chemistry in the Integrated Forecasting System of ECMWF, Geosci. Model Dev., 8, 975-1003, https://doi.org/10.5194/gmd-8-975-2015, 2015.

Friedman, J. H.: Greedy function approximation: A gradient boosting machine, Ann. Stat., 29, 1189-1232, https://doi.org/10.1214/aos/1013203451, 2001.

Ganguly, T., Selvaraj, K. L., and Guttikunda, S. K.: National Clean Air Programme (NCAP) for Indian cities: Review and outlook of clean air action plans, Atmospheric Environment X, 8, 100096, https://doi.org/10.1016/j.aeaoa.2020.100096, 2020.

Gelaro, R., McCarty, W., Suárez, M. J., Todling, R., Molod, A., Takacs, L., Randles, C. A., Darmenov, A., Bosilovich, M. G., Reichle, R., Wargan, K., Coy, L., Cullather, R., Draper, C., Akella, S., Buchard, V., Conaty, A., da Silva, A. M., Gu, W., Kim, G.-K., Koster, R., Lucchesi, R., Merkova, D., Nielsen, J. E., Partyka, G., Pawson, S., Putman, W., Rienecker, M., Schubert, S. D., Sienkiewicz, M., and Zhao, B.: The Modern-Era Retrospective Analysis for Research and Applications, Version 2 (MERRA-2), J. Climate, 30, 5419-5454, https://doi.org/10.1175/JCLI-D-16-0758.1, 2017.

Goff, J. A.: Saturation pressure of water on the new Kelvin temperature scale, Transactions of the American Society of Heating and Ventilating Engineers, 63, 347-354, 1957.

Gong, J.: Clarifying the standard deviational ellipse, Geogr. Anal., 34, 155-167, https://doi.org/10.1111/j.1538-4632.2002.tb01082.x, 2002.

Granier, C., Bessagnet, B., Bond, T., D'Angiola, A., Denier van der Gon, H., Frost, G. J., Heil, A., Kaiser, J. W., Kinne, S., and Klimont, Z.: Evolution of anthropogenic and biomass burning emissions of air pollutants at global and regional scales during the 1980–2010 period, Climatic Change, 109, 163-190, https://doi.org/10.1007/s10584-011-0154-1, 2011.

Green, D. and Fuller, G. W.: The implications of tapered element oscillating microbalance (TEOM) software configuration on particulate matter measurements in the UK and Europe, Atmos. Environ., 40, 5608-5616, https://doi.org/10.1016/j.atmosenv.2006.04.052, 2006.

Guenther, A., Karl, T., Harley, P., Wiedinmyer, C., Palmer, P. I., and Geron, C.: Estimates of global terrestrial isoprene emissions using MEGAN (Model of Emissions of Gases and Aerosols from Nature), Atmos. Chem. Phys., 6, 3181-3210, https://doi.org/10.5194/acp-6-3181-2006, 2006.

Gui, K., Che, H., Zeng, Z., Wang, Y., Zhai, S., Wang, Z., Luo, M., Zhang, L., Liao, T., and Zhao, H.: Construction of a virtual PM2. 5 observation network in China based on high-density surface meteorological observations using the Extreme Gradient Boosting model, Environ. Int., 141, 105801, https://doi.org/10.1016/j.envint.2020.105801, 2020.

Guo, S., Hu, M., Zamora, M. L., Peng, J., Shang, D., Zheng, J., Du, Z., Wu, Z., Shao, M., Zeng, L., Molina, M. J., and Zhang, R.: Elucidating severe urban haze formation in China, P. Natl. A. Sci., 111, 17373-17378, https://doi.org/10.1073/pnas.1419604111, 2014.

Hall, E. and Gilliam, J.: Reference and Equivalent Methods Used to Measure National Ambient Air Quality Standards (NAAQS) Criteria Air Pollutants - Volume I, https://doi.org/10.13140/RG.2.1.3471.8329, 2016.

Hammer, M. S., van Donkelaar, A., Li, C., Lyapustin, A., Sayer, A. M., Hsu, N. C., Levy, R. C., Garay, M. J., Kalashnikova, O. V., and Kahn, R. A.: Global estimates and long-term trends of fine particulate matter concentrations (1998–2018), Environ. Sci. Technol., 54, 7879-7890, https://doi.org/10.1021/acs.est.0c01764, 2020.

Hao, H., Wang, K., Wu, G., Liu, J., and Li, J.: PM2.5 concentrations based on near-surface visibility at 4011 sites in the Northern Hemisphere from 1959 to 2022, National Tibetan Plateau Data Center [dataset], https://doi.org/10.11888/Atmos.tpdc.301127, 2024.

Hastie, T. and Tibshirani, R.: Generalized Additive Models: Some Applications, J. Am. Stat. Assoc., 82, 371-386, https://doi.org/10.1080/01621459.1987.10478440, 1987.

He, Q., Gao, K., Zhang, L., Song, Y., and Zhang, M.: Satellite-derived 1-km estimates and long-term trends of PM2. 5 concentrations in China from 2000 to 2018, Environ. Int., 156, 106726, https://doi.org/10.1016/j.envint.2021.106726, 2021.

Hsu, N., Lee, J., Sayer, A., Carletta, N., Chen, S. H., Tucker, C., Holben, B., and Tsay, S. C.: Retrieving near-global aerosol loading over land and ocean from AVHRR, J. Geophys. Res-Atmos., 122, 9968-9989, https://doi.org/10.1002/2017JD026932, 2017.

Huang, W., Tan, J., Kan, H., Zhao, N., Song, W., Song, G., Chen, G., Jiang, L., Jiang, C., and Chen, R.: Visibility, air quality and daily mortality in Shanghai, China, Sci. Total Environ., 407, 3295-3300, https://doi.org/10.1016/j.scitotenv.2009.02.019, 2009.

Huijnen, V., Pozzer, A., Arteta, J., Brasseur, G., Bouarar, I., Chabrillat, S., Christophe, Y., Doumbia, T., Flemming, J., Guth, J., Josse, B., Karydis, V. A., Marécal, V., and Pelletier, S.: Quantifying uncertainties due to chemistry modelling – evaluation of tropospheric composition simulations in the CAMS model (cycle 43R1), Geosci. Model Dev., 12, 1725-1752, https://doi.org/10.5194/gmd-12-1725-2019, 2019.

Husar, R. B., Husar, J. D., and Martin, L.: Distribution of continental surface aerosol extinction based on visual range data, Atmos. Environ., 34, 5067-5078, https://doi.org/10.1016/s1352-2310(00)00324-1, 2000.

Inness, A., Ades, M., Agustí-Panareda, A., Barré, J., Benedictow, A., Blechschmidt, A.-M., Dominguez, J. J., Engelen, R., Eskes, H., and Flemming, J.: The CAMS reanalysis of atmospheric composition, Atmos. Chem. Phys., 19, 3515-3556, https://doi.org/10.5194/acp-19-3515-2019, 2019.

Jaswal, A.: Changes in total cloud cover over India based upon 1961-2007 surface observations, Mausam, 61, 455-468, https://doi.org/10.54302/mausam.v61i4.882, 2010.

Jaswal, A., Kore, P., and Singh, V.: Variability and trends in low cloud cover over India during 1961-2010, Mausam, 68, 235-252, https://doi.org/10.54302/mausam.v68i2.627, 2017.

Jaswal, A. K., Kumar, N., Prasad, A. K., and Kafatos, M.: Decline in horizontal surface visibility over India (1961–2008) and its association with meteorological variables, Nat. hazards, 68, 929-954, https://doi.org/10.1007/s11069-013-0666-2, 2013.

Jin, C., Wang, Y., Li, T., and Yuan, Q.: Global validation and hybrid calibration of CAMS and MERRA-2 PM2.5 reanalysis products based on OpenAQ platform, Atmos. Environ., 274, 118972, https://doi.org/10.1016/j.atmosenv.2022.118972, 2022.

Kaiser, J. W., Heil, A., Andreae, M. O., Benedetti, A., Chubarova, N., Jones, L., Morcrette, J. J., Razinger, M., Schultz, M. G., Suttie, M., and van der Werf, G. R.: Biomass burning emissions estimated with a global fire assimilation system based on observed fire radiative power, Biogeosciences, 9, 527-554, https://doi.org/10.5194/bg-9-527-2012, 2012.

Kammann, E. E. and Wand, M. P.: Geoadditive Models, J. R. Stat. Soc. C-appl., 52, 1-18, https://doi.org/10.1111/1467-9876.00385, 2003.

Kendall, M. G.: Rank correlation methods, 1948.

Kim, K.-H., Kabir, E., and Kabir, S.: A review on the human health impact of airborne particulate matter, Environ. Int., 74, 136-143, https://doi.org/10.1016/j.envint.2014.10.005, 2015.

Kong, L., Tang, X., Zhu, J., Wang, Z., Li, J., Wu, H., Wu, Q., Chen, H., Zhu, L., Wang, W., Liu, B., Wang, Q., Chen, D., Pan, Y., Song, T., Li, F., Zheng, H., Jia, G., Lu, M., Wu, L., and Carmichael, G. R.: A 6-year-long (2013–2018) high-resolution air quality reanalysis dataset in China based on the assimilation of surface observations from CNEMC, Earth Syst. Sci. Data, 13, 529-570, https://doi.org/10.5194/essd-13-529-2021, 2021.

Kuklinska, K., Wolska, L., and Namiesnik, J.: Air quality policy in the US and the EU–a review, Atmos. Pollut. Res., 6, 129-137, https://doi.org/10.5094/APR.2015.015, 2015.

Lelieveld, J., Evans, J. S., Fnais, M., Giannadaki, D., and Pozzer, A.: The contribution of outdoor air pollution sources to premature mortality on a global scale, Nature, 525, 367-+, https://doi.org/10.1038/nature15371, 2015.

Li, C., Martin, R. V., Boys, B. L., van Donkelaar, A., and Ruzzante, S.: Evaluation and application of multi-decadal visibility data for trend analysis of atmospheric haze, Atmos. Chem. Phys., 16, 2435-2457, https://doi.org/10.5194/acp-16-2435-2016, 2016.

Li, C., Martin, R. V., van Donkelaar, A., Boys, B. L., Hammer, M. S., Xu, J.-W., Marais, E. A., Reff, A., Strum, M., and Ridley, D. A.: Trends in chemical composition of global and regional population-weighted fine particulate matter estimated for 25 years, Environ. Sci. Technol., 51, 11185-11195, https://doi.org/10.1021/acs.est.7b02530, 2017.

Li, J., Han, X., Jin, M., Zhang, X., and Wang, S.: Globally analysing spatiotemporal trends of anthropogenic PM2. 5 concentration and population's PM2. 5 exposure from 1998 to 2016, Environ. Int., 128, 46-62, https://doi.org/10.1016/j.envint.2019.04.026, 2019.

Li, J., Garshick, E., Hart, J. E., Li, L., Shi, L., Al-Hemoud, A., Huang, S., and Koutrakis, P.: Estimation of ambient PM2.5 in Iraq and Kuwait from 2001 to 2018 using machine learning and remote sensing, Environ. Int., 151, https://doi.org/10.1016/j.envint.2021.106445, 2021.

Li, J., Carlson, B. E., Yung, Y. L., Lv, D., Hansen, J., Penner, J. E., Liao, H., Ramaswamy, V., Kahn, R. A., Zhang, P., Dubovik, O., Ding, A., Lacis, A. A., Zhang, L., and Dong, Y.: Scattering and absorbing aerosols in the climate system, Nat. Rev. Earth. Environ., 3, 363-379, https://doi.org/10.1038/s43017-022-00296-7, 2022.

Li, S., Chen, L., Huang, G., Lin, J., Yan, Y., Ni, R., Huo, Y., Wang, J., Liu, M., and Weng, H.: Retrieval of surface PM2. 5 mass concentrations over North China using visibility measurements and GEOS-Chem simulations, Atmos. Environ., 222, 117121, https://doi.org/10.1016/j.atmosenv.2019.117121, 2020.

Liao, H., Chang, W., and Yang, Y.: Climatic Effects of Air Pollutants over China: A Review, Adv. Atmos. Sci., 32, 115-139, https://doi.org/10.1007/s00376-014-0013-x, 2015.

Lim, C.-H., Ryu, J., Choi, Y., Jeon, S. W., and Lee, W.-K.: Understanding global PM2. 5 concentrations and their drivers in recent decades (1998–2016), Environ. Int., 144, 106011, https://doi.org/10.1016/j.envint.2020.106011, 2020.

Liu, M., Bi, J., and Ma, Z.: Visibility-based PM2. 5 concentrations in China: 1957–1964 and 1973–2014, Environ. Sci. Technol., 51, 13161-13169, https://doi.org/10.1021/acs.est.7b03468, 2017.

Liu, M., Huang, X., Song, Y., Tang, J., Cao, J., Zhang, X., Zhang, Q., Wang, S., Xu, T., Kang, L., Cai, X., Zhang, H., Yang, F., Wang, H., Yu, J. Z., Lau, A. K. H., He, L., Huang, X., Duan, L., Ding, A., Xue, L., Gao, J., Liu, B., and Zhu, T.: Ammonia emission control in China would mitigate haze pollution and nitrogen deposition, but worsen acid rain, P. Natl. A. Sci., 116, 7760-7765, https://doi.org/10.1073/pnas.1814880116, 2019.

Liu, S., Geng, G., Xiao, Q., Zheng, Y., Liu, X., Cheng, J., and Zhang, Q.: Tracking daily concentrations of PM2. 5 chemical composition in China since 2000, Environ. Sci. Technol., 56, 16517-16527, https://doi.org/10.1021/acs.est.2c06510, 2022.

Ma, Z., Hu, X., Sayer, A. M., Levy, R., Zhang, Q., Xue, Y., Tong, S., Bi, J., Huang, L., and Liu, Y.: Satellite-based spatiotemporal trends in PM2. 5 concentrations: China, 2004–2013, Environ. Health Persp., 124, 184-192, https://doi.org/10.1289/ehp.1409481, 2016.

Mandal, S., Madhipatla, K. K., Guttikunda, S., Kloog, I., Prabhakaran, D., Schwartz, J. D., and Team, G. H. I.: Ensemble averaging based assessment of spatiotemporal variations in ambient PM2. 5 concentrations over Delhi, India, during 2010–2016, Atmos. Environ., 224, 117309, https://doi.org/10.1016/j.atmosenv.2020.117309, 2020.

Mann, H. B.: Nonparametric Tests Against Trend, Econometrica, 13, 245-259, https://doi.org/10.2307/1907187, 1945.

Meng, X., Hand, J. L., Schichtel, B. A., and Liu, Y.: Space-time trends of PM2. 5 constituents in the conterminous United States estimated by a machine learning approach, 2005–2015, Environ. Int., 121, 1137-1147, https://doi.org/10.1016/j.envint.2018.10.029, 2018.

Miao, Y. and Liu, S.: Linkages between aerosol pollution and planetary boundary layer structure in China, Sci. Total Environ., 650, 288-296, https://doi.org/10.1016/j.scitotenv.2018.09.032, 2019.

Molnár, A., Mészáros, E., Imre, K., and Rüll, A.: Trends in visibility over Hungary between 1996 and 2002, Atmos. Environ., 42, 2621-2629, https://doi.org/10.1016/j.atmosenv.2007.05.012, 2008.

Nagaraja Rao, C., Stowe, L., and McClain, E.: Remote sensing of aerosols over the oceans using AVHRR data Theory, practice and applications, Int. J. Remote Sens., 10, 743-749, https://doi.org/10.1080/01431168908903915, 1989.

NOAA, DOD, FAA, and USN: Automated Surface Observing System (ASOS) User's Guide, 1998.

Pant, P., Lal, R. M., Guttikunda, S. K., Russell, A. G., Nagpure, A. S., Ramaswami, A., and Peltier, R. E.: Monitoring particulate matter in India: recent trends and future outlook, Air. Qual. Tmos. Hlth., 12, 45-58, https://doi.org/10.1007/s11869-018-0629-6, 2019.

Park, A., Guillas, S., and Petropavlovskikh, I.: Trends in stratospheric ozone profiles using functional mixed models, Atmos. Chem. Phys., 13, 11473-11501, https://doi.org/10.5194/acp-13-11473-2013, 2013.

Polansky, L. and Robbins, M. M.: Generalized additive mixed models for disentangling long-term trends, local anomalies, and seasonality in fruit tree phenology, Ecol. Evol., 3, 3141-3151, https://doi.org/10.1002/ece3.707, 2013.

Provençal, S., Buchard, V., da Silva, A. M., Leduc, R., and Barrette, N.: Evaluation of PM surface concentrations simulated by Version 1 of NASA's MERRA Aerosol Reanalysis over Europe, Atmos. Pollut. Res., 8, 374-382, https://doi.org/10.1016/j.apr.2016.10.009, 2017.

Pui, D. Y. H., Chen, S.-C., and Zuo, Z.: PM2.5 in China: Measurements, sources, visibility and health effects, and mitigation, Particuology, 13, 1-26, https://doi.org/10.1016/j.partic.2013.11.001, 2014.

Qi, G., Wei, W., Wang, Z., Wang, Z., and Wei, L.: The spatial-temporal evolution mechanism of PM2. 5 concentration based on China's climate zoning, J. Environ. Manage., 325, 116671, https://doi.org/10.1016/j.jenvman.2022.116671, 2023.

Ramanathan, V., Crutzen, P. J., Kiehl, J., and Rosenfeld, D.: Aerosols, climate, and the hydrological cycle, Science, 294, 2119-2124, https://doi.org/10.1126/science.1064034, 2001.

Ramanathan, V., Chung, C., Kim, D., Bettge, T., Buja, L., Kiehl, J. T., Washington, W. M., Fu, Q., Sikka, D. R., and Wild, M.: Atmospheric brown clouds: Impacts on South Asian climate and hydrological cycle, P. Natl. A. Sci., 102, 5326-5333, https://doi.org/10.1073/pnas.0500656102, 2005.

Randles, C. A., da Silva, A. M., Buchard, V., Colarco, P. R., Darmenov, A., Govindaraju, R., Smirnov, A., Holben, B., Ferrare, R., Hair, J., Shinozuka, Y., and Flynn, C. J.: The MERRA-2 Aerosol Reanalysis, 1980 Onward. Part I: System Description and Data Assimilation Evaluation, J. Climate, 30, 6823-6850, https://doi.org/10.1175/JCLI-D-16-0609.1, 2017.

Ravindra, K., Rattan, P., Mor, S., and Aggarwal, A. N.: Generalized additive models: Building evidence of air pollution, climate change and human health, Environ. Int., 132, 104987, https://doi.org/10.1016/j.envint.2019.104987, 2019.

Ravindra, K., Vakacherla, S., Singh, T., Upadhya, A. R., Rattan, P., and Mor, S.: Long-term trend of PM2.5 over five Indian megacities using a new statistical approach, Stoch. Env. Res. Risk A., 38, 715-725, https://doi.org/10.1007/s00477-023-02595-x, 2024.

Ryu, Y.-H. and Min, S.-K.: Long-term evaluation of atmospheric composition reanalyses from CAMS, TCR-2, and MERRA-2 over South Korea: Insights into applications, implications, and limitations, Atmos. Environ., 246, 118062, https://doi.org/10.1016/j.atmosenv.2020.118062, 2021.

Samset, B. H., Lund, M. T., Bollasina, M., Myhre, G., and Wilcox, L.: Emerging Asian aerosol patterns, Nat. Geosci., 12, 582-584, https://doi.org/10.1038/s41561-019-0424-5, 2019.

Sen, P. K.: Estimates of the Regression Coefficient Based on Kendall's Tau, J. Am. Stat. Assoc., 63, 1379-1389, https://doi.org/10.1080/01621459.1968.10480934, 1968.

Shen, Z., Cao, J., Zhang, L., Zhang, Q., Huang, R.-J., Liu, S., Zhao, Z., Zhu, C., Lei, Y., and Xu, H.: Retrieving historical ambient PM2. 5 concentrations using existing visibility measurements in Xi'an, Northwest China, Atmos. Environ., 126, 15-20, https://doi.org/10.1016/j.atmosenv.2015.11.040, 2016.

Shi, Y., Matsunaga, T., Yamaguchi, Y., Li, Z., Gu, X., and Chen, X.: Long-term trends and spatial patterns of satellite-retrieved PM2. 5 concentrations in South and Southeast Asia from 1999 to 2014, Sci. Total Environ., 615, 177-186, https://doi.org/10.1016/j.scitotenv.2017.09.241, 2018.

Singh, A., Avis, W. R., and Pope, F. D.: Visibility as a proxy for air quality in East Africa, Environ. Res. Lett., 15, 084002, https://doi.org/10.1088/1748-9326/ab8b12, 2020.

Singh, V., Singh, S., and Biswal, A.: Exceedances and trends of particulate matter (PM2.5) in five Indian megacities, Sci. Total Environ., 750, 141461, https://doi.org/10.1016/j.scitotenv.2020.141461, 2021.

Smith, A., Lott, N., and Vose, R.: The Integrated Surface Database: Recent Developments and Partnerships, B. Am. Meteorol. Soc., 92, 704-708, https://doi.org/10.1175/2011BAMS3015.1, 2011.

Su, L., Gao, C., Ren, X., Zhang, F., Cao, S., Zhang, S., Chen, T., Liu, M., Ni, B., and Liu, M.: Understanding the spatial representativeness of air quality monitoring network and its application to

PM2.5 in the mainland China, Geosci. Front., 13, 101370, https://doi.org/10.1016/j.gsf.2022.101370, 2022.

Sun, E., Xu, X., Che, H., Tang, Z., Gui, K., An, L., Lu, C., and Shi, G.: Variation in MERRA-2 aerosol optical depth and absorption aerosol optical depth over China from 1980 to 2017, J. Atmos. Sol-Terr. Phy., 186, 8-19, https://doi.org/10.1016/j.jastp.2019.01.019, 2019.

Tan, S., Wang, Y., Yuan, Q., Zheng, L., Li, T., Shen, H., and Zhang, L.: Reconstructing global PM2.5 monitoring dataset from OpenAQ using a two-step spatio-temporal model based on SES-IDW and LSTM, Environ. Res. Lett., 17, 034014, https://doi.org/10.1088/1748-9326/ac52c9, 2022.

Theil, H.: A Rank-Invariant Method of Linear and Polynomial Regression Analysis, in: Henri Theil's Contributions to Economics and Econometrics: Econometric Theory and Methodology, edited by: Raj, B., and Koerts, J., Springer Netherlands, Dordrecht, 345-381, https://doi.org/10.1007/978-94-011-2546-8_20, 1992.

Ukhov, A., Mostamandi, S., da Silva, A., Flemming, J., Alshehri, Y., Shevchenko, I., and Stenchikov, G.: Assessment of natural and anthropogenic aerosol air pollution in the Middle East using MERRA-2, CAMS data assimilation products, and high-resolution WRF-Chem model simulations, Atmos. Chem. Phys., 20, 9281-9310, https://doi.org/10.5194/acp-20-9281-2020, 2020.

Van Donkelaar, A., Martin, R. V., and Park, R. J.: Estimating ground-level PM2. 5 using aerosol optical depth determined from satellite remote sensing, J. Geophys. Res., 111, https://doi.org/10.1029/2005JD006996, 2006.

Van Donkelaar, A., Martin, R. V., Brauer, M., and Boys, B. L.: Use of satellite observations for long-term exposure assessment of global concentrations of fine particulate matter, Environ. Health Persp., 123, 135-143, https://doi.org/10.1289/ehp.1408646, 2015.

Van Donkelaar, A., Martin, R. V., Li, C., and Burnett, R. T.: Regional estimates of chemical composition of fine particulate matter using a combined geoscience-statistical method with information from satellites, models, and monitors, Environ. Sci. Technol., 53, 2595-2611, https://doi.org/10.1021/acs.est.8b06392, 2019.

Van Donkelaar, A., Martin, R. V., Brauer, M., Kahn, R., Levy, R., Verduzco, C., and Villeneuve, P. J.: Global estimates of ambient fine particulate matter concentrations from satellite-based aerosol optical depth: development and application, Environ. Health Persp., 118, 847-855, https://doi.org/10.1289/ehp.0901623, 2010.

Van Donkelaar, A., Martin, R. V., Brauer, M., Hsu, N. C., Kahn, R. A., Levy, R. C., Lyapustin, A., Sayer, A. M., and Winker, D. M.: Global estimates of fine particulate matter using a combined geophysical-statistical method with information from satellites, models, and monitors, Environ. Sci. Technol., 50, 3762-3772, https://doi.org/10.1021/acs.est.5b05833, 2016.

van Donkelaar, A., Hammer, M. S., Bindle, L., Brauer, M., Brook, J. R., Garay, M. J., Hsu, N. C., Kalashnikova, O. V., Kahn, R. A., Lee, C., Levy, R. C., Lyapustin, A., Sayer, A. M., and Martin, R. V.: Monthly Global Estimates of Fine Particulate Matter and Their Uncertainty, Environ. Sci. Technol., 55, 15287-15300, https://doi.org/10.1021/acs.est.1c05309, 2021.

Verbeke, G. and Lesaffre, E.: A Linear Mixed-Effects Model with Heterogeneity in the Random-Effects Population, J. Am. Stat. Assoc., 91, 217-221, https://doi.org/10.1080/01621459.1996.10476679, 1996.

Viana, M., Kuhlbusch, T. A. J., Querol, X., Alastuey, A., Harrison, R. M., Hopke, P. K., Winiwarter, W., Vallius, A., Szidat, S., Prevot, A. S. H., Hueglin, C., Bloemen, H., Wahlin, P., Vecchi, R., Miranda, A. I., Kasper-Giebl, A., Maenhaut, W., and Hitzenberger, R.: Source apportionment of particulate matter in Europe: A review of methods and results, J. Aerosol Sci., 39, 827-849,

https://doi.org/10.1016/j.jaerosci.2008.05.007, 2008.
Wang, K., Dickinson, R. E., and Liang, S.: Clear Sky Visibility Has Decreased over Land Globally from 1973 to 2007, Science, 323, 1468-1470, https://doi.org/10.1126/science.1167549, 2009.
Wang, K. C., Dickinson, R. E., Su, L., and Trenberth, K. E.: Contrasting trends of mass and optical properties of aerosols over the Northern Hemisphere from 1992 to 2011, Atmos. Chem. Phys., 12, 9387-9398, https://doi.org/10.5194/acp-12-9387-2012, 2012.
Wang, Q., Kwan, M.-P., Zhou, K., Fan, J., Wang, Y., and Zhan, D.: The impacts of urbanization on fine particulate matter (PM2. 5) concentrations: Empirical evidence from 135 countries worldwide, Environ. Pollut., 247, 989-998, https://doi.org/10.1016/j.envpol.2019.01.086, 2019.
Wang, Z., Li, J., Wang, Z., Yang, W., Tang, X., Ge, B., Yan, P., Zhu, L., Chen, X., Chen, H., Wand, W., Li, J., Liu, B., Wang, X., Wand, W., Zhao, Y., Lu, N., and Su, D.: Modeling study of regional severe hazes over mid-eastern China in January 2013 and its implications on pollution prevention and control, Sci. China Earth Sci., 57, 3-13, https://doi.org/10.1007/s11430-013-4793-0, 2014.
Wei, J., Li, Z., Peng, Y., and Sun, L.: MODIS Collection 6.1 aerosol optical depth products over land and ocean: validation and comparison, Atmos. Environ., 201, 428-440, https://doi.org/10.1016/j.atmosenv.2018.12.004, 2019a.
Wei, J., Huang, W., Li, Z., Xue, W., Peng, Y., Sun, L., and Cribb, M.: Estimating 1-km-resolution PM2.5 concentrations across China using the space-time random forest approach, Remote Sens. Environ., 231, https://doi.org/10.1016/j.rse.2019.111221, 2019b.
Wei, J., Li, Z., Lyapustin, A., Sun, L., Peng, Y., Xue, W., Su, T., and Cribb, M.: Reconstructing 1-km-resolution high-quality PM2. 5 data records from 2000 to 2018 in China: spatiotemporal variations and policy implications, Remote Sens. Environ., 252, 112136, https://doi.org/10.1016/j.rse.2020.112136, 2021.
Wei, J., Li, Z., Cribb, M., Huang, W., Xue, W., Sun, L., Guo, J., Peng, Y., Li, J., and Lyapustin, A.: Improved 1 km resolution PM 2.5 estimates across China using enhanced space–time extremely randomized trees, Atmos. Chem. Phys., 20, 3273-3289, https://doi.org/10.5194/acp-20-3273-2020, 2020a.
Wei, J., Li, Z., Cribb, M., Huang, W., Xue, W., Sun, L., Guo, J., Peng, Y., Li, J., Lyapustin, A., Liu, L., Wu, H., and Song, Y.: Improved 1 km resolution PM2.5 estimates across China using enhanced space-time extremely randomized trees, Atmos. Chem. Phys., 20, 3273-3289, https://doi.org/10.5194/acp-20-3273-2020, 2020b.
Wood, S. N., Pya, N., and Säfken, B.: Smoothing Parameter and Model Selection for General Smooth Models, J. Am. Stat. Assoc., 111, 1548-1563, https://doi.org/10.1080/01621459.2016.1180986, 2016.
Wu, J., Zheng, H., Zhe, F., Xie, W., and Song, J.: Study on the relationship between urbanization and fine particulate matter (PM2. 5) concentration and its implication in China, J. Cleaner Prod., 182, 872-882, https://doi.org/10.1016/j.jclepro.2018.02.060, 2018.
Wu, W. and Zhang, Y.: Effects of particulate matter (PM2.5) and associated acidity on ecosystem functioning: response of leaf litter breakdown, Environ. Sci. Pollut. R., 25, 30720-30727, https://doi.org/10.1007/s11356-018-2922-1, 2018.
Xue, T., Zheng, Y., Tong, D., Zheng, B., Li, X., Zhu, T., and Zhang, Q.: Spatiotemporal continuous estimates of PM2. 5 concentrations in China, 2000–2016: A machine learning method with inputs from satellites, chemical transport model, and ground observations, Environ. Int., 123, 345-357, https://doi.org/10.1016/j.envint.2018.11.075, 2019.
Yang, X., Zhao, C., Yang, Y., Yan, X., and Fan, H.: Statistical aerosol properties associated with fire

events from 2002 to 2019 and a case analysis in 2019 over Australia, Atmos. Chem. Phys., 21, 3833-3853, https://doi.org/10.5194/acp-21-3833-2021, 2021.

Zeng, Z., Gui, K., Wang, Z., Luo, M., Geng, H., Ge, E., An, J., Song, X., Ning, G., and Zhai, S.: Estimating hourly surface PM2. 5 concentrations across China from high-density meteorological observations by machine learning, Atmos. Res., 254, 105516, https://doi.org/10.1016/j.atmosres.2021.105516, 2021.

Zhang, Q., Zheng, Y., Tong, D., Shao, M., Wang, S., Zhang, Y., Xu, X., Wang, J., He, H., Liu, W., Ding, Y., Lei, Y., Li, J., Wang, Z., Zhang, X., Wang, Y., Cheng, J., Liu, Y., Shi, Q., Yan, L., Geng, G., Hong, C., Li, M., Liu, F., Zheng, B., Cao, J., Ding, A., Gao, J., Fu, Q., Huo, J., Liu, B., Liu, Z., Yang, F., He, K., and Hao, J.: Drivers of improved PM_{2.5} air quality in China from 2013 to 2017, P. Natl. A. Sci., 116, 24463-24469, https://doi.org/10.1073/pnas.1907956116, 2019.

Zhang, S., Wu, J., Fan, W., Yang, Q., and Zhao, D.: Review of aerosol optical depth retrieval using visibility data, Earth-Sci. Rev., 200, 102986, https://doi.org/10.1016/j.earscirev.2019.102986, 2020.

Zhang, Z., Wu, W., Wei, J., Song, Y., Yan, X., Zhu, L., and Wang, Q.: Aerosol optical depth retrieval from visibility in China during 1973-2014, Atmos. Environ., 171, 38-48, https://doi.org/10.1016/j.atmosenv.2017.09.004, 2017.

Zhao, B., Su, Y., He, S., Zhong, M., and Cui, G.: Evolution and comparative assessment of ambient air quality standards in China, J. Integr. Environ. Sci., 13, 85-102, https://doi.org/10.1080/1943815X.2016.1150301, 2016a.

Zhao, S., Yu, Y., Yin, D., He, J., Liu, N., Qu, J., and Xiao, J.: Annual and diurnal variations of gaseous and particulate pollutants in 31 provincial capital cities based on in situ air quality monitoring data from China National Environmental Monitoring Center, Environ. Int., 86, 92-106, https://doi.org/10.1016/j.envint.2015.11.003, 2016b.

Zhong, J., Zhang, X., Gui, K., Liao, J., Fei, Y., Jiang, L., Guo, L., Liu, L., Che, H., and Wang, Y.: Reconstructing 6-hourly PM 2.5 datasets from 1960 to 2020 in China, Earth Syst. Sci. Data, 14, 3197-3211, https://doi.org/10.5194/essd-14-3197-2022, 2022.

Zhong, J., Zhang, X., Gui, K., Wang, Y., Che, H., Shen, X., Zhang, L., Zhang, Y., Sun, J., and Zhang, W.: Robust prediction of hourly PM2. 5 from meteorological data using LightGBM, Natl. Sci. Rev., 8, nwaa307, https://doi.org/10.1093/nsr/nwaa307, 2021.